AUTOMATIC FAULT DETECTION IN DOMESTIC HEAT PUMPS

Ivan Bellanco Bellanco

UNIVERSITAT ROVIRA i VIRGILI

Automatic Fault Detection in domestic heat pumps

Ivan Bellanco Bellanco

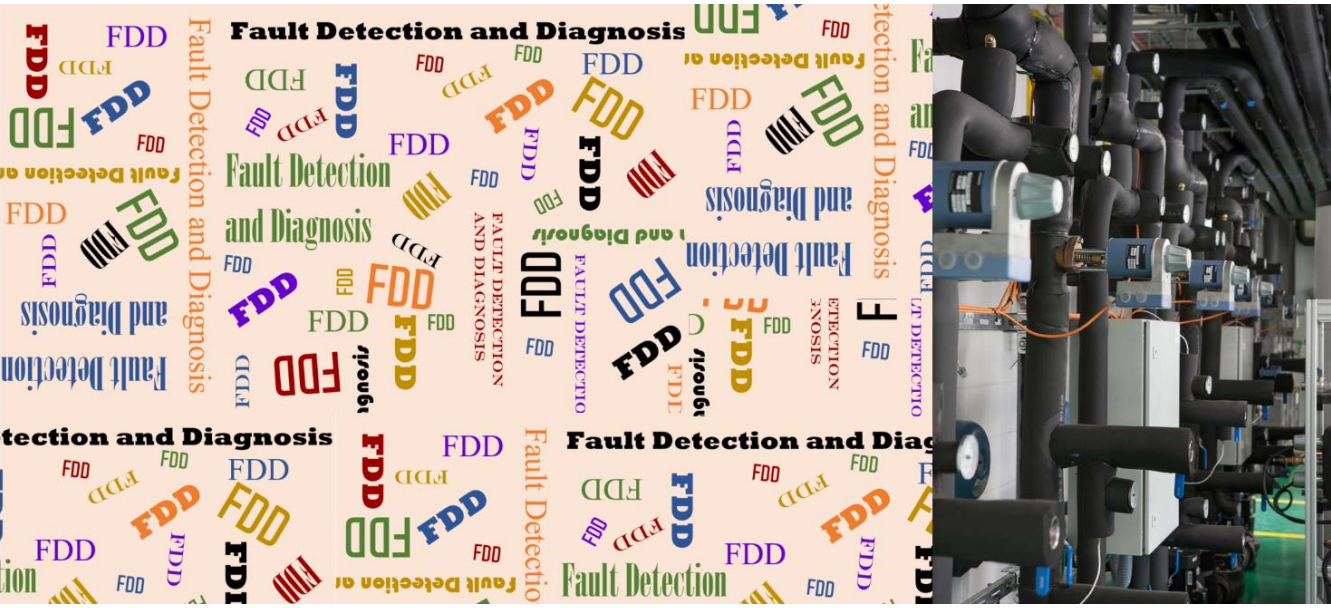

DOCTORAL THESIS
2022

UNIVERSITAT ROVIRA I VIRGILI
AUTOMATIC FAULT DETECTION IN DOMESTIC HEAT PUMPS
Ivan Bellanco Bellanco

UNIVERSITAT ROVIRA I VIRGILI
AUTOMATIC FAULT DETECTION IN DOMESTIC HEAT PUMPS
Ivan Bellanco Bellanco

UNIVERSITAT ROVIRA I VIRGILI
AUTOMATIC FAULT DETECTION IN DOMESTIC HEAT PUMPS
Ivan Bellanco Bellanco

Ivan Bellanco Bellanco

Automatic Fault Detection in domestic heat pumps

DOCTORAL THESIS

Supervised by

Dr Manel Vallès
Dr Jaume Salom

Department of Mechanical Engineering

UNIVERSITAT ROVIRA i VIRGILI

Tarragona, 2022

UNIVERSITAT ROVIRA I VIRGILI
AUTOMATIC FAULT DETECTION IN DOMESTIC HEAT PUMPS
Ivan Bellanco Bellanco

UNIVERSITAT
ROVIRA i VIRGILI
DEPARTAMENT D'ENGINYERIA MECÀNICA
Escola Tècnica Superior d'Enginyeria Química
(ETSEQ). Avgda Paisos Catalans, 26; 43007
Tarragona (Spain)

Declaration

WE STATE that the present study, entitled, "Automatic fault detection in domestic heat pumps", presented by Ivan Bellanco Bellanco for the award of the degree of Doctor, has been carried out under our supervision at the Department of Mechanical Engineering of the University Rovira I Virgili (URV) and at the Institut de Recerca en Energia de Catalunya (IREC), and it fulfils the requirements to be eligible for the International Doctorate Award.

Tarragona, 23th August 2021

VALLES RASQUERA JOAN MANEL - 39680747C
Firmado digitalmente por VALLES RASQUERA JOAN MANEL - 39680747C
Fecha: 2022.08.25 14:04:29 +02'00'

Doctoral Thesis Supervisor
Dr. Manel Vallès

Jaume Salom Tormo
Firmado digitalmente por Jaume Salom Tormo
Nombre de reconocimiento (DN): cn=Jaume Salom Tormo, o=IREC, ou, email=jsalom@irec.cat, c=ES
Fecha: 2022.08.26 07:12:17 +02'00'

Doctoral Thesis Supervisor
Dr. Jaume Salom

UNIVERSITAT ROVIRA I VIRGILI
AUTOMATIC FAULT DETECTION IN DOMESTIC HEAT PUMPS
Ivan Bellanco Bellanco

Acknowledgements

First of all, I would like to express my deepest gratitude to my supervisors, Dr Jaume Salom and Dr Manel Vallès. I am grateful for their patience and their guidance throughout the thesis. Their constructive criticism has helped me to open my mind and teach me a lot about research and myself.

I would also like to show my gratitude to all my colleagues in IREC, especially to Francisco Belío, for his constant support throughout the project and for cheering me up when I needed it. I want to thank Thibault, Alba and Daniel Ramon for their support along the TRI-HP project. I would also want to thank Elena Fuentes for her development of the fault parametrization equations and Angel Carrera for his work with the TRNSYS model of the heat pump.

I would like to express my gratitude to Dr Daniel Carbonell to allowed me to work in their research group in SPF. Many thanks to Maike, Robert, Kevin, Andy and all the members of SPF for being so kind and giving me such an educational experience regarding laboratory testing. Danke schön!

I want to thank all the members of the TRI-HP project and the European Union for giving me the opportunity to work on such an interesting project and with a great professional team. Specially to Ángel for his development of the Dymola model and to Raphael for his bast knowledge about heat pumps.

També m'agradaria agrair a la Generalitat de Catalunya pel suport financer d'aquesta tesi a través de la beca de contractació de personal investigador novell 2019FI_B 00928, i en general agrair al sistema

d'educació pública que m'ha permès arribar fins a aquest punt.

Y finalmente me gustaría agradecer a mi familia. Primero, me gustaría darle las gracias a aquellos que ya no están, pero que dejaron en mi recuerdos, vivencias y lecciones que nunca he olvidado. Seguidamente, quiero agradecer a mis padres sin los que, gracias a su duro trabajo y su amor incondicional no habría podido llegar hasta aquí. También me gustaría agradecer a mi hermana por siempre haber estado ahí y por aguantarme y cuidarme. Gracias también a mi familia política, que me acogieron como uno más e hicieron suyas mis alegrías y mis tristezas. Y para acabar, no podría estar más inmensamente agradecido a Judit, la persona con la que tengo la suerte de compartir mi vida y que logra sacar lo mejor de todas las personas. Gracias por darle sentido a este mundo.

Muchas gracias a todos.

Glossary

feature in the context of FDD, a measurement that gives information to perform the detection or the diagnosis.

hard faults faults that do not allow the system to cover the demand.

liquid line tube or pipe carrying the refrigerant liquid from the condenser or receiver of a heat pump or vapor compression system to a pressure-reducing device.

non-condensable gas gas that cannot be liquefied at normal operating pressures and temperatures.

quasi steady-state a situation that is changing slowly enough that it can be considered to be constant.

rooftop air conditioners packaged air conditioners mounted on a roof, the conditioned air being discharged directly into the rooms below or through a duct system.

sensible heat ratio ratio of the sensible heat to the sensible plus latent heat to be removed from a conditioned space.

soft faults faults that allow the system to cover the demand but reduce its efficiency.

subcooling that a defined pressure, the difference between a given liquid temperature and the bubble point temperature.

Acronyms

MSR ratio between the refrigerant mass flow rate and compressor speed (g/rev).

$NMSR$ normalized value of MSR.

Q_{heat} heat duty (kW).

T_{cond} condensing temperature (^{o}C).

T_{co} compressor outlet temperature (^{o}C).

T_{evap} evaporation temperature (^{o}C).

T_{ll} liquid line temperature (^{o}C).

T_{sc} subcooling(^{o}C).

T_{sh} superheating (^{o}C).

W_{comp} compressor power consumption (kW).

f compressor frequency (Hz).

m_r refrigerant mass flow (g/s).

A coil heat transfer surface area.

AHU air handling units.

ANN artificial neural networks.

COP coefficient of performance.

CVL compressor or 4-way valve leakage.

DHW domestic hot water.

Dt detection time.

EEV electronic expansion valve.

FAR false alarm rate.

FDD Fault Detection and Diagnosis.

FI fault intensity.

FIR fault impact ratio.

FXO fixed oriffice.

GHG greenhouse gases.

HiL Hardware-in-the-loop.

HVAC heating, ventilating and air conditioning.

IEA International Energy Agency.

IHXF indoor heat exchanger fouling fault.

IMC indoor unit mechanical component failure.

LL liquid line restriction.

LMTD log mean temperature difference.

MDR missed detection rate.

MR missdiagnosis rate.

NON non-condensable gas in the refrigerant.

OC refrigerant overcharge.

OHXF outdoor heat exchanger fouling fault.

OMC outdoor unit mechanical component failure.

PCA principal component analysis.

RMSE root-mean-square error.

RTU roof top unit.

SEILAB Semi-Virtual Energy Integration Laboratory.

SGDR stochastic gradient descent regression.

SHR sensible heat ratio.

SSD steady-state detector.

TRL Technology Readiness Level.

TXV thermostatic expansion valve.

U overall heat transfer coefficient.

UC refrigerant undercharge.

UN United Nations.

VSHP variable speed heat pumps.

List of Figures

UNIVERSITAT ROVIRA I VIRGILI
AUTOMATIC FAULT DETECTION IN DOMESTIC HEAT PUMPS
Ivan Bellanco Bellanco

List of Tables

Publications and outreach activities

In the framework of this doctoral thesis, different research articles, congress presentations and other dissemination actions were made. In this section, those action are listed.

Journal articles

I.Bellanco, E.Fuentes, M.Vallès, J.Salom, "A review of the fault behavior of heat pumps and measurements, detection and diagnosis methods including virtual sensors", *Journal of Building Engineering*, vol.39, 2021. DOI: 10.1016/j.jobe.2021.102254

I. Bellanco, F.Belío, M.Vallès, R.Gerber, J.Salom, "Common fault effects on a natural refrigerant, variable-speed heat pump", *International Journal of Refrigeration*, vol.133, pp.259-266,2022. DOI:10.1016/j.ijrefrig.2021.10.017

Conference papers

I.Bellanco, J. Salom, "Overview of fault detection and diagnostics methods for domestic heat pumps", in *9th International Seminar on Thermodynamic Engineering of Fluids*, Tarragona, Spain, 2019. ISBN: 978-84-09-14637-6

I.Bellanco, M. Vallès, J.Salom, "Experimental determination of faults effects for variable-speed heat pumps", in *proceedings of the 10th International Seminar on Thermodynamic Engineering of Fluids*, Tarragona, Spain, 2021.

I.Bellanco, F.Belío, M.Vallès, R.Gerber, J.Salom, "FDD method for a variable-speed heat pump with natural refrigerants", in *proceedings of the conference CLIMA 2022 The 14th REHVA HVAC World Congress*, Rotterdam, The Netherlands, 2022. DOI:https:10.34641/clima.2022.433

Data sets

I.Bellanco, F.Belío, R.Gerber, J.Salom, "Common faults tested on a variable-speed propane-charged heat pump on heating mode", dataset hosted on Zenodo. DOI: 10.5281/zenodo.5155136.

Other contributions

E.Fuentes, I.Bellanco, J.Salom, A.Àlvarez-Pardiñas, R.Gerber,L.Alonso, "Self-diagnosis algorithm description", Confidential report from the project *Trigeneration systems based on heat pumps with natural refrigerants and multiple renewable sources*(TRI-HP), 2020

I.Bellanco, F.Belío, J.Salom, "Validation of the self-diagnosis efficiency system", Public report from the project *Trigeneration systems based on heat pumps with natural refrigerants and multiple renewable sources*(TRI-HP), 2021. DOI:10.5281/zenodo.6380812

R.Haberl, M.Schubert, T.Péan, I.Bellanco, F.Belío, J. Salom, "Concise Cycle Test (CCT) method definition", Public report from the project *Trigeneration systems based on heat pumps with natural refrigerants and multiple renewable sources*(TRI-HP), 2021. DOI:10.5281/zenodo.5960592

I.Bellanco, F.Belío, M.Vallès, R.Gerber, J.Salom, "Fault detection and diagnosis monitor for domestic heat pumps", oral presentation in *the 11th International Seminar on Thermodynamic Engineering of Fluids*, Tarragona, Spain, 2022.

R. Haberl, M.Schubert, T.Péan, I.Bellanco, F.Belío, J.Salom, D. Carbonell, "Concise cycle test methods to evaluate heating/cooling systems with multiple renewable sources", *proceedings of the conference CLIMA 2022 The 14th REHVA HVAC World Congress*, Rotterdam, The Netherlands, 2022. DOI:10.34641/clima.2022.390

T.Péan, D.R.Lumbieres, A.Colet, I.Bellanco, M.J.Neugebauer, D. Carbonell, J.Iturralde Iñarga, C.Corchero García, J.Salom, "Co-simulation studies of optimal control for natural refrigerant heat pumps", *proceedings of the conference CLIMA 2022 The 14th REHVA HVAC World Congress*, Rotterdam, The Netherlands, 2022. DOI:10.34641/clima.2022.432

Internships

Host institution: Institut für Solartechnik (SPF) from the Ostschweizer Fachhochschule, Rapperswil (Switzerland)

Supervisor at host institution: Dr. Daniel Carbonell

Period: 10th January - 11th March 2022

Topic: system test of a variable speed heat pump charged with propane and coupled with an ice-slurry tank to use the solar energy as a source, in the framework of the European project TRI-HP.

UNIVERSITAT ROVIRA I VIRGILI
AUTOMATIC FAULT DETECTION IN DOMESTIC HEAT PUMPS
Ivan Bellanco Bellanco

Contents

UNIVERSITAT ROVIRA I VIRGILI
AUTOMATIC FAULT DETECTION IN DOMESTIC HEAT PUMPS
Ivan Bellanco Bellanco

Summary

In the current context of climate emergency, governments around the world are taking actions to reduce greenhouse gases (GHG) emissions, which are the main agents of climate change. The European Union has set the goal to cut emissions by 55% by 2030 and to become climate neutral by 2050. Among the sectors that more energy consumes, buildings accounted for 32% of the total energy consumption worldwide. In domestic buildings of the European Union, water heating and space heating production represented more than 75% of the final use of energy. For space and water heating, the main sources of energy come from fossil fuels.

Heat pumps could provide water heating and space heating and cooling with high efficiency and, coupled with renewable electric sources, with low GHG emissions. Within this context, heat pumps have been selected as the main providers of heating, cooling and ventilation for buildings, to achieve Net Zero by 2050. Hence, the number of units installed worldwide will increase from the current 180 million to 600 million by 2030.

Despite their high efficiency, different studies have tackled the health status of heat pumps in field, founding that half of the units could be working at 80% of their efficiency. These performance losses could be caused by faults that increase the energy consumption while the equipment could still cover the demand, and therefore they could pass undetected for long periods of time. Fault Detection and Diagnosis (FDD) monitors are focused on the detection of performance losses and the diagnosis of faults. Despite there were several methodologies for FDD solutions, they have been mainly focused on the industrial sector and less oriented to the domestic market.

The main objective of this doctoral thesis is the development of an FDD monitor for domestic heat pumps which could work with variable speed compressors and diagnose different faults. The first part of this thesis is dedicated to the description of the causes and the effects of the different faults found in vapour compression systems. An overview of the faults incidence on in-field equipment is given, followed by an analysis of the origin and the repercussions of the faults. Additionally, a review of the methods for fault emulation is given, discerning between emulation in laboratory and simulation with virtual models and comparing the emulation techniques.

The next part of the thesis is focused on the development and first validation of the FDD monitor. The monitor counts with several modules dedicated to different processes of the FDD. The fault detection is based on the comparison between the real measurements and the results from models that replicate the fault-free behaviour of the equipment. From the comparison of different FDD methodologies, polynomial regressions were selected to generate the fault-free models. The diagnosis is based on expert knowledge, where knowing the trends of the features, the fault could be determined. Furthermore, the monitor also counts with a novel methodology for the detection of steady-state points to filter the incoming data. The Input Space module divides the operational space to classify the data into groups, where each of these groups could have a fault-free model. To prevent the detection of measurement outliers or measurement noise as false alarms, an additional module ensures that the fault persists over time before triggering a warning.

The monitor was firstly validated with simulated data of a variable-speed heat pump from a TRNSYS model, where the effects of faults were emulated with a fault parametrization method developed for that purpose. The monitor detected a fault before a 5% COP degradation was reached. A thorough literature research gave as a result a diagnosis table, used for the diagnosis of faults. With this methodology, the monitor could diagnose the faults indoor and outdoor heat exchanger fouling, compressor valve leakage, liquid line restriction, undercharge and overcharge.

The following section puts the spotlight on the methodology and the results of testing different faults on a variable speed heat pump.

The tests were performed under laboratory conditions on a 10 kW water-to-water, variable-speed heat pump charged with propane. The faults outdoor heat exchanger fouling, compressor valve leakage, liquid line restriction and overcharge were emulated for heat duties of 10 kW and 12 kW and with different fault intensities. The results showed that compressor valve leakage was the fault that had the highest effect on the heat pump, while outdoor heat exchanger fouling had the least. Some differences were found between the results obtained from the tests and the ones from the literature. However, the differences between the equipment architectures could explain the dissimilarities.

Thus, the FDD monitor was validated with the data from the faults tests. Real data has more noise than the simulated data from the first validation. This increases the uncertainty of the fault-free models prediction. Nevertheless, the monitor could detect faults before an 8% of COP degradation, without triggering any false alarm. The diagnosis table used for the fault diagnosis had to be changed to adapt to the different effects of the faults for that specific heat pump. All the faults were correctly diagnosed, except outdoor heat exchanger fouling, which was detected as a fault but could not be discerned from the others.

This thesis provides a new solution to reduce energy losses for domestic heat pumps. The experimental faults tests increases the knowledge about fault effects in variable speed heat pumps, which is scarce. More work needs to be done to increase the flexibility of the diagnosis to different heat pump typologies. However, the FDD monitor performed well with simulated and real data and different conditions.

Resumen

En el contexto actual de emergencia climática, los gobiernos alrededor del mundo están tomando acciones para reducir las emisiones de gases de efecto invernadero (GHG), que son los mayores agentes del cambio climático. La Unión Europea ha fijado el objetivo de disminuir las emisiones un 55% para 2030 y convertirse en neutral climáticamente para 2050. De entre los sectores que más energía consume, la edificación representa un 32% de la energía consumida mundialmente. En las viviendas domesticas de la Unión Europea, la calefacción y el agua caliente sanitaria representan más de un 75% del uso final de la energía. Para el calentamiento de agua e interiores, la principal fuente de energía proviene de combustibles fósiles.

Las bombas de calor pueden producir agua caliente, calefacción y refrigeración con gran eficiencia y, usando fuentes renovables de energía eléctrica, produciendo pocas emisiones de GHG. En este contexto, las bombas de calor han sido seleccionadas como la principal opción para producir calor, frío y ventilación a edificios para alcanzar emisiones cero en 2050. Para ello, el número de unidades instaladas en todo el mundo aumentará de los actuales 180 millones a 600 millones para 2030.

Pese a su gran eficiencia, diferentes estudios han abordado el estado de salud de bombas de calor en campo, hallando que la mitad de las unidades podrían estar trabajando al 80% de su eficiencia. Estas pérdidas de eficiencia podrían estar causadas por fallos que incrementan el consumo de energía mientras que el equipo aún puede cubrir la demanda y, por lo tanto, pueden pasar desapercibidas por largos periodos de tiempo. Los monitores de detección y diagnóstico de fallos (FDD) están orientados a la detección de pérdidas de eficiencia

y diagnóstico de fallos. Pese a haber varias metodologías para soluciones FDD, han estado principalmente enfocadas al sector industrial y menos orientadas al sector doméstico.

El principal objetivo de esta tesis doctoral es el desarrollo de un monitor FDD para bombas de calor domésticas que pueda trabajar con compresores de velocidad variable y diagnosticar diferentes fallos. La primera parte de esta tesis se ha dedicado a la descripción de las causas y los efectos de los diferentes fallos que se pueden encontrar en sistemas de compresión de vapor. Se ha proporcionado una visión general de la incidencia de fallos en equipamiento en campo, seguido de un análisis del origen y las repercusiones de los fallos. Además, se ha hecho una revisión de los métodos para la emulación de fallos, diferenciando entre emulación en laboratorio y simulación con modelos virtuales, y comparando las técnicas de emulación.

La siguiente parte de la tesis está enfocada en el desarrollo y primera validación del monitor FDD. El monitor cuenta con varios módulos dedicados a diferentes procesos de la FDD. La detección de fallos se basa en la comparación entre las mediciones reales y los resultados de modelos que replican el comportamiento libre de fallos del equipamiento. A partir de una revisión de la literatura donde diferentes metodologías FDD fueron comparadas, la regresión polinómica fue seleccionada para generar los modelos libres de fallos. El diagnóstico está basado en conocimiento experto donde, conociendo las tendencias de diferentes medidas, el fallo puede ser determinado. Además, el monitor también cuenta con una nueva metodología para la detección de puntos en estado estacionario para filtrar los datos entrantes. El módulo *Input Space* divide el espacio operacional para clasificar los datos en grupos, donde cada uno de estos grupos puede tener un modelo libre de fallos. Para prevenir la detección de valores atípicos o ruido en la medida como falsas alarmas, un módulo adicional se asegura de que el fallo es persistente en el tiempo antes de dar alarma.

El monitor fue validado primero con datos de un modelo de una bomba de calor con velocidad variable. Pese a que los fallos no pudieron ser emulados directamente en el modelo, un nuevo método de parametrización de fallos fue desarrollado basándose en datos de la literatura y simulaciones. El monitor detectó fallos antes de alcanzar un 5% de degradación en el COP. También pudo diagnosticar los fal-

los de intercambiador de calor externo e interno obstruidos, fuga en la válvula del compresor, restricción de la línea liquida, carga insuficiente y sobrecarga.

La siguiente sección pone el foco en la metodología y los resultados de testear diferentes fallos en una bomba de calor con velocidad variable. Los experimentos se realizaron en condiciones de laboratorio con una bomba de calor de velocidad variable de 10 kW, agua-agua cargada con propano. Los fallos intercambiador externo obstruido, fuga en la válvula del compresor, restricción de línea líquida y sobrecarga fueron emulados para demandas de calor de 10 kW y 12 kW, y con diferentes intensidades de fallo. Los resultados muestran que el fallo de fuga en la válvula del compresor tuvo el efecto más grande en la bomba de calor, mientras que intercambiador externo obstruido tubo el más pequeño. Algunas diferencias se encontraron entre los resultados obtenidos con los experimentos y la literatura. Sin embargo, las diferentes arquitecturas de los equipos pueden explicar estas diferencias.

De este modo, el monitor FDD fue validado con los datos de los experimentos con fallos. Los datos reales tienen más ruido que los datos de la simulación de la primera validación, hecho que incrementa la incertidumbre de las predicciones de los modelos sin fallos. No obstante, el monitor pudo detectar fallos antes de que se alcanzara un 8% de degradación en el COP, sin que se presentase ninguna falsa alarma. La tabla de diagnóstico usada para el diagnóstico de fallos, tuvo que ser cambiada para adaptarse a los efectos diferentes de los fallos para esa bomba de calor en específico. Todos los fallos fueron correctamente diagnosticados, excepto intercambiador de calor externo obstruido, que fue detectado como un fallo, pero no se pudo discernir de los otros.

Esta tesis proporciona una nueva solución para reducir las pérdidas de energía en bombas de calor domésticas. Los experimentos con fallos incrementan el conocimiento sobre los efectos de los fallos en bombas de calor con velocidad variable, que es escaso. Se necesita hacer más trabajo para incrementar la flexibilidad del diagnóstico con diferentes tipologías de bomba de calor. Sin embargo, el monitor FDD tuvo un buen desempeño con los datos simulados y reales con diferentes condiciones.

CHAPTER 1

Motivation and objectives

UNIVERSITAT ROVIRA I VIRGILI
AUTOMATIC FAULT DETECTION IN DOMESTIC HEAT PUMPS
Ivan Bellanco Bellanco

1.1 Motivations

1.1.1 Climate emergency

Climate change refers to the long-term shifts in temperatures and weather patterns. Human activities since the 1800s have been the main driver of the acceleration of climate change [1]. The burning of fossil fuels like gas, oil or coal has increased greenhouse gas emissions, mainly carbon dioxide and methane. Those emissions increased the global temperature, being about 1.1^{o}C warmer than in the pre-industrial era [2]. The consequences of climate change, among others, include water scarcity, an increase in forest fires, floods, and in general, more severe and more common natural disasters [1].

There are several international organisms that are committed to find solutions to mitigate the effects of climate change. One of the most known is the United Nations (UN) and its United Nations Framework Convention on Climate Change, that from 1995, every year celebrates the Conference of the Parties (COP), being COP 3 in Kyoto (1997) and the COP 21 in Paris (2015) the most relevant ones.

COP 3 resulted in the Kyoto Protocol, which committed industrialized countries and economies in transition to limit and reduce greenhouse gases (GHG) emissions in accordance with agreed targets [3]. In COP 21, the Paris Agreement committed every country without differentiating between industrialized countries or economies in transition, and the targets were voluntary and each country sets its own goals [4]. The main compromises of the Paris Agreement were:

- Avoid the increase of 2^{o}C in global temperature from the pre-industrial era, while pursuing efforts to limit the increase even further to 1.5 degrees.
- Review countries' commitments every five years
- Provide financing to developing countries to mitigate climate change, strengthen resilience and enhance abilities to adapt to climate impacts

The actions defined by the Paris Agreement are not decreasing fast enough climate change, becoming an emergency situation. In that regard, on 28th November 2019, the European Parliament declared a climate emergency [5] which is defined as a situation in which immediate action is needed to reduce or stop climate change and prevent serious and permanent damage to the environment. The European Union set the goals to cut emissions by 55% by 2030 and to become climate neutral by 2050, which means emitting no more GHG than the ecosystem could safely absorb.

1.1.2 Heat pumps to decarbonise buildings

Net zero emissions by 2050 in the European Union entails a huge social, economic and governmental effort. The fossil fuels use is present in almost every sector of society, from transport to energy production. Between the different sectors, buildings accounted for 32% of worldwide energy use and 19% of energy-related GHG emissions [6]. Figure 1.1 shows that space and water heating represent 56% of the residential energy consumption worldwide.

For the European Union, space heating and water heating represents more than 75% of the final energy consumption in households [7]. Figure 1.2 shows that a high percentage of the energy needed for space and water heating in the European Union comes from fossil fuels.

Heat pumps represent an efficient solution to provide water heating and space heating and cooling. Since heat pumps need electrical energy to work, if renewable electrical sources are used, they could shift the current pathway. The International Energy Agency (IEA) reported that heat pumps could easily supply more than 90% of global space and water heating despite, in 2020, represented no more than 7% of the supply [8].

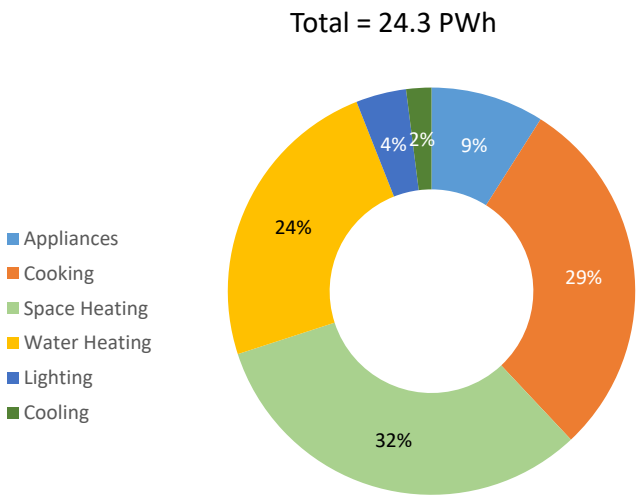

Figure 1.1: World building final energy consumption by end-use in 2010 for residential sector. Adapted from: O.Lucon et al. *2014: Buildings in Climate Change 2014: Mitigation of Climate Change. Contribution of Working Group III to the Fifth Assessment Report of the Intergovernmental Panel of Climate Change.* Cambridge University Press, 2014.

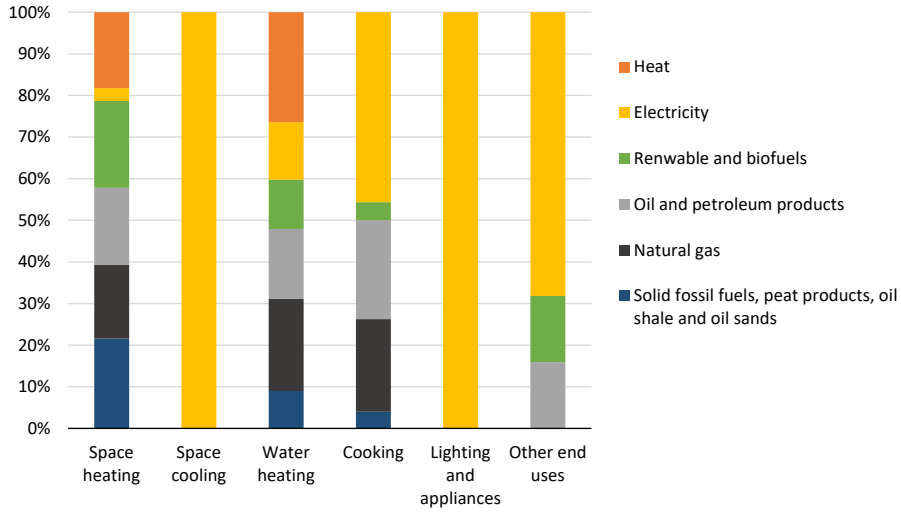

Figure 1.2: Part of the main energy products in the final energy consumption in the residential sector for each type of end-use in the European Union in 2020 [7].

The Energy Performance of Buildings Directive of the European Union entails a commitment to modernise the building sector and to increase building renovations [9]. It stated that for 2021 all new buildings must be nearly zero-energy buildings (NZEB), reducing considerably the energy consumption of the building sector. Heat pumps have been selected one of the main technologies to provide heating, cooling and ventilation for buildings to achieve Net Zero by 2050 [10]. This entails an increase of units installed worldwide from the present 180 million to 600 million by 2030 to pave the way to Zero Emissions by 2050 [8].

1.1.3 The need of fault detection and diagnosis monitors

The European heat pump market is growing every year [11] and expecting to grow even more to achieve the GHG goals. Heat pumps count with a high efficiency, which is improving steadily every year [8]. However, like every other piece of equipment, if they are not correctly maintained, faults could develop in the system. The faults could be categorized into"hard faults", that let the equipment out of service or severely reduce their work capacity, and "soft faults" that increase the energy consumption of the equipment but it still could cover the demand [12]. Hard faults will usually be detected by the users when they feel discomfort, while soft faults could be unnoticed for long periods of time. If heat pumps are going to be the main provider of heating for buildings, the reduction of the possible inefficiencies takes more relevance.

Different studies have tackled the health status of compression systems installed in field, and despite they were made before 2005, they could give an overview of the situation. A study of a database with 1468 registers of in-field unitary air conditionings revealed that, at least two-thirds of those units needed servicing, which comprises from coil cleaning to major repairs such as compressor replacement. They estimated that 50% had an 80% performance compared to factory conditions, and 20% of the units had 70% performance or less [13]. Another study showed that 65% of 13000 air conditioners required repairs [14]. Other studies showed that most of the faults were related to thermo-

static expansion valve (TXV) defects or with the quantity of refrigerant charged [15, 16].

Despite those types of faults increase the energy consumption, the equipment could still cover the demand without affecting the user's comfort. This implies that the fault could pass undetected for long periods of time [17]. Fault Detection and Diagnosis (FDD) methodologies tackle the issue by monitoring the equipment and warning when a fault is occurring and the origin of the fault.

An FDD monitor learns the behaviour of the equipment when no faults are present. The comparison between what the monitor has learned and the measurements from the device is used to detect a possible fault. There are several FDD methodologies and tools already developed [17] based on FDD for the whole building sector and big heating, ventilating and air conditioning (HVAC) equipment, however, the household market has attracted less attention [18]. The main reasons are that big HVAC equipment and whole building ventilation give service to many users at the same time, therefore, the downtime of the equipment could be translated into economic losses and is more critical than for domestic installations. In the same line, FDD solutions uses the equipment measurements to reach the diagnosis. These measurements come from sensors installed in the equipment or additional sensors installed for the monitoring system. For big HVAC the cost of installing additional sensors is smaller than the price of the whole equipment, whereas for domestic heat pumps the cost impact is bigger. Furthermore, variable speed compressors have became an standard for heat pumps [19], nevertheless the FDD studies have been mostly focused on the systems with fixed speed compressors [20].

In conclusion, to tackle the current climate emergency, heat pumps will be used to substitute more pollutant solutions for domestic water and space heating. Not enough attention has been given to the faults that increase the energy consumption of domestic heat pumps. FDD solutions are used to detect those faults but they have been oriented to commercial buildings and big HVAC equipment. Therefore, the development of FDD solutions for residential equipment takes more relevance every year.

1.2 Objectives of the thesis

The main objective of this doctoral thesis is the development of a fault detection and diagnosis monitor to detect performance losses and to diagnose faults in domestic heat pumps. The monitor will take into account the current heat pumps technologies present in the residential market, as variable speed compressors.

To achieve the main objective of the thesis, the following specific objectives were set:

- To analyse the most common faults in domestic heat pumps so the monitor could diagnose them.
- To investigate the different fault detection and diagnosis methodologies to select the most appropriated for developing the monitor.
- To develop an FDD monitor with the aim of working with different models of variable speed heat pumps.
- To get the monitor to be able to detect in less than an hour the presence of a fault that generates a degradation of 10% of the COP.
- To validate the monitor in a real heat pump with a variable speed compressor.
- To characterize the fault effects in a heat pump with variable speed compressor and to provide the experimental data in an open access format to the scientific community, aiming to increase the scarce data available in this field.

1.3 Framework and structure of the thesis

1.3.1 Framework

The thesis has been developed within the framework of the TRI-HP project, a Horizon 2020 project from the European Union [21]. The overall goal of the TRI-HP project is the development and demonstration of flexible energy-efficient and affordable trigeneration systems. The systems will be based on electrically driven natural refrigerant heat pumps coupled with renewable electricity generators (PV), using cold (ice slurry), heat and electricity storages to provide heating, cooling and electricity to multi-family residential buildings with a self-consumed renewable share of 80%.

TRI-HP systems include advanced controls, managing electricity, heat and cold in a way that optimizes the performance of the system and increases its reliability via failure self-detection. Three different heat sources are being used: solar (with ice/water as storage medium), ground and ambient air. The innovations proposed aim to reduce the system cost by at least 10-15% compared to current heat pump technologies with equivalent energetic performances.

Two natural refrigerants with very low global warming potential, propane and carbon dioxide, are used as working fluids for adapted system architectures that specifically target the different heating and cooling demands across Europe. The newly-developed systems will find application in both new and refurbished multi-family buildings, allowing to cover the major part of Europe's building stock. The new systems reduce GHG emissions by 75% compared to gas boilers and air chillers.

The TRI-HP project provides the most appropriate knowledge and technical solutions in order to cope with stakeholder's needs, building demand characteristics, local regulations and social barriers. Two system concepts were developed for two different combinations of heat sources, i) dual ground/air source and ii) solar with ice-slurry as intermediate storage. These two concepts combined with the two heat pump types developed (CO2 and propane) lead to three complete sys-

tems (CO2-ice, propane-ice and propane-dual) that are being tested in the laboratory.

Figure 1.3 shows the system test of the propane heat pump with the solar source in heating mode. As can be seen, the slurry ice tank is coupled with the Evaporator-Supercooler, which provides cooling to the tank. The solar source is used to provide domestic hot water and to melt the ice of the tank. The condenser is used to provide domestic hot water and space heating. The system also includes an electric part with PV-Modules, battery, appliances and the grid. The electric and the thermal part will be controlled by the advanced control solutions.

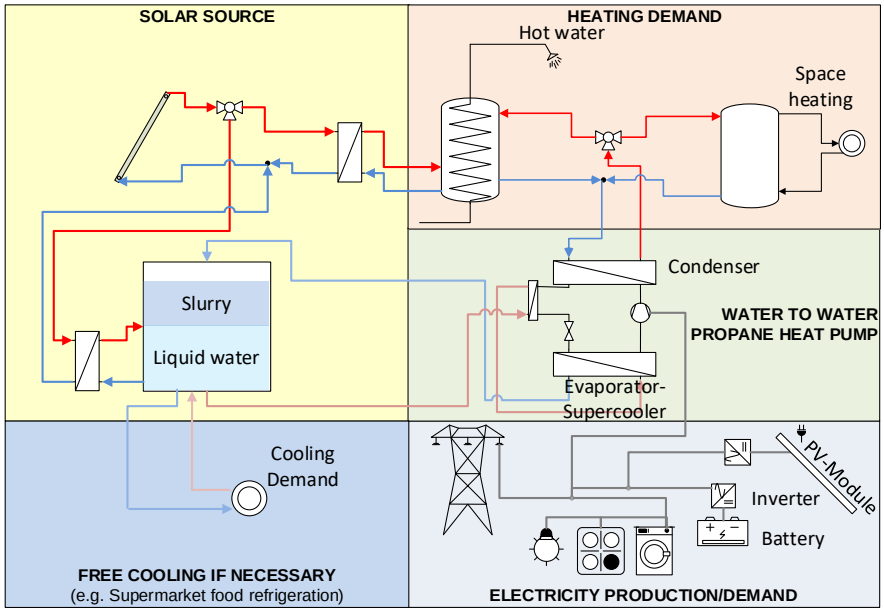

Figure 1.3: Concept of the propane heat pump with an ice slurry system for the heating season.

In the framework of the TRI-HP project, the FDD monitor presented in this thesis has been developed to increase the reliability of the systems with failure self-detection. Thus, both funding through the project and a grant for the recruitment of new research staff (FI) of the *Generalitat de Catalunya*, have provided the opportunity to develop an FDD monitor and to test it in one of the developed heat pump prototypes of the TRI-HP project.

1.3.2 Structure of the thesis and methodology approach

Following this first introductory chapter, the remaining of the thesis is structured as follows.

Chapter 2 describes the causes, the effects and the emulation of faults on vapour compression systems. First, the incidence of faults in-field is studied. Then, an analysis of the most common faults of vapour compression systems is made, indicating the origin of the fault and the effects on the equipment. Finally, the laboratory emulation and virtual simulation of those faults are described.[1]

Chapter 3 focuses on the development of the FDD monitor. A review of the existing literature is made to know the state of the art of FDD. The monitor is composed of different modules that handle different functions of the solution. Each of these modules is described, from their working fundaments to how they are applied. These developments are validated with simulation data. This data comes from a TRNSYS model where the effects of faults are emulated with a fault parametrization method developed for that purpose.

Chapter 4 reports the experimental testing of different faults in a current variable speed heat pump. The methodology followed to emulate the faults and the different levels tested are explained. The effects of these faults on the equipment are analysed and compared with the ones from the literature. [2]

Chapter 5 relates the performance of the FDD monitor with the experimental data from chapter 4. The performance of the different modules is described and compared with results from the validation in chapter 3.

[1]The work of this chapter is embodied in the review: I.Bellanco, E.Fuentes, M.Vallès, J.Salom, "A review of the fault behavior of heat pumps and measurements, detection and diagnosis methods including virtual sensors", *Journal of Building Engineering*, vol.39, 2021. DOI: 10.1016/j.jobe.2021.102254

[2]These results are disseminated in the scientific article: I. Bellanco, F.Belío, M.Vallès, R.Gerber, J.Salom, "Common fault effects on a natural refrigerant, variable-speed heat pump", *International Journal of Refrigeration*, vol.133, pp.259-266,2022. DOI:10.1016/j.ijre-frig.2021.10.017

Finally, Chapter 6 concludes the thesis with a summary of the results and key points, giving an outlook to further developments.

Figure 1.4 shows the graphical representation of the methodology followed throughout the thesis.

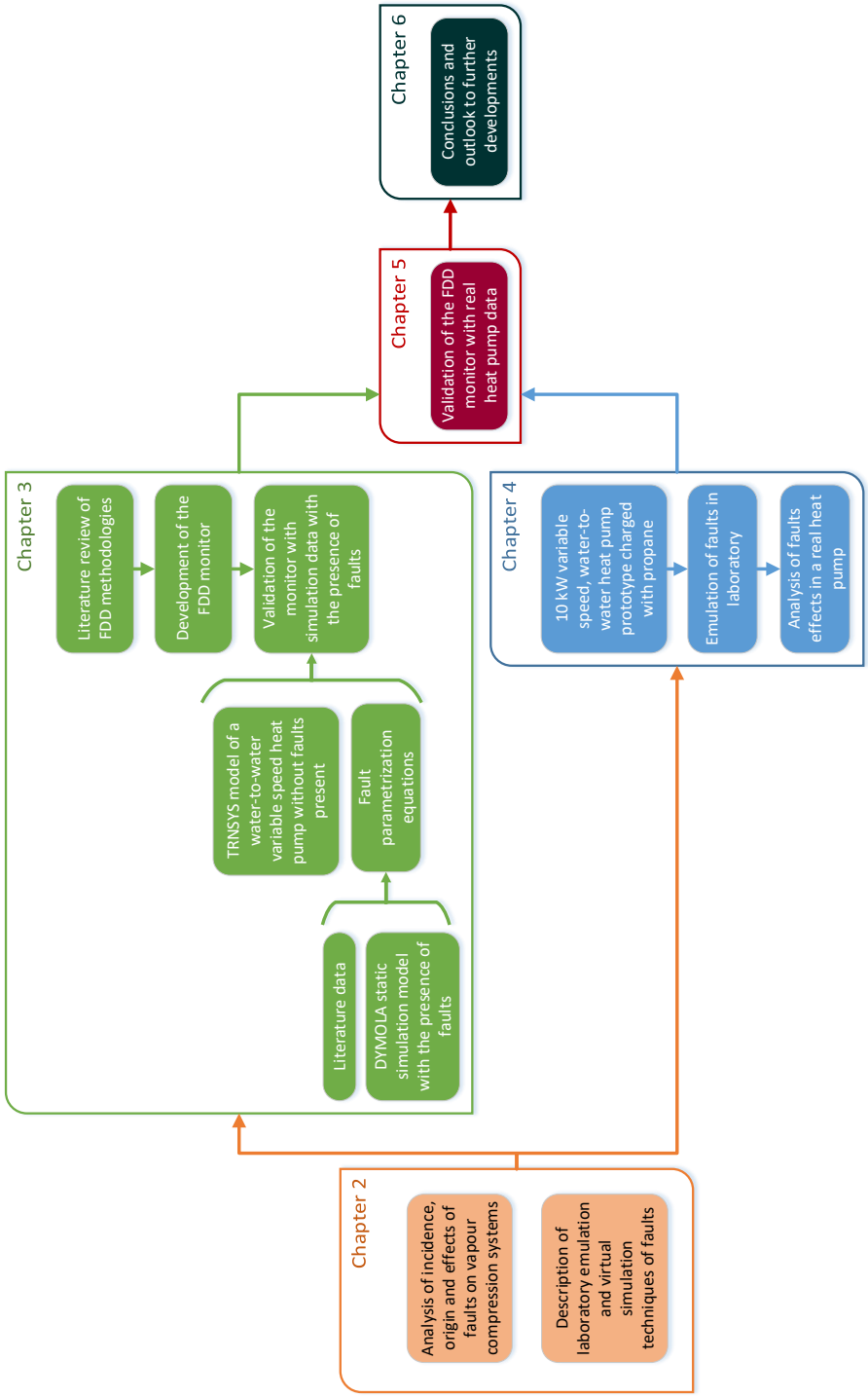

Figure 1.4: Graphical representation of the methodology followed in this doctoral thesis.

UNIVERSITAT ROVIRA I VIRGILI
AUTOMATIC FAULT DETECTION IN DOMESTIC HEAT PUMPS
Ivan Bellanco Bellanco

CHAPTER 2

Faults on vapour compression systems: causes, effects and emulation

UNIVERSITAT ROVIRA I VIRGILI
AUTOMATIC FAULT DETECTION IN DOMESTIC HEAT PUMPS
Ivan Bellanco Bellanco

2.1 Introduction

This chapter of the thesis tackles the study of the faults that affect vapour compression systems. It starts with an analysis of the incidence of faults on in-field equipment to know their occurrence. From a literature research, the origin and the effects of common faults is described, quantifying the effects on coefficient of performance (COP) and capacity of several faults for different typologies of heat pumps. The different techniques for reproducing the fault effects are evaluated, considering laboratory emulation and virtual simulation approaches. The acquired knowledge about different techniques used to reproduce each fault is summarized, also giving the intensities of the faults used. The information found in this chapter serves to define the faults that the Fault Detection and Diagnosis (FDD) monitor should detect, and the methodologies to reproduce them.

2.2 Fault incidence on in-field equipment

Despite the heat pump is a common equipment in European households, the data about fault incidence on in-field equipment is scarce. The main source of this data are the private and manufacturers maintenance services. These services are usually requested when there is a problem that compromises the comfort of the equipment owners. These types of faults are known as "hard faults" [12] because the demand cannot be covered nor the comfort conditions achieved. In some cases, the fault found by those services could not be the actual root of the problem. The origin of hard faults could be"soft faults" that have not been repaired in time [22]. Soft faults decrease the efficiency but allow the equipment to continue to cover the demand [12]. These soft faults are not perceived by the user and are hard to detect for the maintenance services.

The main source of knowledge about the incidence of faults in field is the scientific literature. The maintenance services and the manufacturers could count with statistic of faults on their equipment but, these data are not usually available. Thus, the present review is

based mainly on previous research published in scientific journal papers and conferences. From the literature, Breuker and Braun [12] focused on the common faults of rooftop air conditioners. To this end, they analysed a database from a service company with 6000 separate faults between 1989 and 1995. The faults that led to inadequate building comfort, in decreasing order of occurrences, were: control errors, electrical problems, refrigerant leaks, condenser-related faults, air handling, evaporator-related faults, compressor problems, cooling water loop problems, plugged filters, personnel error, expansion devices and others that were not classified. However, motor failures were classified with associated equipment (e.g. faults in evaporator motor fans are classified as evaporator related). Compressor faults were related to electrical faults (short to ground and open windings), mechanical faults (locked rotor and broken compressor internals) and compressor valve leakage or other leakage paths. Another cause of early compressor failure was high compressor temperature, which may be caused by low airflow in the condenser, liquid line restriction or a low refrigerant charge. For the condenser, the faults were related to mechanical and electrical problems in the fan and fouling of the condenser. The evaporator faults were fouling and coil rupture/damage. If the repair cost is analysed, compressor, control and condenser faults were the most expensive.

Brownell et al. [23] published a case study about a large refrigeration system with control problems. They found different malfunctions on the equipment that increase the energy consumption. Those malfunctions were: plugged liquid line filter, low refrigerant charge and refrigeration system control not working properly. They concluded that, besides the faults, changing the control system can significantly reduce the operational cost of the device as the controller was not properly tuned.

Ahn et al. [24] focused on the fouling of fin-and-tube indoor heat exchangers of air conditioners. They collected operational data from heat pumps installed in inns, offices and restaurants during their opening hours. The cooling capacity and the indoor air quality were negatively affected by the equipment ageing. The type and concentration of pollutants and the structure of the heat exchanger influenced the degree of fouling.

Madani and Rocatello [25] examined the repair orders of Swedish heat pump producers during the warranty period, focusing on four different types of heat pumps: Air-to-Air, Air-to-Water, Brine-to-Water and Exhaust Air-to-Water. They concluded that control and electronics, and temperature sensor faults were among the most common and costly faults.

Those studies focused on the health status of in-field vapour compression systems. However, they may not be representative of the actual health status of the devices. Some of them [12][23] studied equipment assembled before the year 2000. Since then, heat pump production has changed dramatically, in particular, everything related with electronics and controls, devices with thermostatic expansion valve (TXV) or electronic expansion valve (EEV) and variable speed compressors [26]. Madani and Rocatello's study [25], despite being relatively recent, focuses only on repair orders during warranty periods. So it can be assumed that the user had noticed a malfunction and that most faults would be hard faults. Also, because it was limited to the warranty period, faults due to the ageing of the components were hardly represented. Therefore, it is necessary to have updated information about the health status of compressions systems installed in field.

2.3 Faults effects in vapour compression systems

Besides in-field studies, the researchers have studied the causes and the effects of the different faults emulating them under laboratory conditions. Research into common faults and their detection is more prolific for larger systems [18] such as air conditioning for buildings [27]. This is because the cost impact of increasing the number of sensors in these systems is considerably lower than for domestic units. Also, the cost of repairing a fault and the economic impact of having the equipment out of service on such systems are more significant [28]. Nevertheless, although this section uses data of big heating or ventilation equipment, some faults can be found in all vapour compression systems.

Figure 2.1 shows an scheme of the refrigeration circuit of a water-to-water heat pump working in heating mode.

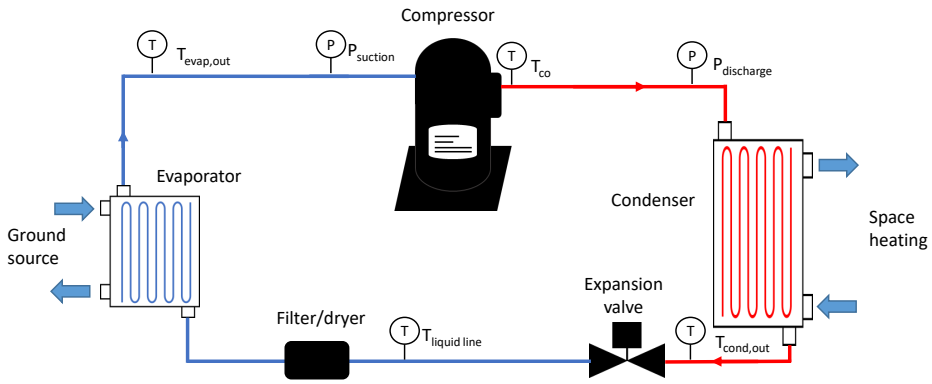

Figure 2.1: Scheme of the different parts that compose a heat pump. In that case, a water-to-water heat pump for space heating.

Heat pumps can provide heating, cooling and hot water with the refrigeration cycle. In Figure 2.1, the evaporator is a heat exchanger (outdoor heat exchanger) that transfers heating power with a ground source. Water absorbs the heat from the ground and this heat is used to boil the refrigerant. The compressor uses electrical energy to compress the refrigerant to a high pressure, which leads to a rise in temperature. The condenser is another heat exchanger (indoor heat exchanger) which releases the heat into the house heating system while the refrigerant condenses to liquid. The expansion valve lowers the pressure of the refrigerant to enter into the evaporator. The filter/dryer located in the liquid line (after the expansion valve) eliminates the debris and moisture of the refrigerant, which can damage the heat pump. The compressor could have fixed speed, working with an on-off behaviour, or variable speed, adapting the frequency to the demand.

The main faults that could affect to a vapour compression system are: outdoor heat exchanger fouling fault (OHXF), outdoor unit mechanical component failure (OMC), indoor heat exchanger fouling fault (IHXF), indoor unit mechanical component failure (IMC), compressor or 4-way valve leakage (CVL), refrigerant overcharge (OC), refrigerant undercharge (UC) and liquid line restriction (LL).

The key variables affected by those faults are:

- the coefficient of performance (COP), which is the ratio between the heating power provided and the electrical power consumption of the compressor.
- the compressor power consumption (W_{comp}).
- the condensing temperature (T_{cond}) which depends on the discharge line pressure ($P_{discharge}$).
- the evaporation temperature (T_{evap}) which depends on the suction line pressure ($P_{suction}$).
- the subcooling (T_{sc}) which is the difference between the temperature at the condenser outlet ($T_{cond,out}$) and T_{cond}.
- the superheating (T_{sh}) which is the difference between the temperature at the evaporator outlet ($T_{evap,out}$) and T_{evap}.

Table 2.1 lists the studies presented in the literature and shows the comparison between the quantifiable effects on COP and thermal capacity of these faults. All the studies emulated the faults under laboratory conditions. The table only takes into account the references that give a quantitative value of the effect, and for each fault, the value showed is for a fault intensity level around 10%.

Sections from 2.3.1 to 2.3.9 describes the origin and the effect of each fault. Because the effect of the faults depends on the type of heat pump and whether the system is in cooling or heating mode, the description of the faults effects of this section has been done considering an air-to-air heat pump working in cooling mode. With that hypothesis, the outdoor part will be the condenser and the indoor will be the evaporator.[1]

[1]Note that the term outdoor and indoor here does not represent the actual location of the heat exchanger. E.g. in a compact unit, there are no differences in the the heat exchangers location; but there is a heat exchanger that exchanges with the outdoor (air, borehole, etc.) and another that exchanges with the indoor (household, office, etc.).

Table 2.1: Summary of the quantifiable effects on thermal capacity and COP of common faults for different types of heat pump. For changes below 0.5% the parameter has been assumed to remain the same. Comp.: compressor, FS: fixed speed, VS: variable speed.

Fault type	Type of pump	Comp.	Mode	Effect	Ref.
OHXF	Air-to-Air	FS	Cooling	COP decreases 9%, Capacity decreases 14%	[29]
	Air-to-Water	VS	Heating	COP decreases 0.77%	[30]
	Air-to-Air	FS	Heating	COP decreases 1.34%, Capacity remains	[31]
IMC	Air-to-Air	FS	Cooling	COP increases 33%, Capacity decreases 13%	[29]
IHXF	Air-to-Water	VS	Heating	COP remains	[30]
	Air-to-Air	FS	Heating	COP and Capacity remains	[31]
CVL	Air-to-Air	FS	Cooling	COP decreases 15%, Capacity decreases 24%	[29]
	Air-to-Air	FS	Heating	COP decreases 4.4%, Capacity decreases 4.7%	[31]
OC	Air-to-Air	FS	Cooling	COP increases 22%, Capacity decreases 36%	[29]
	Water-to-Water	VS	Cooling	COP decreases 2%, Capacity remains	[32]
	Water-to-Water	VS	Heating	COP and Capacity remains	[32]
	Air-to-Water	VS	Heating	COP decreases 3.4%	[30]
	Air-to-Air	FS	Heating	COP decreases 2.7%, Capacity increases 1.5%	[31]
UC	Air-to-Air	FS	Cooling	COP increases 18%, Capacity decreases 29%	[29]
	Water-to-Water	VS	Cooling	COP decreases 4.6%, Capacity decreases 6.6%	[32]
	Water-to-Water	VS	Heating	COP decreases 10.6%, Capacity decreases 15.7%	[32]
	Air-to-Water	VS	Heating	COP increases 1.2%	[30]
LL	Air-to-Air	FS	Cooling	COP increases 8%, Capacity decreases 20%	[29]
	Air-to-Air	FS	Heating	COP and Capacity remains the same	[31]

2.3.1 Outdoor heat exchanger fouling and outdoor mechanical component failure: OHXF and OMC

In real installations the outdoor unit is normally exposed to dirt, debris and other components (fallen leaves) that can accumulate in the filters or gaps in the heat exchanger. There are two types of fouling, one that accumulates at the air inlet of the unit and the other that gets stuck in the internal gaps of the heat exchanger. Both types of fouling reduce the flow of the external stream (air or water). The first type can also increase heat resistance.

Another fault that can affect the outdoor unit is the failure of mechanical components (OMC). The fan or pumps may not work correctly due to a mechanical or a control problem. In this case, the main repercussion is the decrease in external stream.

In field studies, outdoor heat exchanger fouling fault (OHXF) does not significantly affect indoor comfort levels [12]. Only 14% of outdoor unit fouling faults have been found to reduce the comfort in the building [12]. This is supported by Mehrabi and Yuill [33], who show that the fouling effect of field heat pumps had a nearly negligible effect on performance (0.2% reduction) and capacity.

In the literature, to test the fouling fault, different authors reproduced this fault by blocking the air inlet [34, 31] or reducing the water or air flow [30]. In the study on particulate fouling by Bell et al. [35], the impact on coil heat transfer is small, and the main effect is an increase in the air-side pressure drop . Therefore, the effects explained below will consider only the reduction in air flow and not the increase in heat resistance.

For the levels tested in the literature, the reduction in airflow involves an increase in condensing temperature and pressure [36]. The temperature of the discharge line in the compressor and condenser inlet saturation temperature are higher [12, 37]. The COP of the unit is lower, because the power consumption of the compressor increases and the thermal capacity decreases [12, 36, 29, 38, 30].

2.3.2 Indoor unit fouling and indoor mechanical component failure: IHXF & IMC

Even though the indoor unit is not affected by the same type of dirt and debris as the outdoor unit, it can be affected by fouling because of particulates and fibres that create deposits that obstruct air circulation or increase heat transfer resistance. These deposits can also act as substrate for bacteria growth [24], which worsens the air quality. As with the outdoor unit, the fans, pumps or controls of the indoor unit can also have mechanical faults. For systems with fan-coils, the functioning of the fan or the size of the duct can reduce the air flow rate as well.

The fouling in air heat exchangers, could increase or reduce the heat transfer of the device. Depending on the geometry of the exchanger, the fouling could increase the air turbulence, which in turn increases the heat transfer [39]. Therefore, as with the outdoor unit, from the different repercussions of fouling, the reduction in external stream flow rate is the one considered for the explanation below.

Low air flow in the evaporator decreases the saturation temperature at the evaporator exit, while the air temperature drop in the evaporator increases [12, 36, 37, 29]. This means that the sensible heat ratio (SHR) decreases as well, which improves moisture removal [38]. This fault has small effect on COP [31, 30].

2.3.3 Valve leakage: CVL

In the literature, the valve leakage fault refers to a leakage of refrigerant from the discharge line to the suction line. This leakage is normally associated with the valves at the inlet (suction line) and outlet (discharge line) of the compressor. These valve seals can break which, in turn, leads to leakage. Leakage can be also found in the 4-way valve, but because the consequences are the same, they are both classified in the same group [40].

If the valve in the suction line is loose, when the compressor is in the compression phase, high pressure refrigerant may enter the suction

line. If the discharge valve is loose, when the compressor is in the suction phase, high pressure refrigerant from the discharge line may enter the compressor. For the 4-way valve, there is also a refrigerant bypass between the suction and discharge line. Therefore, the high pressure vapour enters the suction line, which decreases the mass flow rate of refrigerant.

The refrigerant saturation temperature at the condenser inlet decreases while the saturation temperature at the evaporator exit increases [29]. For heat pumps equipped with a thermostatic expansion valve (TXV), the actuation of the valve decreases the mass flow rate in response to the increase in the saturation temperature at the outlet of the evaporator [36]. This fault increases the SHR and reduces capacity and COP [12]. In some studies it has degraded COP up to 15% [31].

2.3.4 Non-condensable gas: NON

During the commissioning, before the refrigerant is charged, the circuit must be purged to remove all the air and moisture inside. When the vacuum pump does not work correctly, some air or moisture may remain in the system. The presence of non-condensable gases may raise the system pressure, reducing the efficiency and even causing a TXV malfunction.

Non-condensable gases settle in the condenser, so the condenser pressure is increased by the partial pressure of the non-condensables [37]. This decreases capacity and increases compressor power consumption, and has been identified as the fault that has the largest impact on system performance [22].

2.3.5 Refrigerant overcharge: OC

During the commissioning, the technical service may apply a higher refrigerant charge than the specified by the manufacturer. This fault increases the subcooling value [37] and degrades the COP [31, 30]. In some cases, until a 20% of overcharge, it can increase the capacity of the heat pump [38], but this may depend on the specific characteristics

of each heat pump.

2.3.6 Refrigerant undercharge: UC

During the commissioning, the technical service may apply a lower refrigerant charge than the specified by the manufacturer. Also, any leakage of refrigerant may decrease refrigerant mass so the optimal working point will be lost. In this case there will be a continuous loss of refrigerant, so the fault intensity will increase over time whereas in the first case, the fault intensity remains the same. Mehrabi and Yuill [41] found that, for devices with TXV, when the level of undercharge is below 20%, the effects are nearly negligible.

The features that are most sensitive to this fault are subcooling, which decreases, and superheating that increases [32, 29]. For equipment with variable speed compressor, the compressor frequency and the refrigerant flow rate increases. As a consequence of the undercharge, the equipment could not work with some outdoor conditions that before the fault were part of the operating range of the equipment [30].

Breuker and Braun [12] found that this fault has a greater effect on thermal capacity than on COP for equipment with fixed oriffice (FXO), but Du et al. [38] found that this was one of the faults that most degraded COP in a heat pump with TXV.

2.3.7 Liquid line restriction: LL

Normally, a filter/dryer is installed in the liquid line to remove solid particles and moisture from the refrigerant. These particles may enter the circuit if the technical services do not follow good refrigerant charging practices or if the material is rusty as a consequence of inefficient tube joinery. This debris will clog the filter/dryer and increment the refrigerant flow restriction.

As a consequence, there will be a reduction in refrigerant mass flow rate, an increase in suction superheat and a reduction in cooling

capacity [29, 31]. However, for devices with TXV, the fault effect is negligible for fault levels below 10% [36, 37] and has a greater effect on thermal capacity than COP [12].

2.3.8 Sensor error: SEN

All FDD methods use the measurement of different sensor of the equipment as temperature or pressure to know the current state of the system. These sensors are affected by ageing, which can lead to a loss of accuracy [42]. For methods that use large quantities of sensor data as data mining, the detection of a drift or bias in measurements is especially important [43].

Sensor accuracy will affect not only FDD performance but also the efficiency of the heat pump itself. If a faulty sensor is used for the internal control of the device, the performance and the comfort of the occupants can be affected [44]. Therefore, the sensors measuring the heat pump or FDD operation must be checked to ensure they are providing correct data.

2.3.9 Other errors

The errors explained above have been discussed frequently in the literature, but other errors are less frequent or do not occur in current technology. Some of these faults are: compressor liquid ingestion [45], expansion valve malfunction [46] and excess of oil in the refrigerant circuit [47].

This has been a general description of the fault effects for an specific typology of heat pump. However, as has been mentioned during the section, the effects depends also on the architecture of the equipment. For example, faults have much less effect on heat pumps equipped with a TXV than pumps with fixed orifices as expansion devices [48]. The same occurs for systems with variable speed compressors [20]. Therefore, the faults presented could affect in a different way depending on the compression system.

2.4 Fault emulation on laboratory

Most of the knowledge about the fault effects mentioned before is obtained through the emulation of faults in real equipment in a controlled environment. In this section, more than fifteen research papers of the different emulation techniques used in laboratory are analysed.

Table 2.2 shows a compilation of the different faults tested in real equipment under laboratory conditions. For each fault, the methodology to emulate it is stated in the Emulation technique column. The quantification column indicates how the fault level is determined.

Rossi et al. [49] wrote one of the first articles on reproducing faults under laboratory conditions for an air-to-air conditioner. They emulated condenser fouling, evaporator fouling, leaky compressor valves, liquid line restriction and refrigerant leakage. These are the same faults used by Breuker and Braun [12]. In both articles, condenser fouling corresponds to the fault OHXF. This fault was reproduced by partially blocking the finned area of the coils with paper. Evaporator fouling (IHXF for that case) was reproduced by placing paper on the air-side filter. Compressor or 4-way valve leakage (CVL) was emulated by opening a hot gas bypass line controlled by a manual valve. Liquid line restriction (LL) was implemented by including a valve in the liquid line to increase the pressure loss. Refrigerant leakage (UC for that case) was reproduced by removing the charge from the refrigerant circuit.

Chen and Braun [48] included non-condensable gas in the refrigerant circuit and refrigerant overcharge (OC). To emulate the non-condensable gas in the refrigerant (NON) fault, a fixed quantity of dry nitrogen was added to the refrigerant circuit. The OC was implemented by adding charge to the system.

Working with a water-to-water system, Comstock et al. [22] studied reduced condenser water flow and reduced evaporator water flow, which was reproduced by reducing the speed of the circulating pumps. Excess oil and defective expansion valves were also emulated.

Table 2.2: Summary of faults emulated under laboratory testing on real equipment.

Fault type	Emulation technique	Quantification	Fault level	Ref.
OHXF	Fan/pump speed reduced	% of air flow reduced	10-50	[30, 50]
			30	[51]
			Unspecified	[52]
	Blocking the area of the heat exchanger with paper or cardboard	% of area blocked	14-39	[45]
			3-16	[53]
			10-30	[31]
			5-35	[40]
			10-40	[48]
OMC	Attaching weights to the fan to create mechanical imbalance	Unspecified	Unspecified	[45]
IHXF	Fan/pump speed reduced	% of air flow reduced	40	[51]
			10-30	[31]
			6.82-27.28	[48]
			10-50	[54]
	Blocking the area of the heat exchanger with paper or cardboard	% of area blocked	10-100	[45]
			5-31	[53]
IMC	Fan switched off			[54]
IHXF & IMC	Fan/pump speed reduced		5-33	[40]
CVL	Opening the hot gas bypass valve a specific amount	% Reduction of refrigerant mass flow rate	8-56	[53]
			4-19	[31]
			3-11	[40]
			10-40	[48]
			Unspecified	[45, 51, 52, 55]
NON	Adding dry nitrogen to the refrigerant circuit	% of the amount of nitrogen in the circuit at atmospheric pressure	20-50	[40]
		% of the total refrigerant mass	0.03-0.17	[48]

Continued on next page

Table 2.2 – *Continued from previous page*

OC	Increasing the refrigerant charge	% of refrigerant with respect to the nominal amount	20	[45, 30]
			10-20	[32]
			10	[30, 51]
			11-32	[53]
			10-30	[31, 40]
			5-30	[48]
			Unspecified	[52]
UC	Decreasing the refrigerant charge	% of refrigerant with respect to the nominal amount	20	[45]
			10-30	[32, 31, 40]
			10-50	[50]
			15	[51]
			11-32	[53]
			30-50	[30]
			5-30	[48]
			Unspecified	[52]
LL	Partially closing the needle valve on the liquid line	% of pressure drop increased in liquid line	5-19	[53]
			8-49	[31]
			1-20	[40]
			4.75-18.66	[48]
SEN	Adding a bias to the measurement value of a sensor	ºC added	-4 to 4	[44]
			-0.75 to 0.75	[43]
			1 to 8	[56]
			0.5	[57]
			-1.5 to 1	[58]
			Unspecified	[59]
	Adding a drift to the measurement value of a sensor	ºC/hour added	-0.1 to 0.1	[43]
Others	Compressor switched off			[52]
	Expansion valve malfunction	% of superheat temperature increased	40-130	[46]
	Short cycling			[45]
	Compressor liquid ingestion			[45]

Armstrong et al. [45] based their research of FDD on the variation of the electrical current of a roof top unit (RTU). They tested some of the above-mentioned faults and added mechanical imbalance of fans and compressor liquid ingestion. Weights were placed on the tips of the fan blades to create imbalance and the suction port of the semi-hermetic compressor was injected with a mass of liquid to emulate liquid ingestion.

Xiao [57] and Hou et al. [58] focused on sensor faults in HVAC systems by applying bias in the measurement of critical sensors for the operation of the equipment. Luo et al. [43] differentiated between sensor bias, drift, precision degradation and complete failure.

Namdeo et al. [55] focused on valve leakages, but differentiated between leakage at the suction or the discharge valve. In their study with heat pumps, Kim et al. [40] implemented compressor valve leakage but also included as the same type of fault a leakage in the 4-way valve. This is because the consequences of leakage at the compressor valves or at the 4-way valves are the same (hot gas to the suction line).

Bonvini et al. [59] worked with a model of a real chiller plant and considered a more general description of faults, such as higher energy consumption than expected, a decrease in chiller efficiency or occluded condenser water valves.

2.5 Simulation of faults with virtual models

The laboratory testing of real equipment is costly and time-consuming. In some cases, the faults tested can permanently reduce the performance of the heat pump or even leave it inoperable. Models for heat pumps and fault modelling represent a solution to those issues.

Fault modelling has increasingly being used to validate FDD techniques under a variety of fault free and faulty conditions, including concurrent fault occurrence [60]. Simulations can also provide greater insight into the overall effect of faults on the operation of a system, the interaction between concurrent faults, the energy consumption and

thermal comfort of buildings [60].

Several studies have engaged in FDD by applying heat pump simulations modelled with a grey-box and white-box approach [61, 62, 63]. A grey-box model mixes the use of experimental data and inverse modelling to determine the values of parameters to generate the model [64]. A white-box model uses the knowledge of the physics of the system to create the model based in its principles. The fault modelling methods applied in the literature are summarized in Table 2.3.

For OHXF, IHXF, OMC and IMC faults, grey-box and white-box models have been used to simulate the reduction of the air-flow. Whereas grey-boxes are used to reduce the airflow only across the heat exchanger [61, 62], white-boxes consider the effect on the term UA, which is the product of the overall heat transfer coefficient (U) and the coil heat transfer surface area (A), when introducing a fouling factor for IHXF and OHXF faults [63]. Additionally, white-box models simulate fouling by formulating the degradation of the UA factor [66] or by modifying the log mean temperature difference (LMTD) term in the heat transfer equation [67].

The CVL fault is commonly simulated by reducing the refrigerant mass flow rate and the effect of mixing during suction on the refrigerant's thermodynamic properties is also accounted for [61].

The LL fault is simulated with an additional pressure drop in the liquid line [60, 61]. Even though some authors consider that for NON fault, the non-condesables gases accumulates only within the condenser [68], Cheung and Braun [61] assumed that it accumulates in the hot gas line and the vapour section of the condenser. Therefore, the fault is simulated by calculating the refrigerant and the non-condensable partial pressure and then solving the rest of the heat pump model by considering this influence [61].

Control sensor faults in HVAC systems are frequently modelled by considering both positive and negative offset values, particularly on readings of temperature sensors [67].

Table 2.3: Summary of fault modelling techniques for heat pumps. Percent values are defined with respect to fault free conditions. HX: heat exchanger. R_f: fouling factor. UA: overall heat transfer coefficient times area.

Fault type	Simulation technique	Fault levels	Ref.
OC & UC	Charge variation	70-130%	[61, 62]
IHXF & OHXF air side	*Grey-box*: Reduction of air flow rate by increasing friction factor or reducing fan speed	0-55%	
	White-box:		
	1) Modelling of UA introducing R_f	-	[63, 65]
	2) Modeling UA degradation with degradation coefficient α	$\alpha \in$ [0,1]	[66]
	3) Regressions on air-side effective heat transfer and air pressure drop	-	[39]
	4) Reduction of UA based on changes in LMTD value	-	[67]
IHXF & OHXF water-side	*White-box*: same approaches 1) 2) and 4) of air-side HX fouling	-	[63]
IMC & OMC	Reduction in fan speed	-	[66]
	Reduction in fan efficiency	-	
	Change in fan performance curve	-	
	Change of pump performance curve	-	[60]
LL	Increase in pressure drop across liquid line	0-3500%	[61]
NON	Change in partial and total pressures	0-20%	[61]
CVL	Reduction of refrigerant mass flow	0-50%	[61, 62]
	Effect of mixing on suction enthalpy		
SEN	Addition of offset	$\pm$ 0.5 K	[67]

In most studies, the researchers used a deterministic approach with fixed levels of faults, omitting the increasing degradation with time that happens in real equipment. For example, for UC due to a leakage of refrigerant, the fault level will increase with time, but the fault is emulated at a fixed level or in increasing steps. Otto et al. [69] proposed a stochastic method for studying the distribution of faults by using a probability density function. However, there is a lack of information on the evolution of those gradual faults and their incidence on heat pump systems.

Another key fact is the occurrence of simultaneous faults. This section has only considered isolated faults, however, other authors have studied the option of simultaneous faults [53, 51, 70]. In some cases, the effect of simultaneous faults could be additive [70]. Nevertheless, when simultaneous faults happen in a heat pump, the effects could overlap, hindering the diagnosis process. However, is difficult to stablish the probability of which faults could happen simultaneously because of the lack of in-field equipment data.

2.6 Conclusions

This chapter has put the focus on the description and occurrence of faults. Despite there were studies about fault incidence of in-field equipment, the literature was scarce and, in some cases, outdated. However, an analysis of the incidence has been made to have information about the general health status of in-field equipment.

Then, a thorough description of each common fault, how it occurs and the repercussion was made. There could be different origins for the same fault but the effect tends to be the same. However, the faults effects could depend on the equipment typology and architecture.

There were several techniques for fault emulation, from the use of real equipment to the simulation with virtual models. The use of real equipment has been extensively used to study the faults effects. Despite it requires of measurement and testing apparatus and the possibility of breaking the tested equipment, the experimental emulation of faults gave high valuable data about the repercussion of faults. Virtual

simulation tackles some of the inconveniences of experimental testing as the cost of an experimental campaign. However, the virtual models do not reflect completely the reality and could overlook the cross influence of faults on other parts of the system.

The content of this chapter was an exhaustive state of the art review that covered several aspects about which should be the faults targeted by the FDD monitor and the expected effects. This review covered the lack of updated revisions about the faults and their effects. In the same way, this chapter was the base for elaborating the experimental part of this thesis: the emulation of faults on a current heat pump.

UNIVERSITAT ROVIRA I VIRGILI
AUTOMATIC FAULT DETECTION IN DOMESTIC HEAT PUMPS
Ivan Bellanco Bellanco

CHAPTER 3

Fault Detection and Diagnosis monitor development

UNIVERSITAT ROVIRA I VIRGILI
AUTOMATIC FAULT DETECTION IN DOMESTIC HEAT PUMPS
Ivan Bellanco Bellanco

3.1 Introduction

Fault Detection and Diagnosis (FDD) methodologies have been applied to different systems to increase reliability, security or to improve the maintenance actions. In the case of heating, ventilating and air conditioning (HVAC) equipment, FDD has been extensively investigated in the last three decades [71, 72], developing several FDD methodologies.

In this chapter, the state of the art of the FDD is reviewed in order to choose the different methodologies that will compose the FDD monitor. The development of the monitor is explained as well as the different modules that form it. The monitor is then validated with simulation data and the performance results are analysed.

3.2 State of the art of the fault detection and diagnosis methodologies

In general, the objective of an FDD system is to detect anomalous behaviour of the equipment, which can be associated with a fault, and try to diagnose the cause.

FDD methodologies were first used for applications where safety and money-saving are crucial as aeronautics or nuclear power plants [20]. Then, they were spread to different types of systems. There are several characteristics that are desirable for an FDD methodology. Venkatasubramanian et al. [73] enumerated those characteristics as:

- Speed: the fault should be detected and diagnosed quickly.
- Isolability: the ability to distinguish between different faults.
- Robustness: to be robust to the noise and uncertainties.
- Novelty identifiability: when a novel unknown fault appears, it is need to detect that a fault is happening and not misclassifying it as a known malfunction.

- Error estimate: the possibility of telling the user the classification error or the confidence in the prediction.
- Adaptability: to be adaptable to new conditions or changes.
- Explanation facility: the algorithm should justify its results and explain how it has reached the diagnosis so the operator could act accordingly.
- Modelling requirements: the model complexity should be minimal for fast and easy deployment.
- Storage and computational requirements: they should be as low as possible.
- Multiple fault identifiability: it is important to detect multiple simultaneous faults but could be difficult because of the synergies between the faults.

An FDD solution could be divided into different parts that Rogers et al. [18] described as feature selection, steady-state detection, fault-free modelling, fault detection and fault diagnosis. These parts could be defined as:

- Feature selection is the decision of which measurements will be used for detecting and diagnosing faults. The term feature is used in FDD literature to express a measurement from the equipment that can provide useful information for performing FDD. The measurement can come directly from a sensor installed in the system or indirectly as in the case of virtual sensors where an indirect measurement is calculated or trained with the data from a real sensor.
- The steady-state detection eliminates the noise and the outliers of the data. This ensures that the incoming data does not correspond to a transitory, which could confound the algorithm.
- Fault-free modelling is the generation of a reference model of the equipment in a "healthy" state. The equipment is in healthy state when there is no fault present.

- Fault detection is the comparison between the measured data and the one from the fault-free models. The mismatch between them is a fault indicative.
- Fault diagnosis tells which is the occurring fault depending on the features affected.

From these parts, the literature reviews have been focused on fault-free modelling, fault detection and fault diagnosis, which are the most distinctive part of the different FDD solutions. The steady-state detection is not always mandatory, as its goal is to increase the quality of the incoming data, if the data has enough quality or low uncertainty, its use could be unnecessary. The feature selection depends on the FDD methodology or the sensors available and have not been considered separately from the fault diagnosis or fault detection methodology in FDD reviews. Therefore, the following state of the art is focused on the fault-free modelling, detection and diagnosis.

The series of articles about the general process of FDD of Venkatasubramanian et al. [73, 74, 75] gave an explanation of the different FDD methods classified by the a priori knowledge about the system to perform the FDD. This classification is adapted to building systems by Katipamula and Brambley in two review articles [17, 76]. The first[17], gave an accurate description of the use of FDD in systems such as refrigerators, air conditioners, heat pumps, chillers and air handling units (AHU). Figure 3.1 shows the classification made by Katipmaula and Brambley based on the type of knowledge used to perform the fault diagnosis. This classification divides the FDD methodologies into three main groups:

- Quantitative model-based methods, which use models obtained from basic physical principles to perform the diagnosis.
- Qualitative model-based methods which rely less on the accuracy of the data and uses ranges of values to extract qualitative values (high, normal, low, etc.) from the features. This group consists of methods based on a series of if-then-else rules (rule-based).
- Process history based methods which rely on the empirical relation between output and input data. This group is divided into

two subgroups: black-box models , which do not need any knowledge about the process and perform the diagnosis through the relationship between inputs and outputs of the system, and grey-box models, which need some knowledge of the system studied.

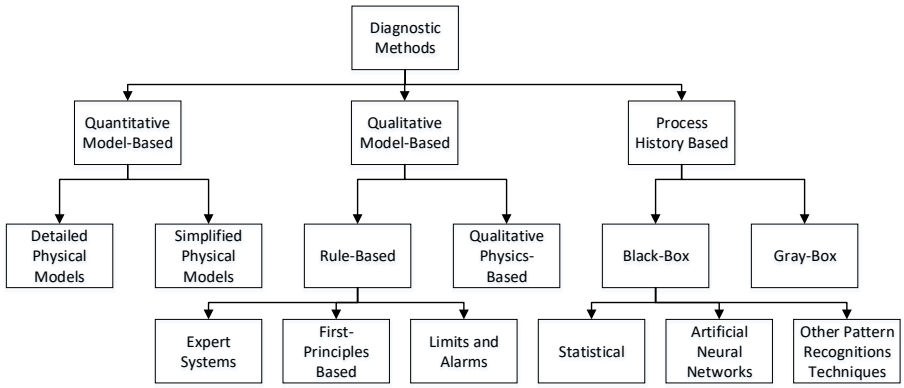

Figure 3.1: Classification of FDD based on the diagnosis methodology, from Katipamula and Brambley. Adapted from"Review article: Methods for fault detection, diagnostics, and prognostics for building systems—a review, part I", S. Katipamula, M.R. Brambley, 2005, *HVAC&R Research, 11.* Copyright 2005 by the American Society of Heating, Refrigerating and Air-Conditioning Engineers, Inc.

The second article [76] described the faults, measurement and FDD methods used for each type of building system. The review by Katipamula and Brambley [17] is the basis for a later review by Kim and Katipamula [77] of FDD for building systems, which focused on the publication trends of each of the methods described in Katipamula's classification between 2005 and 2018. The main conclusion was that process history-based methods were increasingly being used to perform FDD. The main reasons for that increase were the higher process capacity of electronics and the fast deployment of black-box models because they do not required specific knowledge about the process.

Zhao et al. [78] authored a review of artificial intelligence-based FDD methods for buildings as an example of the increasing interest in the area. Zhao et al. pointed out that there was a lack of articles about

FDD methods that could detect both sensor and physical component faults within the same solution.

For HVAC systems, the same increasing trend of using process history-based methods was observed. Yu et al. [27] proposed in 2014 a new classification of methods that took into account new methodologies as shown in Figure 3.2. In this new classification, methods as artificial neural networks (ANN) and principal component analysis (PCA) are included under its own group.

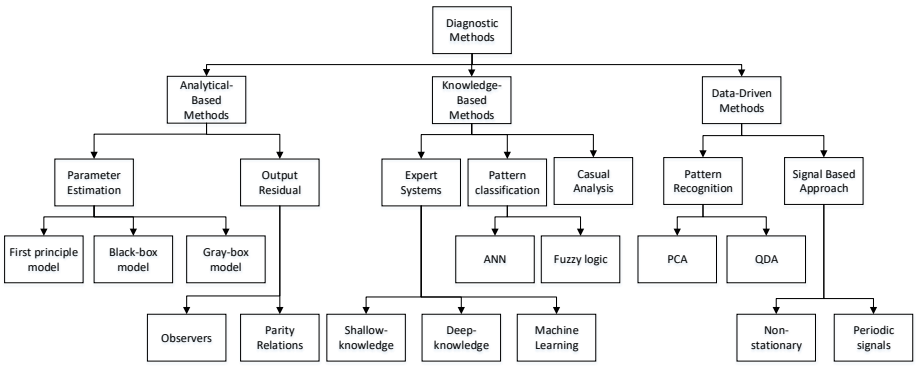

Figure 3.2: Classification of FDD based on the diagnosis methodology, from Yu et al. Adapted from "A review of fault detection and diagnosis methodologies on air-handling units", Y. Yu, D. Woradechjumroen, D. Yu, 2014, *Energy and Buildings, 82.* Copyright 2014 by Elsevier B.V.

The methods classification of Yu et al. and Katipamula and Brambley are very similar. Both uses the diagnosis methodology to classify the methods, but the one from Yu et al. is more specific and differentiates better recent methodologies based on computation.

The same classification could be suitable for the description of the methodology used for the generation of the fault-free models. In the case of an FDD solution where the methodologies used for the fault-free models and the fault diagnosis are different, they could be described separately with Yu et al. classification.

There are different indicators used to characterize the performance of the different FDD methods. Yuill and Braun [79] compare different FDD methodologies using no response, the false alarm rate, the

misdiagnosis rate and missed detection as indicators. Shi and O'Brien [80] used a more statistical point of view, and identified the false positive rate (false alarm), false negative rate (missed detection), precision (accuracy) and detection time as the parameters for validating FDD performance. The issue is that there are few authors that use these indicators to determine the performance of their FDD solutions. From what was found in the literature research, the indicators Accuracy and False Alarm Rate were the most used.

These indicators used the binary outcomes of the model. Taking into account that a positive is a fault, and negative is no-fault, the possible outcomes are:

- True positive: a point in the data that is positive (a fault) and it was predicted as positive (fault detected).
- True negative: a data point that is negative (there is no fault) and it was predicted as negative (no fault detected).
- False positive: a point in the data that is negative (there is no fault) and it was predicted as positive (false alarm).
- False negative: a data point that is positive (a fault) and it was predicted as negative (missed fault).

Taking into account that nomenclature, the accuracy represents the fraction of correct fault warnings (True positive) with respect to the total fault warnings given by the FDD system (True positive + False Positive). This indicator is used when there is a fault present in the system, because of this, True positive are used. The ideal value is 100%.

$$\text{Accuracy} = \frac{\text{True positive}}{\text{True positive} + \text{False Positive}} \tag{3.1}$$

False alarm rate (FAR) represents the fraction of erroneous fault warnings (false alarms) with respect to the sum of non-faulty and erroneous detection by the FDD system. This indicator is used while there is no fault present, because of this, the True Negatives (no fault in the equipment) is used. The desired value is 0%.

$$\text{FAR} = \frac{\text{False Positive}}{\text{False Positive} + \text{True Negative}} \tag{3.2}$$

From a literature research of the different FDD methodologies Table 3.1 summarizes and compares the different methods and their performance values. The category column indicates the main category of the methodology, and the method column indicates the subcategory according to Yu et al. classification (Figure 3.2). For those cases, the methodology for creating the no-fault models and the diagnosis is the same. The device column specifies the equipment used. In the column data, the source of data used (data from real equipment or from a simulation) is stated. The number and type of sensors used to develop the FDD method are specified. Then, the accuracy and FAR values are given. This table quantifies the performance values of different methodologies, indicating the system tested and the type of data used, being helpful to select the most suitable FDD methodology for each situation.

Table 3.1: Performance comparison between different FDD methods. CH: chiller, HP: heat pump, RTU: rooftop unit, MS: multi-split, Simu.:data from simulation, No.Sens.: number of sensors, P: pressure sensor, T: temperature sensor, m: air flow rate sensor, Accu.: Accuracy, FAR:false alarm rate and "-":Unspecified.

Category	Method	Device	Data	No.Sens.	Accu.	FAR	Ref.
Knowledge-based	Machine Learning	HP	Real	4T,3P and 2m		1.6%	[53]
Analytical-based	Grey-box	HP	Real	4-5T		5.3%	[54]
Analytical-based	Black-box	CH	Real	7T,3P	93.0%		[81]
Knowledge-based	Machine Learning	RTU	Simu.	-		35.0%	[82]
Knowledge-based	Machine Learning	RTU	Simu.	-		55.0%	[82]
Knowledge-based	Machine Learning	RTU	Simu.	-		15.0%	[82]
Knowledge-based	Machine Learning	MS	Real	28T	94.0%		[83]
Knowledge-based	Machine Learning	MS	Simu.	28T	80.6%		[83]

Despite some quantitative values were found, it is difficult to directly compare the results of the different methods of Table 3.1 because the faults emulated are not the same for each method. In some cases, the authors have tested conditions quite different from those of the training data, whereas others used data similar to the training phase, so the performance values of the latter may be better. For these reasons, there is a general lack of homogenization in the communication of the results of FDD methods.

3.3 Methodology selection

To select the most appropriated methodology to develop the FDD monitor, it is needed to determine the key requirements of the solution to develop. The main requirements of the current research were:

- Fast detection of coefficient of performance (COP) drift
- Diagnose of different faults
- Need of low computational resources
- Flexible to work with different conditions
- Small quantity of data required for training

One of the main limitations of the current development is the data available for training. No data sets about faults in domestic heat pumps were found, and despite a simulation model is used for the first validation, the experimental tests with a real heat pump is limited in time. Therefore, the monitor have to achieve good results with small quantity of data. This situation limits the number of possible FDD methodologies. The methods that require high quantity of data have been be discarded as the data-driven methods and pattern classification.

The use of first principle model was also discarded because it requires a huge development effort and only works with the specific heat pump for which was developed. To delimit the remaining options, the literature trends [77] showed that Black-box, Grey-box and Expert Systems are the most used.

Grey-box required some knowledge about the system thus, limiting the flexibility to use the same solution for different heat pump types. Black-box models are easy to develop and could be adapted to different heat pumps. However, their results depend of the quantity of data used for training. They could fail easily when new data that was not take into account during training appears (for example, a novel fault). Another limitation is that the process to find the solution in black-box

is opaque, therefore, it is difficult to know how the solution has been found and which parameter needs to be tune to optimize the solution.

Taking this into account, the solution for this thesis would count with different methodologies for diagnosis and generation of fault-free models. For generating the fault-free models, polynomial regressions were selected as they required low computational resources and had good results used for FDD [84]. As the fault data is the most limiting factor, expert knowledge was selected for the fault diagnosis. Expert knowledge uses a series of if-then-else conditions about the state of the heat pump to determine the fault. It requires small quantity of data for training and, in comparison with black-box models, the solution process is transparent and can be followed and explained easily. It relies on the knowledge of an expert about the equipment to diagnose the fault. However, this characteristics makes that the results depend on the knowledge about the system.

3.4 Monitor structure

3.4.1 General structure

To achieve the goals of the thesis, the FDD monitor was developed with different parts as showed in Figure 3.3.

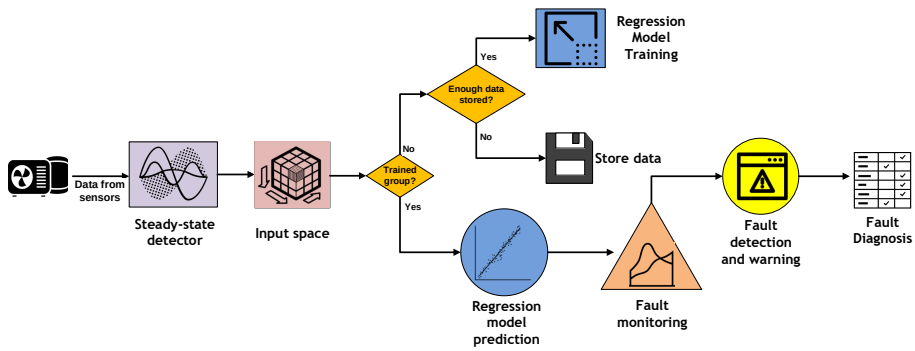

Figure 3.3: Scheme of the different parts that form the FDD monitor developed.

As explained in the last section, the use of an steady-state detector (SSD) filters the data and increases the accuracy of the results. Therefore, it was included to filter the data coming from the heat pump, specially for the tests with real equipment. In the same section, polynomial regressions were selected for the generation of fault-free models. However, it is difficult to have a regression that represented all the operational range of the equipment. Thus, based on the research of Heo et al. [84], a module named Input Space was developed to increase the efficiency of the solution and giving the capability of self-training when new data appears.

When the regression models are trained, their results are compared with the heat pump measurements to detect a possible fault. Finally, based on which features and in which way are affected, the fault is diagnosed based on expert knowledge. The following subsections describes the fundaments and the development of each of the parts of the monitor.

3.4.2 Steady-state detector

During the operation of the equipment, there are moments of transition in which the no-fault model could have poor performance due to non-linearities. These moments could be caused by changing conditions such as the start or stop of the compressor, quick changes in the compressor speed or outliers or noise in the measurements. The objective of the steady-state detector is to identify the stages in which the heat pump is working at quasi steady-state conditions to use this data for training and fault monitoring. The non-steady data is eliminated.

In FDD literature for HVAC, the SSD method most commonly used is the one described by Kim et al. [85]. This process uses a moving window to calculate the mean and the standard deviation. Figure 3.4 shows the process. The moving window takes a number of n values and calculates the mean and the standard deviation of the window. Then, takes in a new point while taking out the oldest one and calculates those values. If the values of the windows are inside the range of plus/minus three times the value of the standard deviations from the mean, the point will be considered in steady-state.

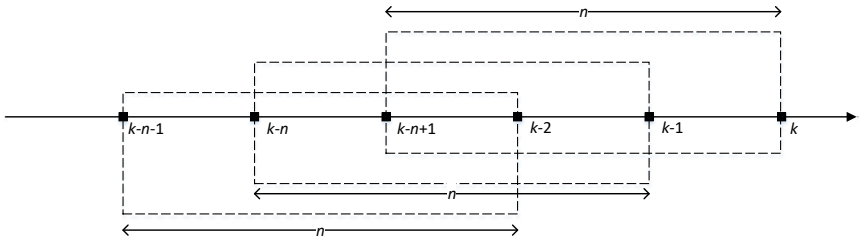

Figure 3.4: Sliding window method. n is the size of the window and k is the position of the data point. Adapted from "Design of a steady-state detector for fault detection and diagnosis of a residential air conditioner", M. Kim, S. H. Yoon, P. A. Domanski, W.V. Payne, 2008, *International Journal of Refrigeration, 31.* Copyright 2008 by the International Institute of Refrigeration.

In the method proposed by Kim et al., the value of the standard deviation is constant and is selected by analysing the data, searching for a series of points in steady-state and using their standard deviation as a reference. Therefore, to apply this methodology, a prior study of the data is needed. To avoid the prior analysis and increase the flexibility, a new approach was considered for the SSD in this thesis.

In statistics, a data series is considered in steady-state when the slope of the mean and the variance are constant, and there is no seasonality. A series has seasonality when the data experiences regular and predictable changes that occur every time period. When real-time data is used, sensor noise and variability due to variable speed operation leads to a non-constant value of the mean and variance. Because of this, the quasi-stationarity is used, where a percentage of change is allowed.

The key of the new SSD is to automatically search this allowed change. Because of that, a structure of queued data windows are used. First, the seasonality is discarded because of the short duration of each window. Figure 3.5 shows a graphical representation of the process. To know if the current point is in quasi-stationarity, the windows are applied from this point and sliding to the previous ones. The first window of n data points is defined. For this origin window called w_o, the mean (μ) and the variance (σ) are calculated. Equations 3.3 and

3.4 shows the calculation of the mean and the variance for the first window.

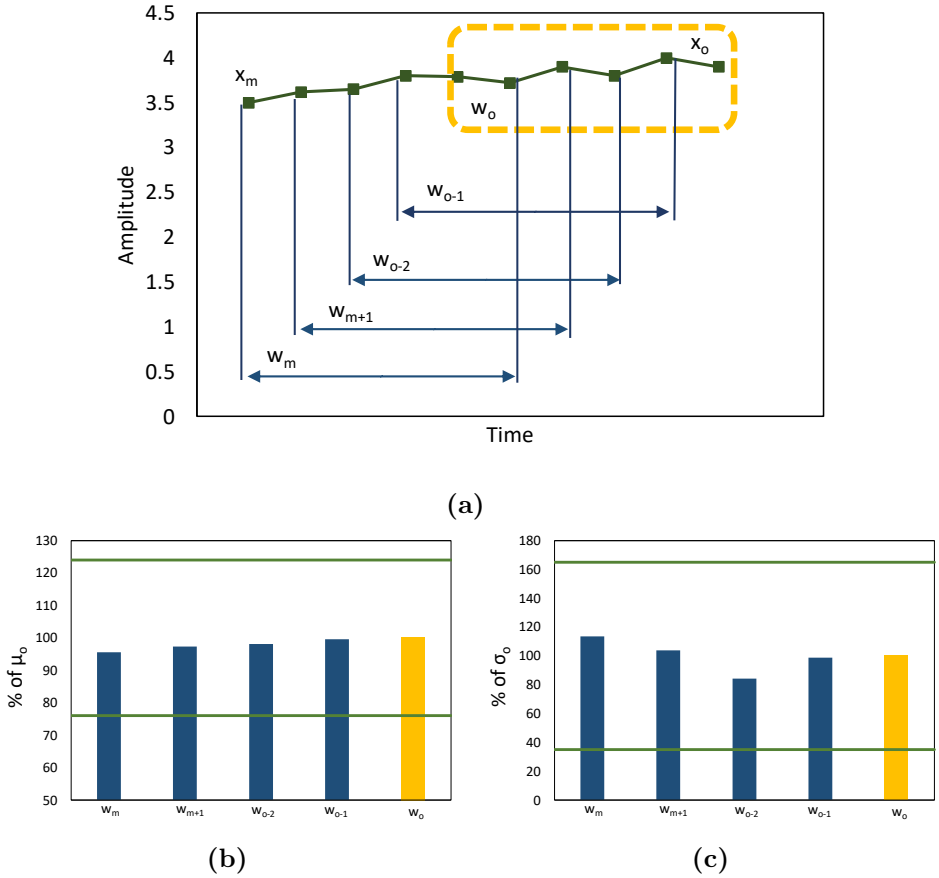

Figure 3.5: Example of the SSD developed applied to a COP signal. a) Series of data points (green). In yellow, the reference window (w_o), in blue, the queue of windows (w_{o-1}, w_{o-2} ...). b) Percentage values of μ (blue) normalized to the reference window mean (yellow). The green lines represent the margin of allowed change. c) Percentage values of σ (blue) normalized to the reference window variance (yellow). The green lines represent the margin of allowed change.

$$\mu = \bar{x} = \frac{1}{n} \sum_{i=o-n+1}^{o} x_i \tag{3.3}$$

$$\sigma = \sqrt{\frac{1}{n} \sum_{i=o-n+1}^{k} (x_i^2 - \bar{x}_{o-1}^2)} \tag{3.4}$$

Then, the window slides to the previous data to calculate the mean and variance of the preceding windows. This creates the queue of windows, which length m depends on the incoming data frequency. After a number of windows have been calculated, the values of the variance and mean are divided by the ones of w_o to know the percentage change. If the values are inside a range of allowed change, the point x_o will be in steady state. Then, the following point is taken in, while the oldest one is taken out, and the process starts again.

The allowed change was determined from experimental data of previous tests in IREC with variable and fixed speed heat pumps showed in Table 3.2. The data comes from three different heat pumps: a water-to-water fixed-speed heat pump working on heating mode (test 1) [86], an air-to-water fixed-speed heat pump in cooling mode (test 2) and an air-to-water variable speed heat pump working on cooling and heating mode (test 3) [87]. A total of thirty-seven steady-state stages were selected manually. For each of these conditions, the sliding window method was applied, obtaining the mean and the variance difference with respect to the original window, for the COP for each stage. In Table 3.2 the averaged difference values of the stages are showed to summarize the results. Different test of the SSD were made using as allowed change the average mean difference from the tests, but it was to restrictive detecting small quantities of steady-state point. Because of that, the maximum values of the mean difference was used. The maximum difference values of the means obtained in each stage was averaged and resulted in 0.24, which give good results for each of the series. For the variance, using the maximum difference values of the variance of the test was too big, detecting nearly all the points as steady. Therefore, the variance difference of all the stages was averaged resulting in 0.65, which give good results.

Table 3.2: Averaged values of the mean (μ) and variance (σ) difference with respect to original window of the COP of different experimental test with heat pumps. w-w: water-to-water, a-w: air-to-water.

Test	Stages	Type	Compressor	μ	Max μ	σ	Max σ
1	8	w-w	fix	0.08	0.64	0.14	2.40
2	8	a-w	fix	0.05	0.14	0.82	3.86
3	21	a-w	variable	0.06	0.12	0.71	3.07

Therefore, the allowed change from the original window (w_o) was 0.24 and 0.65 for the mean and the variance respectively. Figure 3.6 shows the SSD applied to the signal of the variable speed heat pump of the test number 3. The window size (n) was 12 and the queue length (m) was 22.

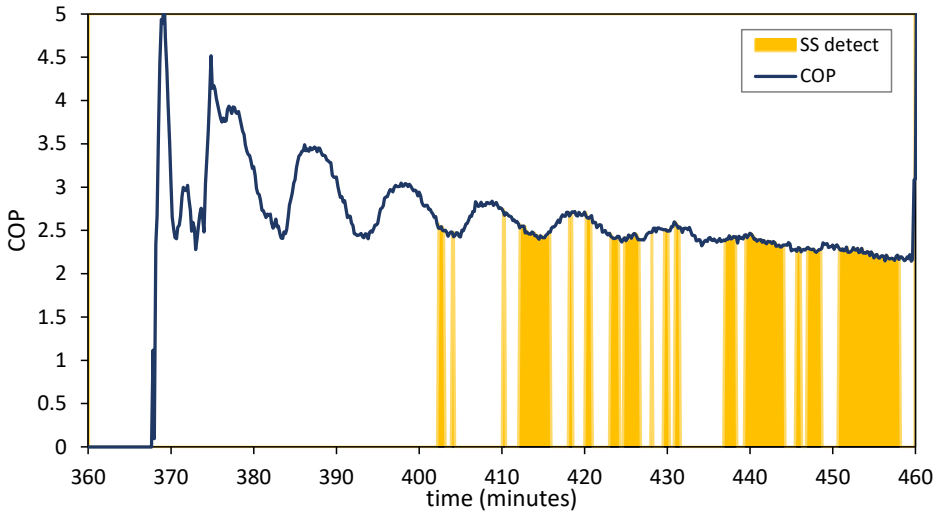

Figure 3.6: SSD detector applied to the COP signal of the variable-speed heat pump of test 3. When a steady-state is detected, the *SS detect* signal have the same value as COP.

3.4.3 Input Space

The majority of previous research on FDD systems for heat pumps has been developed for fixed or limited conditions. Whereas in real installations, the conditions are changing along the year and between different locations. To be practical, the FDD solution should work at different operation points.

In real installations, the data is changing during the year, therefore the FDD solution must be prepared to adapt to those changes. A proposal to adapt FDD to changing conditions is that of Heo et al. who addressed the operation under dynamic conditions on their research [84] about a self-training fault-free model. Their methodology follows the next steps: first, they divide into groups the operational space of the heat pump. This space is defined by the range of the driving variables of the heat pump. For an air-to-air conditioner they selected indoor and outdoor temperatures, and outdoor relative humidity as the driving variables. These groups are shaped like cuboids. Then, the data input is classified to a cuboid depending on the value of its driving variables. Figure 3.7 represents the operational space defined by the driving variables of Heo et al. Each star, represents the centre of a cuboid.

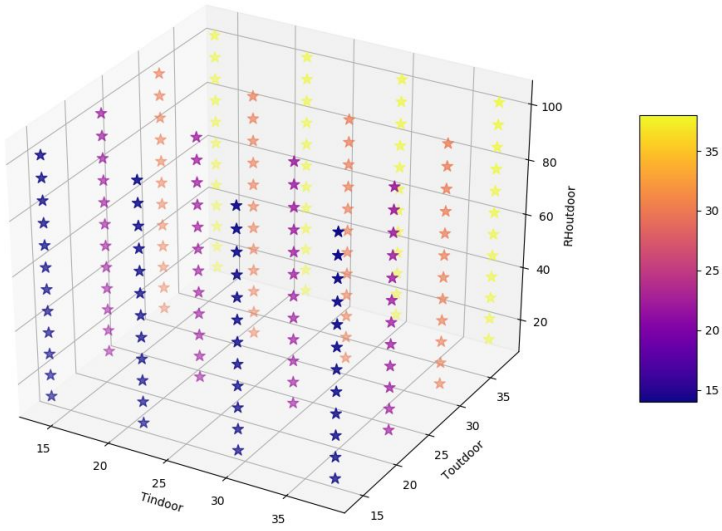

Figure 3.7: Three-dimensional representation of the Input Space of Heo et al. The driving variables indoor and outdoor temperatures and outdoor relative humidity, are the axis of the space. Each star represents a centre of a cuboid. The Toutdoor is coloured to visualize the depth.

For each of those cuboids, a model of the heat pump was trained using the cuboid data. If there were not enough data in a cuboid, it could be trained when more data is available (self-train). Heo et al. used the points near the centre of each cuboid, testing the training with 100, 50, 25 10, 5 and 1 points for each centroid, having the best results with 100 and 50 data points.

Based on that research, the input space of the FDD monitor was developed. The driving variables defined for the Input Space are the inputs of the regression models, that will be presented in the next Section 3.4.4.

For the validation with a real water-to-water heat pump, the variables used were condenser inlet temperature ($T_{cond,in}$) and evaporator inlet temperature ($T_{evap,in}$) as showed in Figure 3.8. This figure represents the data of the fault-free tests at 10 kW and 12 kW loads.

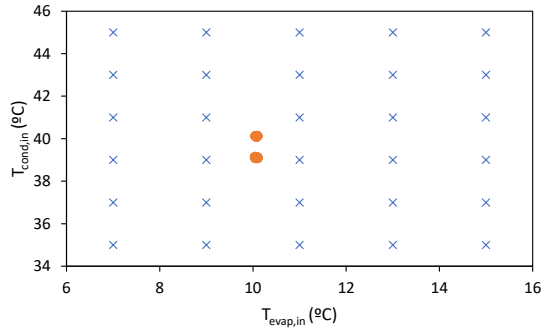

Figure 3.8: Representation of the two-dimension Input Space defined for the validation with data from a real heat pump. The orange points represent the steady-state data of the fault-free tests at 10 kW and 12 kW loads, and the blue crosses represent the centroid of each of the regions of the space.

The Input Space generates an empty variable with the dimension of the input space, which will be used to store the regression model of each of the clusters.

3.4.4 Fault-free models

This part of the algorithm is dedicated to generate a model of the heat pump on normal behaviour, when no fault is present. As explained before, the selected methodology to develop the fault-free models was polynomial regression.

A polynomial regression is included in the group of linear regressions. Linear regressions make predictions by computing the weighted sum of the input features plus a constant (intercept), as shown in Equation 3.5.

$$\hat{y} = \theta_0 + \theta_1 x_1 + \theta_2 x_2 + \cdots + \theta_n x_n \tag{3.5}$$

where $\hat{y}$ is the predicted value, n is the number of features, x_i is the i^{th} feature value, θ_j is the j^{th} model parameter and θ_0 is the intercept. Linear regressions perform well when the relationship between the predicted value and the input features is linear, as shown in Figure 3.9a. In the case of a non-linear series like the one shown in Figure 3.9b, the linear regression could be adjusted to a polynomial regression. In

that case, the equation to solve would be similar to Equation 3.6. For polynomial regression, there are parameters that describe the relationship between the different features (θ_5 in the example). Note that the coefficients are not squared, therefore, the statistical relation is still linear.

$$\hat{y} = \theta_0 + \theta_1 x_1 + \theta_2 x_2 + \theta_3 x_1^2 + \theta_4 x_2^2 + \theta_5 x_1 x_2 \tag{3.6}$$

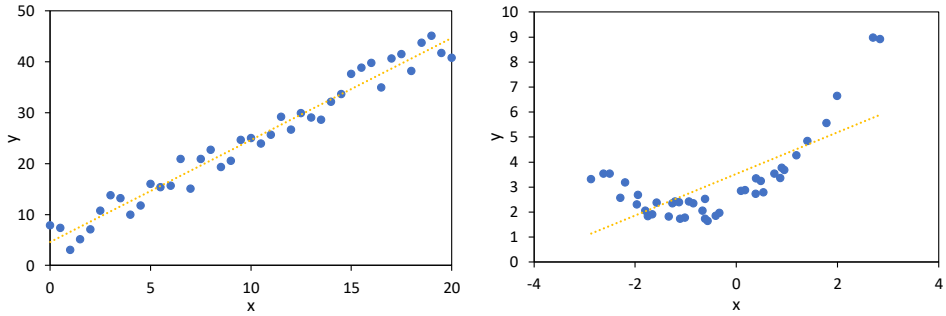

(a) **(b)**

Figure 3.9: Representation of linear regression for linear and non-linear data. a)Linear regression (yellow) of a data series (blue) with a linear behaviour b) Linear regression (yellow) of a data series (blue) with a polynomial behaviour.

The regression searches for the set of parameters (θ) that minimizes the error, typically the root-mean-square error (RMSE). The algorithm recursively searches for this minimum, optimizing the result. Stochastic gradient descent regression (SGDR) from the sklearn library for Python was used as method to optimize the results. This type of optimization picks random solutions to converge to the minimum error, reducing the calculation time and avoiding local minimum solutions.

The predicted value ($\hat{y}$) could be found with one or multiple features ($x_1, x_2 \dots$). These features, also called independent variables, are selected from the driving variables of the equipment.

In the case of Heo et al. [84], the driving variables were indoor and outdoor temperatures and outdoor relative humidity for an air-to-air fixed capacity heat pump. Wang et al. [88] developed an FDD for a

water-to-water chiller system, where they selected chiller water supply and entering condenser water temperatures, and cooling load as the driving variables for their regression method. Li and Braun [89] studied the decoupling of features and the use of virtual sensors, where they stated that the driving variables of a fixed speed compression system are the condenser inlet air temperature, the evaporator air temperature and relative humidity. Therefore the selection of the driving variables depends on the heat pump type, but in general, they must represent the environment and not the internal condition of the heat pump.

For the first validation with simulation data, the model of an air-to-water heat pump was used as it is explained in Section 3.5.1. The independent variables selected were outdoor temperature (T_{amb}), the condenser outlet temperature ($T_{cond,out}$) and the compressor frequency (f) to represent the behaviour of the variable speed compressor. The polynomial equation selected was a third degree equation based on the research of Heo et al. [84], showed in Equation 3.7.

$$\begin{aligned}\hat{y} =&\theta_0 + \theta_1 \mathrm{T_{amb}} + \theta_2 \mathrm{f} + \theta_3 \mathrm{T_{cond,out}} + \theta_4 \mathrm{T^2_{amb}} + \theta_5 \mathrm{f^2} + \theta_6 \mathrm{T^2_{cond,out}} + \\ &\theta_7 \mathrm{T_{amb} f} + \theta_8 \mathrm{T_{amb} T_{cond,out}} + \theta_9 \mathrm{f T_{cond,out}} + \theta_{10} \mathrm{T^3_{amb}} + \theta_{11} \mathrm{f^3} + \\ &\theta_{12} \mathrm{T^3_{cond,out}} + \theta_{13} \mathrm{T_{amb} f T_{cond,out}} + \theta_{14} \mathrm{T^2_{amb} f} + \theta_{15} \mathrm{T^2_{amb} T_{cond,out}} + \\ &\theta_{16} \mathrm{f^2 T_{amb}} + \theta_{17} \mathrm{f^2 T_{cond,out}} + \theta_{18} \mathrm{T^2_{cond,out} T_{amb}} + \theta_{19} \mathrm{T^2_{cond,out} f}\end{aligned} \tag{3.7}$$

For the experimental campaign with the real heat pump, the driving variables were changed to condenser outlet inlet temperature ($T_{cond,in}$) and evaporator inlet temperature ($T_{evap,in}$) for being of a water-to-water type. The compressor frequency was not used because the faults altered the compressor speed, making impossible the fault detection as explained with more detail in Section 5.3. The Equation 3.8 was still used, changing the corresponding variables and making zero the f term, resulting in Equation 3.8 .

$$\begin{aligned}\hat{y} =&\theta_0 + \theta_1 \mathrm{T_{evap,in}} + \theta_2 \mathrm{T_{cond,in}} + \theta_3 \mathrm{T^2_{evap,in}} + \theta_4 \mathrm{T^2_{cond,in}} + \\ &\theta_5 \mathrm{T_{evap,in} T_{cond,in}} + \theta_6 \mathrm{T^3_{evap,in}} + \theta_7 \mathrm{T^3_{cond,in}} + \\ &\theta_8 \mathrm{T^2_{evap,in} T_{cond,in}} + \theta_9 \mathrm{T^2_{cond,in} T_{evap,in}}\end{aligned} \tag{3.8}$$

Those equations could be optimized by looking at the significance of each term and eliminating the irrelevant ones. However, as the time needed to solve the regression model is less than 5 seconds, there were no specific necessity of eliminating terms.

Once the regression model is trained, feeding it the driving variables will produce the expected feature at fault-free conditions. The fault-free models are generated for the features: COP, compressor power consumption (W_{comp}), heat duty (Q_{heat}), subcooling (T_{sc}), superheating (T_{sh}), evaporation temperature (T_{evap}), condensing temperature (T_{cond}), compressor outlet temperature (T_{co}), liquid line temperature (T_{ll}) and refrigerant mass flow (m_r). However, the main indicative of a fault is the COP.

An error margin was applied to the result of the regression to account for the uncertainty of the prediction. The margin used was two times the maximum RMSE obtained during the regression training. When the residual between the measurement and the prediction is outside the margin, it is indicative of a possible fault.

3.4.5 Fault detection

The deviation between the prediction and the real measurement could be a fault indicative. However, this difference could be caused by measurement noise or other outliers in the data. To avoid that, the difference should be maintained in time to ensure the consistency.

The objective of the fault detection module is to look for a maintained fault indication to minimise the possibility of false alarms. The module receives a boolean variable from the regressions analysis that indicates when the residual of the COP is outside the prediction margin. The module starts counting and accumulating the number of efficiency drift events for a predefined time. After this period, if the number of measurements presenting a fault represents more than 80% of the samples taken, a warning flag is triggered. This warning flag indicates that there is a consistent efficiency loss in the heat pump. When the fault ratio does not reach 80% during the predefined time, the module resets the drift count to zero until the next COP drift is detected.

Figure 3.10 shows an example of the operation of the warning module for a data series with 60 seconds sample time and 30 minutes of drift count. The boolean COP flag is zero when the COP is within normal levels and 1 when there is a drift beyond the allowed threshold. When a drift is detected, drift events are added up and the variable Fault number increases during the 30 minutes period. Only when the fault ratio (number of drift counts with respect to total samples) is above the specified minimum value (i.e. 80%), the warning flag is triggered. Once a warning signal is raised, the algorithm requests the diagnosis module to identify the fault.

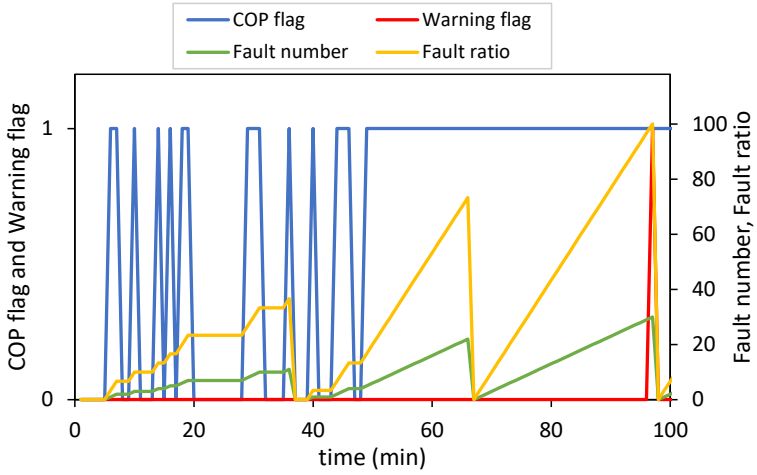

Figure 3.10: Fault monitoring results for an example series with 1 minute frequency and 30 minutes of monitoring. A warning is raised when the fault ratio is above 80%.

For the validation with simulated data, the deviation had to be present 80% in a 50 minutes window, while for experimental data it was 10 minutes. This is because the frequency of data was 10 minutes in the first case and 10 seconds for the last one.

3.4.6 Diagnosis

When there is a consistent efficiency drift, the fault diagnosis module isolates the cause of the fault. The diagnosis methodology used was expert knowledge. Using the knowledge about the fault effects on

different features the fault could be diagnosed.

In Section 3.5.2, a research about the trends of different features when a fault occurs is made. From that research, the diagnosis table showed in Figure 3.11 was created to determine the fault taking into account increasing or decreasing trends of different features. This table was the summary of a literature research about the effects of the different faults. Additionally, the results of a water-to-water, variable speed heat pump virtual model made in the Dymola software, which will be presented in Section 3.5.2, were included to made the diagnosis table.

Feature Fault	COP	W_{comp}	Q_{heat}	T_{sc}	T_{sh}	T_{evap}	T_{cond}	T_{co}	T_{ll}	m_r	Fault code
UC	↓	↑	=	↓		↓ (a-w) = (w-w)	↓	↑		↑	-155-1151
OC	↓	↑	=	↑		↑ (a-w) = (w-w)	↑			↓	155155-1
CVL	↓	↑	=	=	↑			↑		↓	015515-1
IHXF	↓	↑	=				↑	↑			5551155
OHXF	↓	↑	=			↓		↑			55-15155
LL	↓	↑	=	↓	↑				↑		-1155515

Figure 3.11: Fault diagnosis chart. The arrows facing up or down means increasing or decreasing trend, respectively, and the equals means that the feature does not change. For T_{evap}, the trend depends if its an air-to-water (a-w) or water-to-water (w-w) heat pump. Each of the faults has a code based on the tendency of the features starting in T_{sc} and ending in m_r (-1: decreasing, 1: increasing, 0: equals and 5:not relevant).

The features selected to determine the faults were the COP, W_{comp}, Q_{heat}, T_{sc}, T_{sh}, T_{evap}, T_{cond}, T_{co}, T_{ll} and m_r. For each of these features a fault-free model was trained.

After a warning fault is triggered with the COP signal, the diagnosis module gives a value to the trend of the features. The values assigned are -1 if the feature value is decreasing in comparison to no-fault behaviour, +1 if is increasing and 0 if it is within no-fault limits. If the feature is not relevant for the fault, it will be scored with a value of 5, so the algorithm does not look at that trend. This is translated into a code of numbers that describe the trend of each feature. When this code matches any of the fault codes, the diagnosis is completed.

However, it is possible that temporarily the FDD monitor detects an efficiency drift but cannot provide a diagnosis (all the features are not completely affected yet) or there is a novel fault not known before (no match with any fault code). In that case, a warning of a fault will be triggered because of the COP drift but without information about the diagnosis.

3.5 Validation with model data

3.5.1 Model description

Before the tests with a real heat pump in the laboratory, the FDD monitor was validated with virtual data. A TRNSYS simulation model of a domestic installation with a heat pump was developed for that purpose. Figure 3.12 shows the TRNSYS project of the domestic installation.

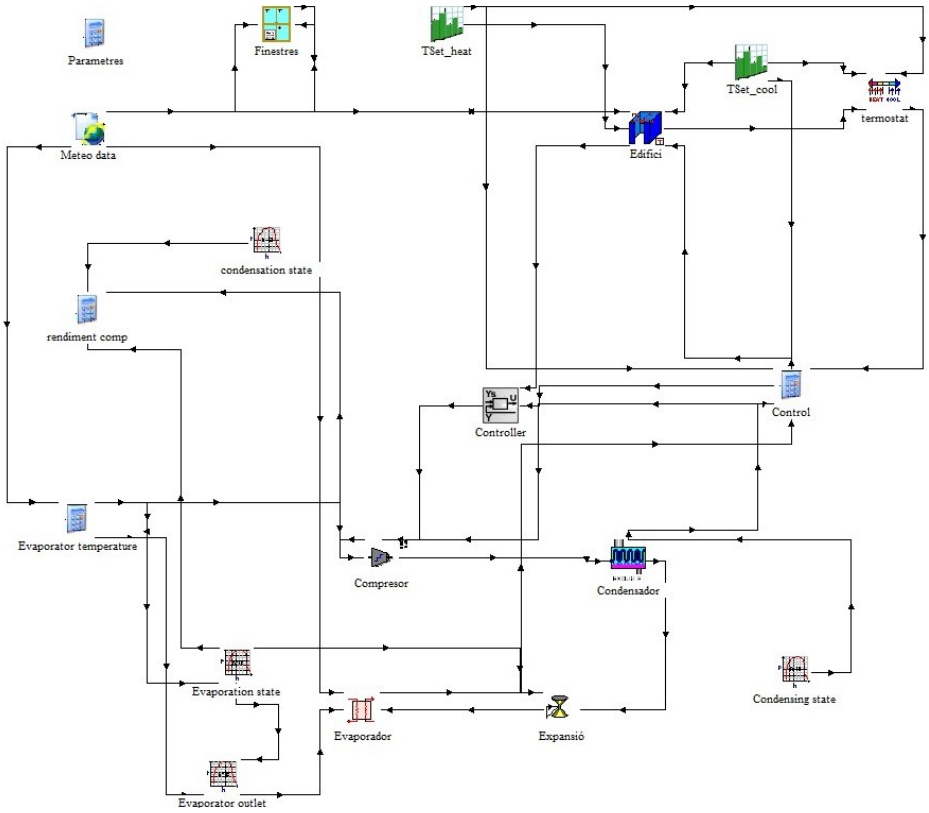

Figure 3.12: Scheme of the TRNSYS project to simulate a variable-speed heat pump within a domestic system.

The installation counted with an air-to-water heat pump model with variable speed compressor. The heat pump model is composed of sub-models for the different internal components, as Table 3.3 shows. The purpose of the model is to cover the heating load of a lumped capacity building model by regulating the heat pump compressor frequency.

Table 3.3: Variable speed heat pump TRNSYS model components specifications.

TRNSYS type	Description	Parameters
660	Simple Lumped Capacitance Multi-Zone Building	Capacitance: 24000 kJ/K Heat loss coefficient: 1000 kJ/(h K)
14	Winter/summer room set point schedule	Winter set point: 17 °C (night), 20 °C (day) Summer set point: 26 °C (night), 24 °C (day) Deadband: 1 °C
108	Five-stage Room Thermostat	Dead band: 1 °C
15	Weather Data Processor	Climate: Madrid Meteonorm
22	Iterative feedback controller	Set point: room temperature
855	Condenser	Subcooling: 5 °C Water supply temp: 45 °C
856	Evaporator	Pinch point temp. diff.: 10 °C Pressure drop: 20 kPa Air flow: 6192 kg/h Superheating: 5 °C
854	Isenthalpic valve	Outlet pressure: evaporation
851	Compressor	Motor power: 2.76 kW Mechanical efficiency: 0.99 Number of poles: 2
857	Coolprop refrigerant properties	Refrigerant: R407C

The compressor model calculates the mass flow of refrigerant using the volumetric efficiency and compressor speed, which is externally regulated with an iterative feedback controller model. The enthalpy of the refrigerant at the suction line is obtained from the refrigerant properties library Coolprop. The discharge enthalpy is calculated from the refrigerant flow, the suction enthalpy and the work delivered to the refrigerant during compression, while the discharge pressure is assumed

to be equal to the condensation pressure and calculated using the Coolprop library. The discharge temperature is then calculated with the thermodynamics database library, using the discharge enthalpy and pressure.

The condenser model considered is a heat exchanger that calculates the heat transfer and refrigerant outlet properties from the inlet properties of the refrigerant, the condensing pressure and the subcooling. The condensing pressure is calculated at the average temperature of the condenser, considering a water supply temperature of 45 °C and a logarithmic mean temperature difference of 10 °C. The evaporator is a heat exchanger model that calculates the heat transfer with the input of the inlet refrigerant properties and the desired enthalpy at the exit of the evaporator, which is calculated considering the saturation pressure and the evaporator outlet temperature. The evaporation temperature is calculated considering the external air temperature, assuming a logarithmic mean temperature difference of 10 °C across the heat exchanger [90]. The expansion valve model calculates the refrigerant outlet properties with the input of the inlet refrigerant data and the desired outlet pressure, which is assumed to be equal to the evaporating pressure. Figure 3.13 shows the evolution of different variables for the TRNSYS model.

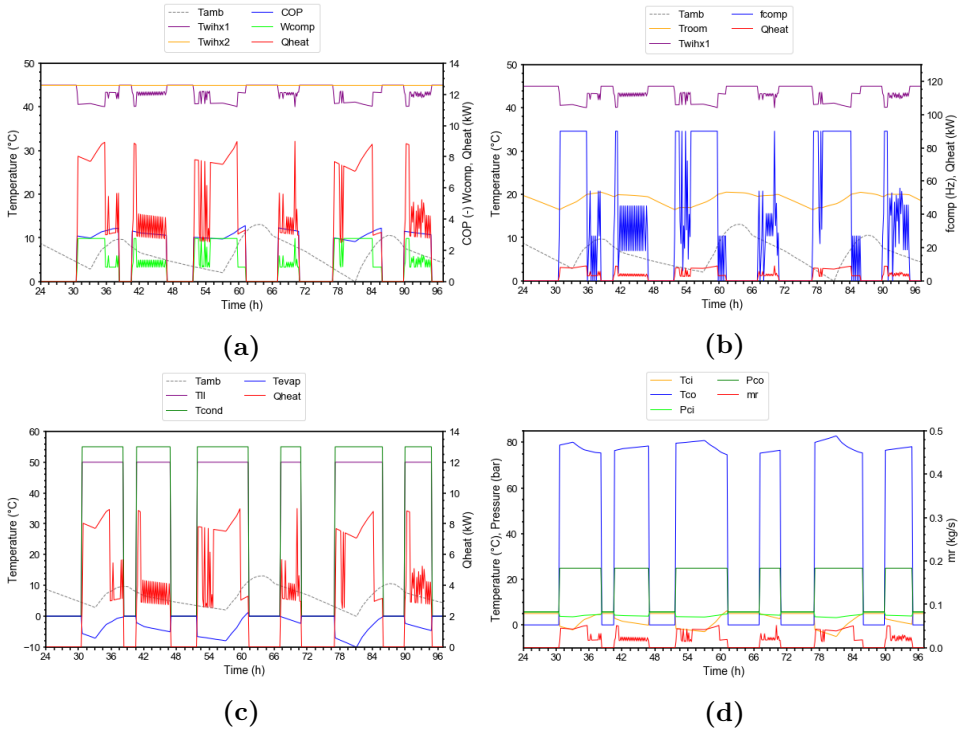

Figure 3.13: Evolution of features under fault free conditions as obtained with variable speed heat pump TRNSYS model. Tamb: ambient temperature, Twihx1: return water temperature of the indoor heat exchanger, Twihx2: supply water temperature of the indoor heat exchanger, Wcomp: compressor power consumption, Qheat: thermal power supplied, Troom: indoor temperature, fcomp: compressor frequency, Tll: liquid line temperature, Tcond: condensing temperature, Tevap: evaporation temperature, Tci: compressor inlet temperature, Tco: compressor outlet temperature, Pci: compressor inlet pressure, Pco: compressor outlet pressure and mr: refrigerant mass flow.

With this heat pump model, the normal behaviour of the heat pump could be simulated. However, the model was not complex enough to simulate faults or their expected effects. Because of this, a series of equations were developed to parametrize the expected effects of faults with time, as explained in the next Section 3.5.2. The TRNSYS model was run to obtain the data of the year. With a Python script, this data was readded, then the parametrization equations were applied obtaining the fault data and then stored in a file to be used for the

validation.

3.5.2 Fault parametrization

The data of faulty heat pumps is scarce, being the data of variable speed heat pumps (VSHP) even more scarce. To validate the algorithm, a series of equations were developed to parametrize the expected effects of different faults along the operation time.

Methodology

Mehrabi and Yuill [41] made a parametrization study from different articles about condenser fouling and refrigerant charge faults. They used the indicator fault impact ratio (FIR) showed in Equation 3.9 to normalize the fault effects of different studies.

$$\mathrm{FIR}_{\mathrm{feature}} = \frac{\mathrm{feature}_{\mathrm{faulted}}}{\mathrm{feature}_{\mathrm{fault-free}}} \tag{3.9}$$

Then, they fitted this data in a second order polynomial regression as showed in Equation 3.10.

$$\mathrm{FIR}_{\mathrm{feature}} = \mathrm{a}_0 + \mathrm{a}_1\mathrm{FI}_{\mathrm{fault}} + \mathrm{a}_2\mathrm{FI}^2_{\mathrm{fault}} \tag{3.10}$$

where a_0, a_1 and a_2 are empirical coefficients obtained from fitting the polynomial regression to the data and FI is the fault intensity level which quantifies the fault severity. The calculation of FI is different for each fault and is detailed later in this section.

Using the same methodology, in this thesis, the data from the studies of Mehrabi and Yuill [91], Noël et al. [30], Cheung and Braun [92] and Kim et al. [93] was used to parametrize their fault effects as in Equation 3.10. Additionally, the data from a simulation of a Dymola model of a heat pump was also used.

Dymola model

A model of a variable-speed, water-to-water, propane heat pump was developed in the Dymola simulation environment. The model was

based on TIL 3.6 library and fluid properties were provided by the TILMedia 3.6 library [94]. The compressor model for mass flow and power consumption was based on a correlation obtained from Copeland scroll compressors manufacturer's data that was dependent on the evaporation and condensing temperature and the compressor frequency. The frequency was controlled in the model to reach the required heating capacity. The heat exchangers were modelled using a detailed approach based on the design and geometry of selected commercial heat exchangers from the ALFA LAVAL brand. The heat transfer coefficients were selected based on typical literature values, being 5000 W/m^2K and 2000 W/m^2K for propane and water, respectively. The expansion valve model was simulated as an orifice with adjustable opening that regulates the flow of propane through the evaporator to attain a given superheating and avoid any liquid entering the compressor. The model also counts with a refrigerant tank to adjust the refrigerant volume.

Simulations with the propane heat pump were performed in space heating mode and steady-state conditions by keeping constant water temperatures at the inlet of the heat exchangers. Simulations were conducted with inlet and outlet temperatures of 47/55 °C and 30/35 °C in the condenser and 12/9 °C in the evaporator.

The Dymola simulation model allowed to induce faults in the system. However, the model could only simulate static points. Because dynamic change of conditions were not possible, it was not used to directly validate the FDD but to generate the parametrization equations. Different fault severity levels were included for each of the faults considered [60].

The faults related to the charge were simulated by varying the refrigerant mass in the circuit with respect to the nominal conditions. Analogously, the liquid line fault was simulated by increasing the pressure drop in the liquid line with respect to normal operation. The compressor leakage was reproduced by circulating a fraction of the refrigerant flow to the inlet of the compressor, which also affects the refrigerant enthalpy at the compressor inlet. The heat transfer reduction in the heat exchangers was simulated with a reduction of the convective heat transfer coefficient. Table 3.4 shows the simulated faults and their intensity.

Table 3.4: Simulated fault intensity minimum and maximum levels in percentage of the fault-free conditions (FI(%)) and normalized quantified values (FI_{fault}) for the DYMOLA model.

Fault type	Simulation method	FI(%)	FI_{fault}
UC	Excess of refrigerant charge	-30, -10	-0.3, -0.1
OC	Defective refrigerant charge	10, 30	0.1, 0.3
CVL	Recirculation of refrigerant in compressor	10,50	-0.1, -0.5
IHX	Reduction of heat transfer coefficient	10, 50	-0.008, -0.065
OHX	Reduction of heat transfer coefficient	10, 50	-0.13,-0.36
LL	Increase of liquid line pressure drop	15, 3600	0.2, 48.2

The FI levels applied in the simulations are normalized with respect to the nominal fault-free values using the definitions by [79], given as:

$$\mathrm{FI_{UC,OC}} = \frac{\mathrm{m_{r\_fault}} - \mathrm{m_{r\_fault-free}}}{\mathrm{m_{r\_fault-free}}} \tag{3.11}$$

$$\mathrm{FI_{IHX,OHX-air}} = \frac{\dot{\mathrm{V}}_{\mathrm{fault}} - \dot{\mathrm{V}}_{\mathrm{fault-free}}}{\dot{\mathrm{V}}_{\mathrm{fault-free}}} \tag{3.12}$$

$$\mathrm{FI_{LL}} = \frac{\Delta \mathrm{P_{fault}}}{\Delta \mathrm{P_{fault-free}}} \tag{3.13}$$

$$\mathrm{FI_{CVL}} = \frac{\dot{\mathrm{m}}_{\mathrm{r\_fault}} - \dot{\mathrm{m}}_{\mathrm{r\_fault-free}}}{\dot{\mathrm{m}}_{\mathrm{r\_fault-free}}} \tag{3.14}$$

where m_{r_fault} is the propane charge for faulty conditions, $m_{r\_fault-free}$ is the nominal propane charge, $\dot{V}_{fault}$ is the fluid mass flow for the current fault level, $\dot{V}_{fault-free}$ is the fluid flow for the no-fault condition, ΔP_{fault} represents the liquid line pressure drop with the fault,

$\Delta P_{fault-free}$ the liquid line pressure drop without the fault, $\dot{m}_{r\_fault}$ is the refrigerant mass flow for the fault condition and $\dot{m}_{r\_fault-free}$ is the refrigerant mass flow when no fault is present.

Parametrizing equations

The results from the Dymola model, together with the ones from the literature [91, 30, 92, 93] are used to parametrize the fault effects. Table 3.5 shows the results of the characterization of fault data from the literature and the model for different features of the heat pump. Each feature could have an increasing or decreasing trend depending on the effect of the fault.

Table 3.5: Parametrizations of FIR for features in VSHP units. "+": indicates an increasing trend, "-": indicates a decreasing trend.

Fault	Feature	Trend	a0	a1	a2	Reference
UC	W_{comp}	+	0.9947	-0.0355	0.3627	Dymola sim., heating, water-to-water, TXV
	T_{sc}	-	-0.30683	19.07352	4.37692	[91], heating, air-to-air, TXV
	T_{evap}	-	0.0623	2.9257	-0.1663	[30], VSHP,heating, EEV
	T_{co}	+	-0.4546	3.34	35.86	Dymola sim., heating, water-to-water, TXV
	mr	+	1.0018	-0.2015	0.0681	Dymola sim., heating, water-to-water, TXV
	T_{cond}	-	-0.64	27.527	35.975	[30], heating, air-to-water, EEV
OC	W_{comp}	+	0.9947	-0.0355	0.3627	Dymola sim., heating, water-to-water, TXV
	T_{sc}	+	-0.30683	19.07352	4.37692	[91], heating, air-to-air, TXV
	mr	-	1.0018	-0.2015	0.0681	Dymola sim., heating, water-to-water, TXV
	T_{evap}	+	0.0623	2.9257	-0.1663	[30], heating, air-to-water, EEV
	T_{co}	+	-0.4546	3.34	35.86	Dymola sim., heating, water-to-water, TXV
	T_{cond}	+	-0.0133	2.5639	28.339	Dymola sim., heating, water-to-water, TXV
LL	COP	-	0.9934	0.1253	-0.4793	[92], heating,air-to-water, EEV
	T_{sc}	-	1.2102	-46.944	29.121	[92], heating,air-to-water, EEV
	T_{ll}	+	0.5397	-16.438	49.951	adapted from [93], cooling, air-to-air, EEV
	T_{sh}	+	0.5397	-16.438	49.951	[92], heating,air-to-water, EEV
IHXF	W_{comp}	+	0.9993	-0.0107	0.1786	[30], heating, air-to-water, EEV
	T_{sc}	+	0.0365	-4.6288	5.8446	[30], heating, air-to-water, EEV
	T_{cond}	+	0.01	-2.7512	3.6204	Dymola sim., heating, water-to-water, TXV
	T_{co}	+	0.0156	-3.9179	5.469	Dymola sim., heating, water-to-water, TXV
OHXF	W_{comp}	+	1.0044	0.1989	0.6576	[30], heating, air-to-water, EEV
	T_{sc}	-	0.0818	4.5071	6.5839	[30], heating, air-to-water, EEV
	T_{co}	+	-0.0189	14.344	48.259	Dymola sim., heating, water-to-water, TXV
	T_{cond}	+	0.1225	4.1881	13.36	[30], heating, air-to-water, EEV
	T_{sh}	+	-0.0337	12.604	19.567	Dymola sim., heating, water-to-water, TXV
	T_{evap}	-	-0.0529	-1.3615	-11.473	[30], heating, air-to-water, EEV
CVL	W_{comp}	+	1.0004	-0.7086	0.2482	Dymola sim., heating, water-to-water, TXV
	mr	-	0.9999	0.2595	-0.0863	Dymola sim., heating, water-to-water, TXV
	T_{sh}	+	0.0675	-42.47	27.29	Dymola sim., heating, water-to-water, TXV
	T_{co}	+	0.0637	-33.42	31.794	Dymola sim., heating, water-to-water, TXV

The criteria used for selecting the fault parametrization equations are the following:

- parametrizations are proposed only for those features whose trend is common between diverse VSHP studies
- parametrizations from experimental studies that have been shown to be valid for different technologies are adopted
- when parametrizations valid for different technologies are not available, the adopted ones were those obtained from the air-to-water VSHP study by Noel et al. [30].
- when no parametrization was available for VSHP air-to-water units, the parametrization were derived using the results from the water-to-water heat pump model Dymola simulations, assuming that a common behaviour is expected between VSHP units of different kind. This hypothesis is to be proved with further experimentation.

Some faults like refrigerant leakage or liquid line restriction do not appear suddenly, and their effect worsens with time. Taking into account this, the fault intensity parametrization in Equation 3.10 were expanded to include a linear time degradation term specific for each fault type as:

$$FIR_{feature}(t) = a_0 + a_1(b_0 + b_1 t)_{fault} + a_2(b_0 + b_1 t)^2_{fault} \qquad (3.15)$$

where b_0 and b_1 are empirical coefficients that define the variation of the fault intensity in time and t is time in hours. Taking into account the information of Sections 2.2 and 2.3 about the incidence of faults and its effects , Table 3.6 shows a conservative value of degradation considered and the coefficients obtained for different faults.

Table 3.6: Parametrizations to estimate the time evolution of fault intensity (FI).

Fault	b0	b1	Degradation
CVL	1.2E-17	-4.00E-6	3.5% refrigerant flow leakage per year
UC	-0.00238	1.33E-05	10% refrigerant mass loss per year
IHXF, OHXF	0.0084	-1.00E-05	8% reduction of water or air flow per year
LL	0.00238	-1.33E-05	10% increase of pressure in liquid line per year

Applying Equation 3.15 and the data from Table 3.5 and 3.6 to the healthy data from the TRNSYS model explained at the beginning of Section 3.5.1, faulty data was obtained to do a preliminary validation of the FDD monitor developed. Figures 3.14 and 3.15 show the FIR on different features for UC and IHXF, respectively.

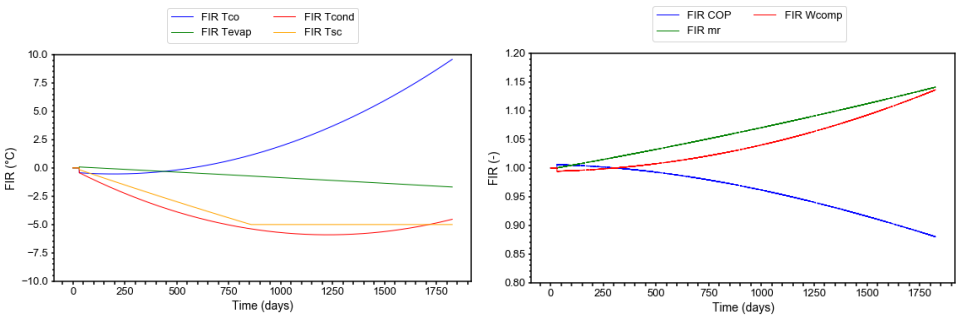

(a) **(b)**

Figure 3.14: Modelled fault impact ratios for different features during 5 years: UC fault.

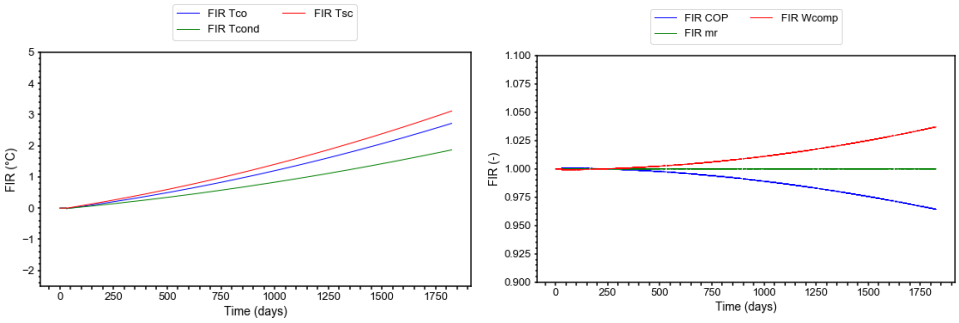

(a) **(b)**

Figure 3.15: Modelled fault impact ratios for different features during 5 years: IHXF fault.

3.5.3 Validation results

Steady-state detector

For the validation of steady-state detection algorithm, it was necessary to define the variable or variables that determine when the system is in steady-state.

The compressor speed regulation poses an additional challenge to the detection of steady-state operation in VSHP, because of the higher variability in the operation variables which results from frequency regulation. To work correctly with the step time of 10 minutes, the window size and queue length of the SSD were changed to 3 and 6, respectively.

Based on the same principle as Kim et al. [93], a method based on performance variables was adopted in the present study to detect quasi-steady state periods. Of the different features considered, COP is the operation variable indicating whether there is a possible efficiency loss. Because of this, COP was selected as one possible candidate to determine steadiness. Along with the COP, compressor electrical consumption (W_{comp}) and thermal power (Q_{heat}) were chosen as key performance variables to detect quasi-steady state.

Figure 3.16 shows the application of the SSD to COP, W_{comp} and Q_{heat} for the same period of time of the TRNSYS simulation. Each

data point represents 10 minutes. When Q_{heat} is in steady-state, W_{comp} and COP were also on steady-state. Therefore, in this case, Q_{heat} was selected as the main indicator of steady-state conditions because being the most restrictive.

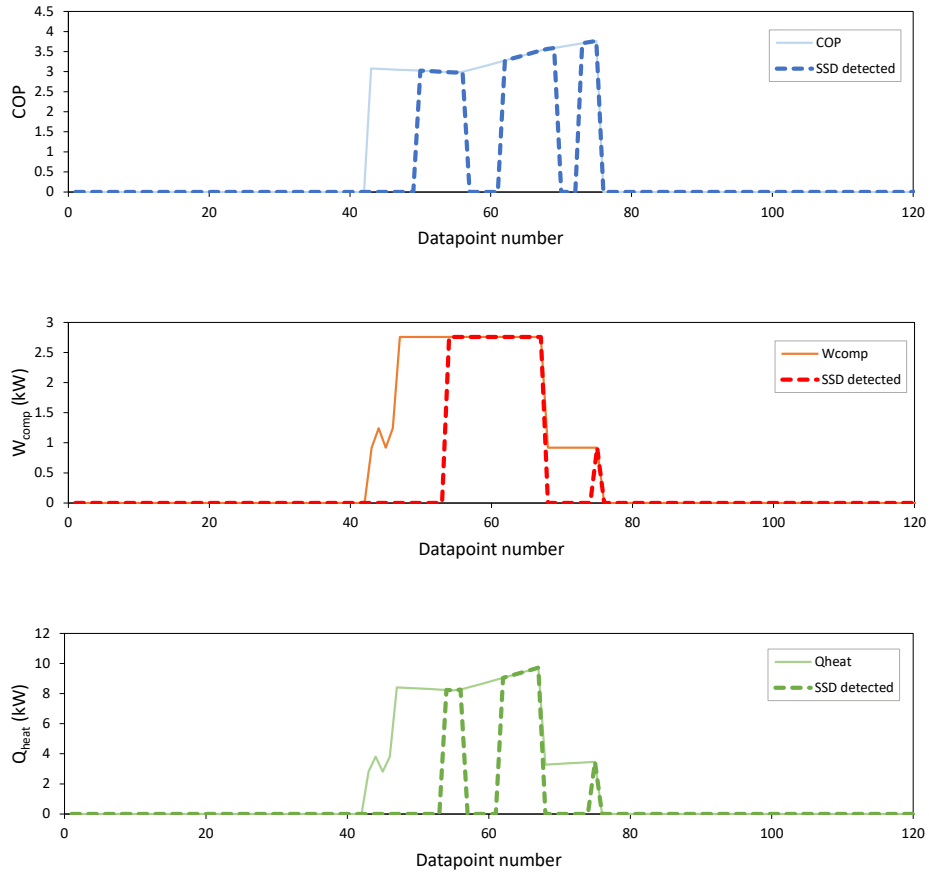

Figure 3.16: SSD applied to different features of the TRNSYS model. The time between data points is 10 minutes. The SSD detected series takes the same value as the feature when steady-state is detected.

The performance of the steady-state detector was robust, meaning that all the points detected were far from the heat pump start periods. However, because of the fluctuation of operation variables resulting from frequency regulation, some steady-state phases are not detected by the algorithm. This could be solved but at the cost of increasing

the number of false positives. However, this configuration was selected to improve the quality of the data sent to the regression models and reduce the false positives.

In Figure 3.17 there is an example of the SSD used with the TRNSYS data. The SSD detected series have the same value as the COP series when steady-state in Q_{heat} is detected. As shown, the detector identified correctly the steady-state points. Because Q_{heat} was more restrictive than COP, some segments of the COP series that could be considered as steady are not detected.

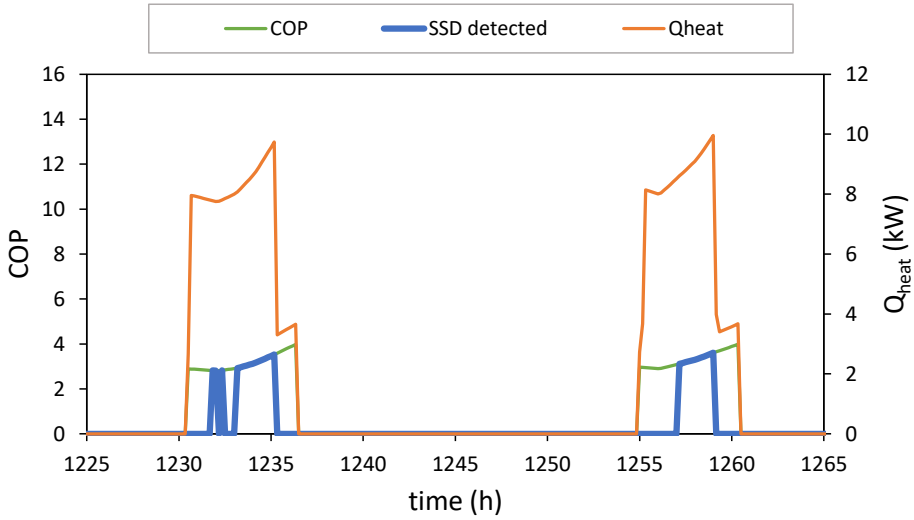

Figure 3.17: Performance of the steady-state detector for the TRNSYS model. The SSD is applied to Q_{heat}. The SSD detected series has the same value as COP when steady-state in Q_{heat} is detected.

Performance of input space and regressions forecasting

The regressions were trained and tested with results from the dynamic TRNSYS model plus the fault parametrization equations. The model generates one year of data with 10 minutes frequency. The data from this period is extended in order to obtain a larger data series of 5 years, so the fault effects from the parametrization methods have enough time to increase. The algorithm training phase lasts one week. After this training phase, the regressions algorithm predicts the features be-

haviour and also self-trains new centroids in case of new data with different conditions from those of the learning period appears.

The data was classified into different clusters of the Input Space, depending on the value of the driving variables T_{amb}, $T_{cond,out}$ and f. For each of these clusters, a fault-free model of the different features was generated by solving the Equation 3.16.

$$\begin{aligned}\hat{y} =& \theta_0 + \theta_1 \mathrm{T_{amb}} + \theta_2 \mathrm{f} + \theta_3 \mathrm{T_{cond,out}} + \theta_4 \mathrm{T_{amb}^2} + \theta_5 \mathrm{f}^2 + \theta_6 \mathrm{T_{cond,out}^2} + \\ & \theta_7 \mathrm{T_{amb}f} + \theta_8 \mathrm{T_{amb}T_{cond,out}} + \theta_9 \mathrm{fT_{cond,out}} + \theta_{10} \mathrm{T_{amb}^3} + \theta_{11} \mathrm{f}^3 + \\ & \theta_{12} \mathrm{T_{cond,out}^3} + \theta_{13} \mathrm{T_{amb}fT_{cond,out}} + \theta_{14} \mathrm{T_{amb}^2 f} + \theta_{15} \mathrm{T_{amb}^2 T_{cond,out}} + \\ & \theta_{16} \mathrm{f}^2 \mathrm{T_{amb}} + \theta_{17} \mathrm{f}^2 \mathrm{T_{cond,out}} + \theta_{18} \mathrm{T_{cond,out}^2 T_{amb}} + \theta_{19} \mathrm{T_{cond,out}^2 f}\end{aligned} \tag{3.16}$$

Table 3.7 shows the value of the regression parameters of COP and T_{co} for the cluster with T_{amb} of 11 ºC, $T_{cond,out}$ of 45 ºC and f at 64 Hz.

Table 3.7: Regression parameters for COP and compressor outlet temperature.

Parameter	COP	T_{co}
θ_0	0.00E+00	0.00E+00
θ_1	3.61E-03	-2.33E-02
θ_2	0.00E+00	0.00E+00
θ_3	0.00E+00	0.00E+00
θ_4	3.72E-03	-2.33E-02
θ_5	3.61E-03	-2.33E-02
θ_6	3.61E-03	-2.33E-02
θ_7	0.00E+00	0.00E+00
θ_8	0.00E+00	0.00E+00
θ_9	0.00E+00	0.00E+00
θ_{10}	3.86E-03	-1.77E-03
θ_{11}	3.72E-03	-1.25E-02
θ_{12}	3.72E-03	-1.25E-02
θ_{13}	3.61E-03	-2.33E-02
θ_{14}	3.61E-03	-2.33E-02
θ_{15}	3.61E-03	-2.33E-02
θ_{16}	0.00E+00	0.00E+00
θ_{17}	0.00E+00	0.00E+00
θ_{18}	0.00E+00	0.00E+00
θ_{19}	0.00E+00	0.00E+00

There are several parameters with a 0 value which can be eliminated to increase the computational efficiency of the solution. Nevertheless, as the time required to reach the solution was small(less than a second), all the parameters were maintained.

The error margin permitted between the prediction and the measurements was two times the RMSE obtained during training. Therefore, for a given feature, if the deviation is larger than this margin it will be considered as a deviation event. Figure 3.18 shows a representation of the COP prediction with the allowed error margin when no fault is present. In this case, the COP prediction by the regressions (Prediction) and the reference simulated data of the TRNSYS model (RealDataFault) are the same and the error margin (red shadowed area) is small because the RMSE of the training was small as well.

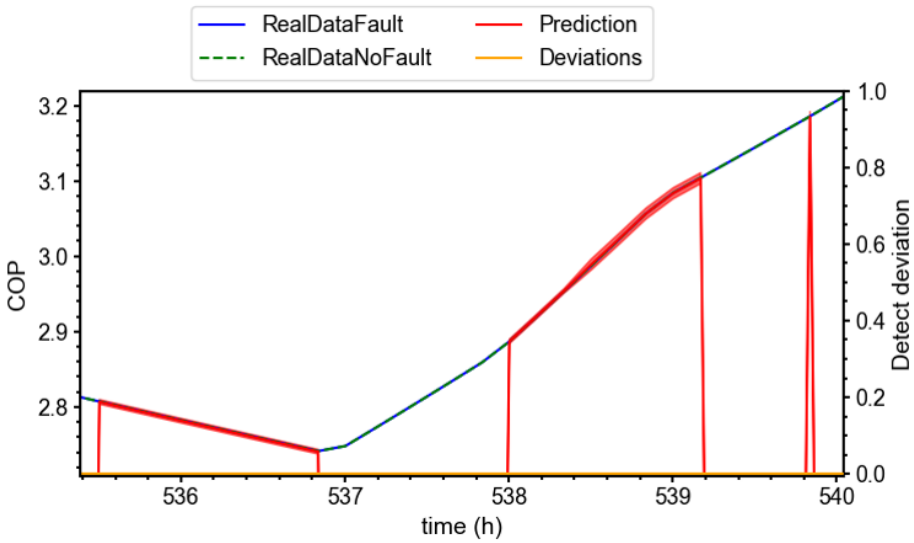

Figure 3.18: Performance of the regression model for the COP during the first year of the TRNSYS model. For the period depicted, the series has no fault present, therefore RealDataFault is equal to RealDataNoFaul.

When testing the algorithm with fault-free data, the features T_{evap} and T_{co} yielded a number of false positives. As explained in the beginning of this chapter, the false alarm rate (FAR) represented the fraction of erroneous fault warnings with respect to the sum of non-faulty and erroneous detections by the FDD system. Those features had a FAR different from zero because their value fluctuated more than features like COP.

For T_{evap}, there were 379 false positives that, in a total of 13167 predictions, made a FAR of 2.87%. For T_{co} , there were 132 deviations from 13167 predictions, making a FAR of 1%. The FAR was still rather low for these features, but this should not affect the FDD performance, since deviations of other features are neglected by the algorithm until there is a significant drift of the COP value.

The quality of the regressions was also assessed by calculating the values of the RMSE. Equation 3.17 shows how the RMSE was calculated.

$$\text{RMSE} = \sqrt{\frac{\sum_{\text{i=1}}^{\text{n}}(\text{Predicted}_\text{i} - \text{Actual}_\text{i})^2}{\text{N}}} \tag{3.17}$$

The RMSE has the same units of the values that are used in the equation and its magnitude is related to the scale of the measurement. The RMSE for the training and the monitoring phases using the fault-free series is shown in Table 3.8.

Table 3.8: RMSE values for the training (one week of data) and the first month of monitoring (when no fault is present) of the different features of the heat pump. The average value of each feature is given to understand the RMSE magnitude

Feature	RMSE Training	RMSE Monitoring	Average value
COP	4.45E-07	3.36E-07	3.09
W_{comp} (kW)	9.51E-09	9.21E-09	2.60
Q_{heat} (kW)	2.61E-06	1.88E-06	7.95
T_{sc} (°C)	1.24E-07	9.26E-08	5.00
T_{sh} (°C)	4.97E-08	9.75E-08	5.00
T_{evap} (°C)	7.74E-05	6.84E-05	-3.90
T_{cond} (°C)	1.38E-05	1.05E-05	55.00
T_{co} (°C)	1.52E-04	1.30E-04	77.90
T_{ihx2} (°C)	1.36E-05	9.55E-06	50.00
m_r (kg/s)	1.17E-10	9.08E-11	0.045

As can be seen, the errors were very small, near zero. This is because the modelled data series were smooth without any noise. Thus, the predictions tend to be accurate. The small RMSE values could be a sign of overfitting, which means that the model performs well on the training data, but it does not generalize well to new data [95]. However, the model is correctly fitted because the RMSE between the training and the monitoring was on the same order, which discards the overfitting.

Even though the RMSE was very small for the features, the regressions yielded false positives for T_{evap} and T_{co}. Event though the deviations between the prediction and the real value were very small, they were outside of the error margin of the prediction, therefore they were detected as deviations of that specific feature. However, the COP

is the feature that triggers the warnings, so, until a deviation in COP is detected, the deviation of other features are only informative, and will be used only for diagnosis.

For an insight on the performance of the regressions for predicting ideal behaviour at detection time, the absolute residuals (i.e. difference between the feature at fault-free conditions and under fault conditions) were compared. Table 3.9 compares the residual of the prediction and the no-fault series at detection. In this table, X_{ff}-X_{fail} represents the difference between one point of the fault free series and the same point with fault. The column X_{pred}-X_{fail} represents the difference between the prediction of the regressions models for that same point of the series, and the fault series.

Table 3.9: Comparison between the prediction and fault-free series for each fault. Where: X_{fail} is the series with fault data, X_{ff} is the fault-free data, X_{pred} is the predicted data by the algorithm.

Fault/feature	X_{ff}-X_{fail}	X_{pred}-X_{fail}
UC		
COP	0.05	0.04
W_{comp} (kW)	-0.012	-0.011
T_{sc} (ºC)	3.6	2.9
T_{evap} (ºC)	0.4	0.4
T_{cond} (ºC)	4.5	3.3
T_{co} (ºC)	-0.1	-0.1
m_r (kg/s)	-2.51E-03	-2.14E-03
OC		
COP	0.05	0.05
W_{comp} (kW)	-0.046	-0.045
T_{sc} (ºC)	-5.8	-5.8
T_{evap} (ºC)	-0.9	-0.9
T_{cond} (ºC)	-3.3	-3.3
T_{co} (ºC)	-3.7	-3.7
m_r (kg/s)	2.50E-03	2.54E-03
CVL		
COP	0.05	0.04
W_{comp} (kW)	-0.044	-0.035 5
T_{sh} (ºC)	-1.0	-0.7
T_{co} (ºC)	-0.8	-0.6
m_r (kg/s)	-3.25E-04	2.64E-04
IHXF		
COP	0.05	0.05
W_{comp} (kW)	-0.012	-0.012
T_{cond} (ºC)	-0.9	-0.9
T_{co} (ºC)	-1.3	-1.3
OHXF		
COP	0.05	0.04
W_{comp} (kW)	-0.013	-0.010
T_{evap} (ºC)	0.9	0.9
T_{co} (ºC)	-0.7	-0.7
LL		
COP	0.05	0.04
W_{comp} (kW)	-0.011	-0.010
T_{sc} (ºC)	5.0	4.5
T_{sh} (ºC)	-4.7	-4.7
T_{r_ihx2} (ºC)	-0.9	-0.9

As can be seen, the values between the columns X_{ff}-X_{fail} and X_{pred}-X_{fail} were almost the same, this means that the prediction values of the regression models (X_{pred}) were similar to the real values (X_{ff}) and therefore, the fault-free models represent accurately the healthy behaviour.

Fault detection

For the validation of the fault detection module, data series generated from the TRNSYS model data and applying the fault parametrizations equations were used as inputs to the FDD monitor. For each fault a series was created, consisting in one month of fault free data and the following 5 years with the presence of a fault. The use of 5 years was required to fully develop the effects of the parametrized faults.

The algorithm used one week of data for the training phase and monitored the heat pump behaviour for the remaining time. The fault detection module analyses the residuals between the measurements and the predictions. When the COP residuals are larger than the deviation allowed, the boolean variable "COP fault" becomes True. When a number of deviations are accumulated in a certain time interval (80% of all collected samples), a warning flag is triggered. For the TRNSYS series, with a sample frequency of 10 minutes, the number of faults needed for a warning flag was five, which is the equivalent to a 50 minute period with consistent drift events.

Figure 3.19 shows an example of fault detection and COP drift warning for the UC fault data series. In Figure 3.19a COP fault is a binary variable representing the state of the deviation between the measurement and the prediction (0: no deviation, 1: deviation). In Figure 3.19a, the fault ratio (number of deviations over total samples) increases as more deviations are detected, but not enough to raise a warning. In Figure 3.19b, the fault ratio reaches a value above the 80% threshold, hence, a warning flag is triggered, meaning that there exists a consistent loss of performance. This activates the diagnosis module, which analyses the residuals of all features to provide a diagnosis.

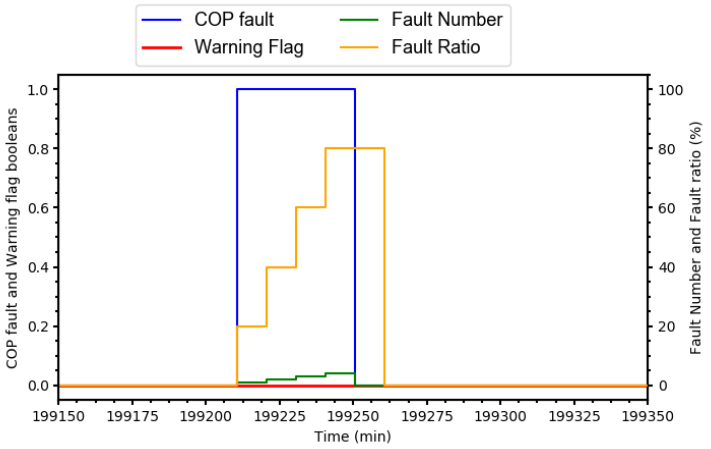

(a)

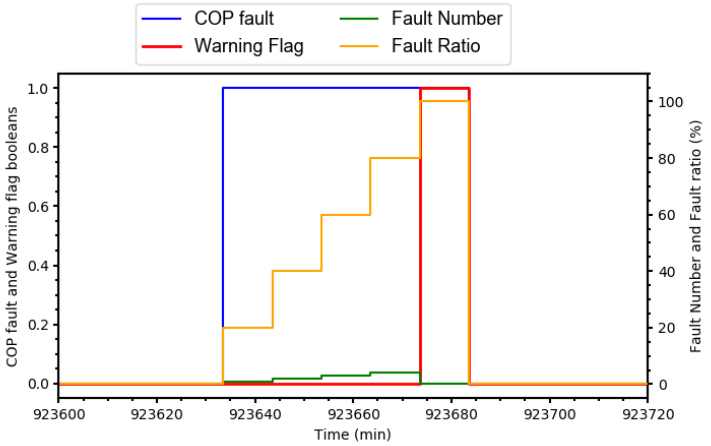

(b)

Figure 3.19: Example of two cases with results of the COP fault detection and drift warning module with the presence of UC fault. Generated by applying the fault parametrizing equations to the TRNSYS model data.a) at the first year, the fault effect is small, b) at the second year, the fault effect is higher, being enough to be detected.

Fault diagnosis

As indicated previously, the fault diagnosis module is called when a consistent COP drift is detected by the FDD monitor. Then, the

other features of the heat pump are compared with their corresponding no-fault model. Depending on the trend of the features, the fault is diagnosed as explained in Section 3.4.6. The result from the fault identification module is an enumerated variable with the following values: -1, no fault; 0 there is a fault that cannot be diagnosed; 1, UC fault; 2, OC fault; 3, CVL fault; 4, IHXF fault; 5, OHXF fault and 6, LL fault.

The diagnosis results by the FDD monitor for each of the parametrized faults are shown in Figure 3.20. In some cases, the algorithm detected a fault (fault identifier equals 0) but it was still not possible to diagnose it until the incidence increases.

It also should be noted that for LL and OHXF, there were fault warnings (fault identifier equals 0) before the hour 500, however, the FIR parametrizations caused a misdiagnosis after that period as Figures 3.20d and 3.20f show. This was because, the parametrization models are non-monotonic, meaning that the fault effects go from increasing to decreasing along the time. To avoid that, the models could be improved by increasing the regression polynomial order. However, the data below 500 h for LL and OHXF was neglected as it could mislead the results

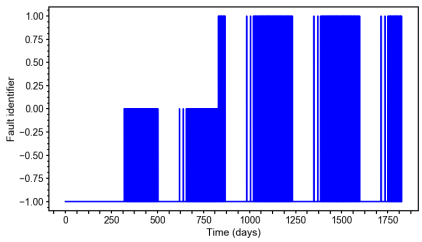

(a) Fault identification for UC

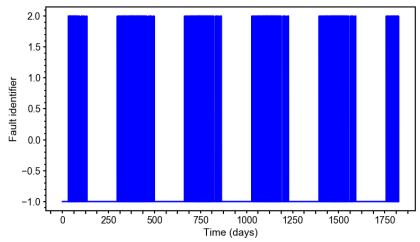

(b) Fault identification for OC

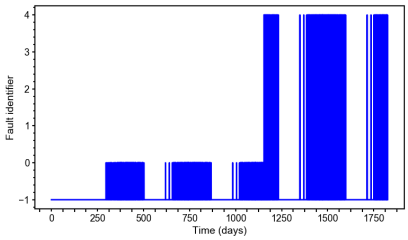

(c) Fault identification for IHXF

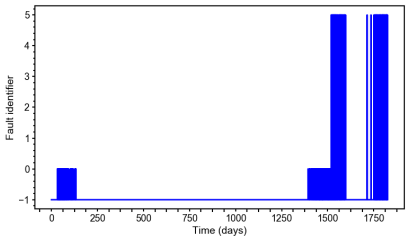

(d) Fault identification for OHXF

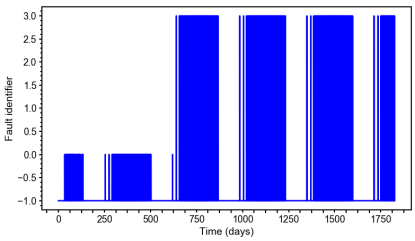

(e) Fault identification for CVL

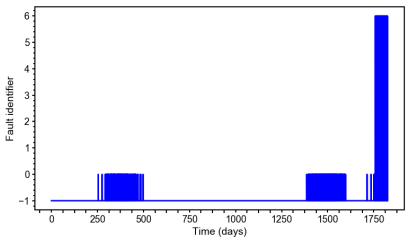

(f) Fault identification for LL

Figure 3.20: Results of the diagnosis module for different faults where fault identification is indicated with an enumerated variable. The heat pump was turned off during the cooling season. Fault identifier: -1: no fault, 0: fault detected but not identified, 1: UC fault, 2: OC fault, 3: CVL fault, 4: IHXF fault, 5: OHXF fault, 6: LL fault.

On the one hand, the fault detection time in these results (fault identification equals 0) was short for the cases of OC, OHXF and CVL, being not realistic since the effects of measurement noise and limitations due to sensor accuracy are neglected. This leads to detection of COP losses below 0.05. On the other hand, the fault diagnosis takes more time (fault identification between 1 and 6). The diagnosis is only possible when all the required features have deviated following a given trend and after surpassing a established limit, which is included in the

diagnosis logic. This limit is used to decouple faults and is inclusive of sensor accuracy limits. Those situations explain the large time separation between the fault detection (fault identification equals 0) and the fault diagnosis (fault identification between 1 and 6), as could be seen in Figures 3.20a and 3.20c. It should be noted that the fault parametrization equations induced a fault that worsens with time. Therefore, it was normal that the diagnosis required time until the fault effects were enough severe.

For tests with real equipment, it is expected that detection and diagnosis will be closer, because the fault detection will not be as fast due to the noise and other limitations of sensors. The exception are sudden faults as OC that appears suddenly on the equipment, and are diagnosed immediately as Figure 3.20b shows.

General performance

In Section 3.2 the indicators accuracy and false alarm rate (FAR) were described. In the present section, these and other performance indicators were applied to the results obtained in the first validation with the simulation model.

Aside from accuracy and FAR, the indicators missed detection rate (MDR), missdiagnosis rate (MR), and detection time (Dt) were used to quantify the performance of the monitor. For the nomenclature, it is considered *Positive* when the system detects a fault, *Negative* when not, *True* when the result of the algorithm matches reality and *False* when the algorithm results do not match reality. For reference, the data series without faults was used to determine the True and False conditions with respect to reality. In the definitions below, a fault warning was an alarm raised by the FDD when a consistent drift of the COP was detected.

Missed detection rate (MDR): it represents the fraction of undetected faults with respect to the sum of detected and undetected faults by the FDD system. In the equation of MDR below, a False Negative implies that, under the presence of a fault, the algorithm does not raise any warnings.

$$\text{MDR} = \frac{\text{False Negative}}{\text{False Negative} + \text{True Positive}} \tag{3.18}$$

Detection time (Dt): time since the COP residual is higher than 0.05 until the system raises a warning on COP drift.

$$\text{Dt} = \text{t}_{\text{COPWarning}} - \text{t}_{\text{faultStart}} \tag{3.19}$$

Misdiagnosis rate (MR): This indicator represents the capability of the FDD to correctly diagnose the faults detected. In the equation below False Diagnosis implies that a fault is detected, but the diagnosis does not match the real fault.

$$\text{MR} = \frac{\text{False Diagnosis}}{\text{False Diagnosis} + \text{True Diagnosis}} \tag{3.20}$$

$\text{FIR}_{\text{COPdiagno}}$ is additionally use to quantify the performance loss until the fault is diagnosed. This indicator represents the fault impact ratio (FIR) value for the COP when the system is able to diagnose a fault. It gives an indication of the degree of deterioration of the system when the FDD monitor is able to isolate a fault. $\text{COP}_{\text{fault}_\text{d}\text{iagnosed}}$ is the COP when a fault is diagnosed, and $\text{COP}_{\text{fault}-\text{free}}$ is the COP value without fault.

$$\text{FIR}_{\text{COPdiagno}} = \frac{\text{COP}_{\text{fault}_\text{d}\text{iagnosed}}}{\text{COP}_{\text{fault}-\text{free}}} \tag{3.21}$$

Table 3.10 lists all the key indicators for the different faults calculated using the 5 years data generated for algorithm testing. As described above, during the first month the data represented a system without faults, while the fault function was applied at the beginning of the second month until the end of the data set. The first week of data was used to train the algorithm, period after which the algorithm monitored the performance of the heat pump or activated self-training if the operating conditions surpassed the operation limits of the initial training period.

Table 3.10: Key indicators for the FDD performance.

Fault	FAR(%)	MDR(%)	MR(%)	Accuracy(%)	Dt(h)	$FIR_{COPdiagno}$
UC	0	0.11	0	100	0.5	0.974
OC	0	35.16	0	100	0.0	0.984
CVL	0	3.37	0	100	49.5	0.958
IHX	0	4.64	0	100	985.0	0.985
LL	0	0.28	0	100	119.0	0.974
OHX	0	0.58	0	100	0.0	0.983

To determine the false alarm rate, it was calculated all the false positives by the algorithm in the fault free region of each fault data series (i.e. in the period comprising the first month and the remaining time until fault detection). Similarly, for calculating MDR, the False negatives where undetected drifts calculated for the period in which the COP residual was above 0.05 after the first month. The same reference was used for Dt, being $t_{faultStart}$ the first point when the COP residual (COP-$COP_{fault-free}$) was higher than 0.05. A residual limit of 0.05 (equivalent to about FIR=0.986 and 1% loss of COP) was adopted to evaluate the algorithm performance for these indicators as it was considered that a deviation below this value would not be detectable in a real system due to sensors accuracy.

As shown in Table 3.10, the FAR was 0 for all cases and the accuracy was 100%, which means that the algorithm did not generate false alarms in the non-faulty region. In the case of the MDR, all the values were small, with the exception of the OC fault. In the case of OC, due to the automatic self-training, the module trains with faulty data after overcharge. To reduce this possibility, the algorithm will need to stop training when a warning occurs. However, this was not implemented in the current version of the FDD monitor.

Regarding Dt, for OC and LL there was an immediate warning for COP drift, with a value of 0 for these faults, while for UC the detection time Dt was 0.5 h. For CVL, IHXF and OHXF the detection time ranged from 49 to 985 hours (41 days) after the COP has deviated for the first time by a value of 0.05. This longer detection time was due to the COP residual value fluctuating slowly in the period since the COP residual reaches 0.05, until a consistent drift occurs and sufficient information has been collected for a warning to be raised.

The indicator MR was 0 in all cases but this could be the result of using the same knowledge about feature trends for generating the fault parametrizing equations and the diagnosis table. Testing MR was nonetheless useful to consolidate the implementation and confirm that the algorithm logic works correctly. However, additional experimental testing is needed to assess the chart definitions used for diagnosis.

On the other hand, the indicator $FIR_{COPdiagno}$ (FIR of COP at diagnosis) shows that the deterioration of system performance was still very small at diagnosis, with a COP loss between 1.5 % to 4.2 %. This indicates that the long time required to reach the diagnosis showed in Figure 3.20 was due to the parametrizing equations that caused a slow decrease of the COP.

3.6 Conclusions

This section has described the development effort done to generate the FDD and its first validation. The state of the art on FDD methodologies has served to select the better methodology for the research. Polynomial regression and expert knowledge were selected as fault-free model generation and diagnosis methodologies respectively.

The FDD monitor was developed in different modules to increase the efficiency of the solution. A novel steady state detector was developed to fix the disadvantages of other SSD, as the need of tuning for each new signal. The use of the input space, ensured the adaptability to different types of conditions and the capability of self-training. The verification of consistent fault makes sure that no false alarms were triggered.

At the first stages of the doctoral thesis there was not data available therefore, a variable-speed heat pump model was developed in TRNSYS to use in the validation. However, the model was not complex enough to simulate faults in the system, therefore, a novel methodology to parametrize the fault effects into equations was generated. These equations were the result of summarizing literature research and the results from a Dymola simulation model of a variable speed heat pump with faults. The parametrizing equations also take into account

the increasing of fault intensity in time.

Those equations were applied to the results of the TRNSYS model to obtain faulty data. The validations showed a good performance of each of the modules of the FDD monitor. A fault could be detected and diagnosed before a 5% of COP drift, with no false alarms triggered. All the faults were correctly diagnosed, but the faults parametrization required long time to fully develop the effects of the faults on all the features. Nevertheless, the FDD monitor has fulfilled with the expectations for this first validation.

CHAPTER 4

Laboratory fault emulation: methodology and results

UNIVERSITAT ROVIRA I VIRGILI
AUTOMATIC FAULT DETECTION IN DOMESTIC HEAT PUMPS
Ivan Bellanco Bellanco

4.1 Introduction

This chapter describes the testing procedures to emulate different faults in one real heat pump in a laboratory environment. This tests are made to increase the knowledge about the fault effects in a variable-speed heat pump and to use this data to validate the Fault Detection and Diagnosis (FDD) monitor with a real heat pump.

The chapter starts with the description of the SEILAB, the laboratory where test were made. Then, the tested heat pump is described. Finally, the faults that were tested and the emulation procedure are explained.

The heat pump had a nominal heating capacity of 10 kW. All the tests were performed at nominal capacity (10.2 kW) and with higher capacity (12.3 kW), to see if the effects were the same at different capacities. The indicator fault intensity (FI) was used to indicate the severity of the fault.

The tests results are analysed and compared with similar studies. All the results from the faults test are available as a dataset in the open-access repository Zenodo [96].

4.2 Semi-virtual environment laboratory framework

The fault tests on a real heat pump were carried out on the Semi-Virtual Energy Integration Laboratory (SEILAB). This laboratory is located in the IREC facilities in Tarragona and its main focus is the testing of HVAC equipment with the Hardware-in-the-loop (HiL) methodology. HiL tesing allows to test equipment in realistic operating conditions provided by dynamic simulations [97]. The simulations send the thermal loadings, user behaviour and climatic conditions, which are replicated by the laboratory. To do so, the SEILAB counts with a walk-in climate chamber to generate the environmental air characteristics and hydraulic thermal test benches for emulating the heat and

the load sources. The test benches consist of a set of hydraulic loops equipped with flow meters, motorized valves, pressure meters and temperature proves to control and measure the system.

The tests are performed by means of a control system created in the laboratory. A LabVIEW interface enables to communicate with the different elements tested in the lab and to collect all the data from the laboratory measurements. The data acquisition system saves the measured data at a sampling time of 10 seconds.

The FDD monitor was running in the same computer of the LabVIEW interface to read the measurements of the heat pump registered by it. The data exchange between the LabVIEW and the FDD monitor was every 10 seconds. At the same time, the FDD monitor was also running in a pocket sized computer. This computer counts with a 64-bit 1,4GHz processor, 1 GB of RAM and the hard drive is an SD card. The pocket sized computer exchanged data every 10 seconds trough TCP/IP connection to the main laboratory interface. Figure 4.1 shows the schematic of the general process.

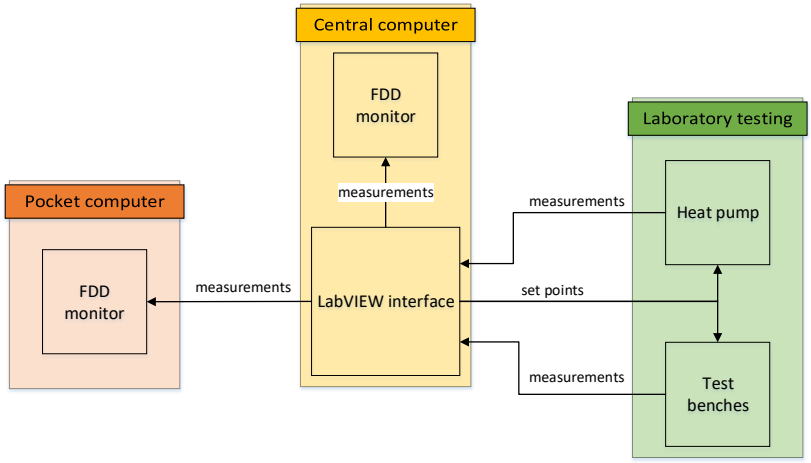

Figure 4.1: General scheme of the laboratory communications.

The heat pump tested was a water-to-water compact unit working in heating mode. The tests were carried out in static conditions to ensure the comparison between the different fault levels. Thus, there

were not dynamic experiments; the required conditions were set as set points in the interface of the laboratory.

The heat pump counted with three different water loops: domestic hot water, space heating and ground source. Each of this loops where coupled with an hydraulic test bench. Nevertheless, the domestic hot water loop was not used during fault emulation because it induced a high fluctuation in the measurements. Figure 4.2 shows a picture of the heat pump prototype and Figure 4.3 shows the scheme of the hydraulic configuration of the tests.

Figure 4.2: Picture of the compact unit tested in SEILAB.

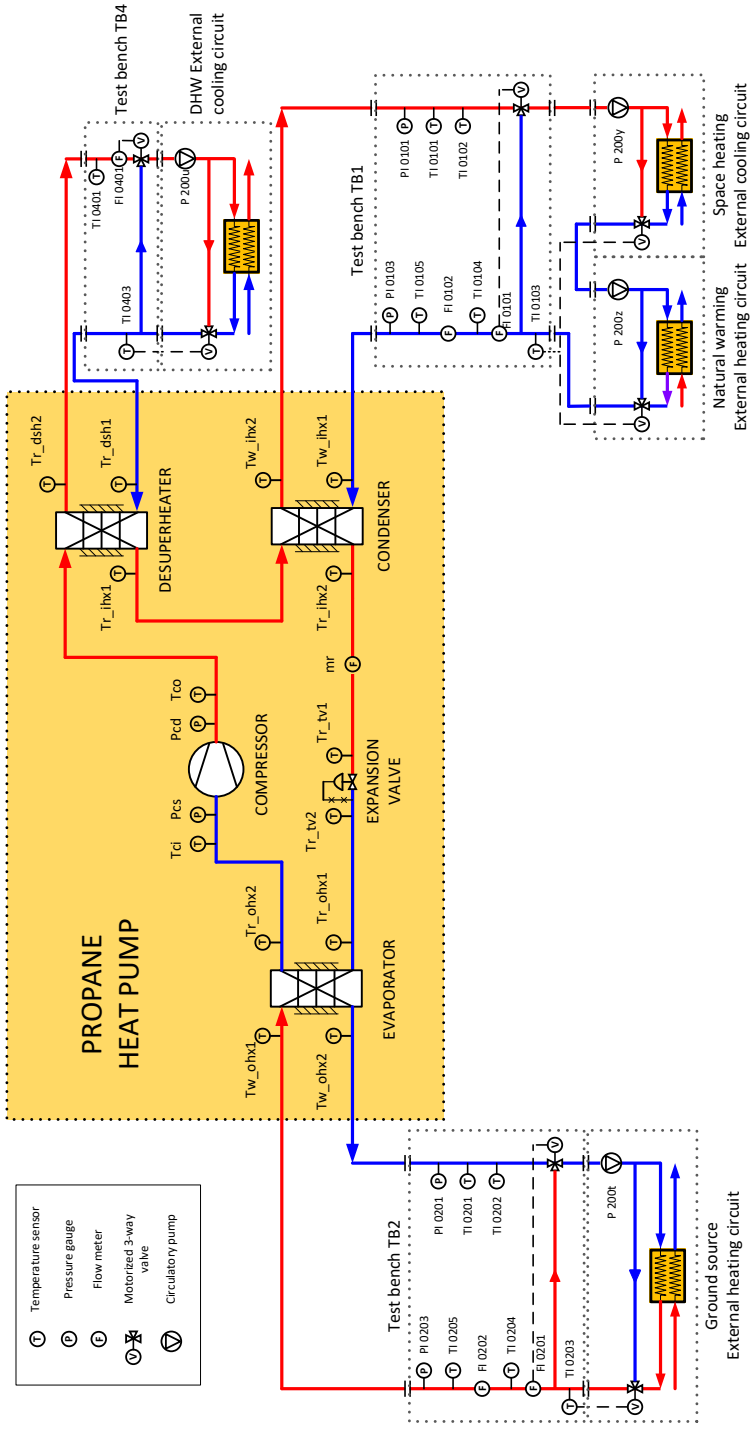

Figure 4.3: Schematic of the mechanical and control systems, illustrating the principle of the semi-virtual environment.

4.3 Description of the tested heat pump

For the present study, a 10 kW, variable-speed water-to-water heat pump was tested. The heat pump used was a prototype charged with 720 grams of propane as the refrigerant. Figure 4.4 shows the heat pump architecture.

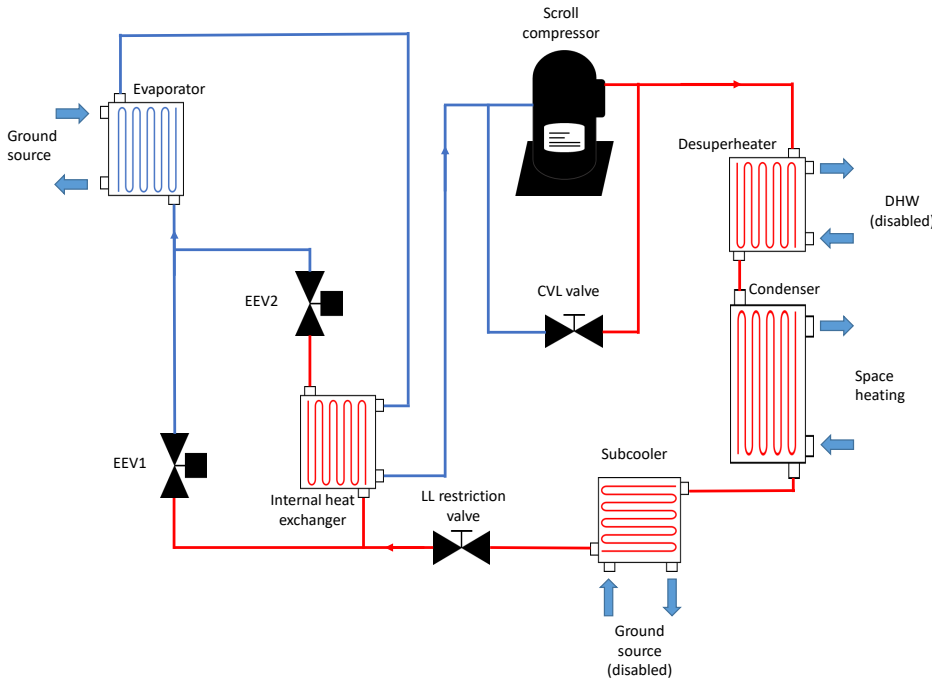

Figure 4.4: Heat pump scheme. The desuperheater and subcooler were not used during the fault tests.

The compressor used was a hermetic scroll type YHV0461U from Emerson. It was specifically designed for propane applications and to meet the requirements of flammable refrigerants. A Carel inverter type power+ was used to control the compressor. Despite the frequency can be controlled by the inverter, there was no speed control by default, therefore in internal control, the speed was always fixed, except for the start-up and shut-down.

Both the condenser and evaporator were brazed plate heat exchangers in countercurrent arrangement. The desuperheater was used

for DHW production. The internal heat exchanger used the heat from the condensed liquid to function as a suction gas superheater and condensed liquid subcooler. Its capacity was fixed by a separate expansion valve (EEV2) controlled by the own heat pump.

The prototype had internal pressure and temperature sensors and a Coriolis flowmeter after the condenser, for the refrigerant mass flow measurement. As explained before, the heat pump has no internal speed control however, an external compressor frequency set point could be sent. A PID control was developed to adapt the compressor frequency to the difference between the condenser water supply temperature and a set point.

The temperatures of the refrigerant circuit were obtained with NTC temperature probes at the suction line and with Pt1000 for the rest of the circuit. The heat duty was measured on the waterside with Pt100 probes and flowmeters. The pressure measurements were obtained with pressure transducers. The compressor speed lecture was provided by the inverter and the power consumption was measured with a multimeter. Table 4.1 shows the manufacturer accuracy data of each sensor. The uncertainty of the tests were calculated using the Guide to Uncertainty in Measurement methods [98].

Table 4.1: Manufacturer's accuracy of the sensors.

Magnitude	Type	Accuracy
Pressure	Piezo-resistive	±1.00%
Refrigerant mass flow meter	Coriolis	±0.10%
Temperature refrigerant liquid side	Pt1000	±0.15 K
Temperature refrigerant gas side	NTC	±0.30 K
Temperature water side	Pt100	±0.25 K
Electrical power	Multimeter	±1.00%
Water Flow	Electromagnetic	±0.50%

4.4 Fault emulation

4.4.1 Outdoor heat exchanger fouling

The outdoor heat exchanger fouling (OHXF) represents a circulating pump malfunction or the accumulation of dirt in the circuit, which reduces the flow on that heat exchanger. For the tested heat pump, the outdoor heat exchanger worked as an evaporator, which used water as a secondary fluid. Therefore, the fault was emulated by reducing the evaporator water flow below the nominal value. The indicator fault intensity (FI) is used to characterize each fault level [79]. The $\mathrm{FI_{OHXF}}$ is shown in Equation 4.1.

$$\mathrm{FI_{OHXF}} = \frac{\dot{\mathrm{V}}_{\mathrm{fault}} - \dot{\mathrm{V}}_{\mathrm{ff}}}{\dot{\mathrm{V}}_{\mathrm{ff}}} \tag{4.1}$$

where $\dot{V}_{fault}$ is the evaporator volumetric water flow for the current fault level and $\dot{V}_{ff}$ is the evaporator volumetric water flow for the no-fault condition. Table 4.2 shows the experimental plan followed for the steady-state tests.

Table 4.2: OHXF steady-state tests experimental plan.

Code	Load (kW)	FI_{OHXF}
OHXF10.1	10.2	-0.100
OHXF10.2	10.2	-0.157
OHXF10.3	10.2	-0.214
OHXF10.4	10.2	-0.271
OHXF10.5	10.2	-0.328
OHXF10.6	10.2	-0.385
OHXF10.7	10.2	-0.442
OHXF10.8	10.2	-0.500
OHXF12.1	12.3	-0.100
OHXF12.2	12.3	-0.157
OHXF12.3	12.3	-0.214
OHXF12.4	12.3	-0.271
OHXF12.5	12.3	-0.328
OHXF12.6	12.3	-0.385
OHXF12.7	12.3	-0.442
OHXF12.8	12.3	-0.500

4.4.2 Compressor valve leakage

The compressor or 4-way valve leakage (CVL) fault represents the refrigerant bypass between the high and low-pressure sides of the circuit. This leakage can appear in the compressor or in the reversing valves. A pipe that bypasses the suction and discharge lines of the compressor was installed to emulate the fault, as shown in Figure 4.5a. Figure 4.5b shows the valve that controls the aperture of the bypass line.

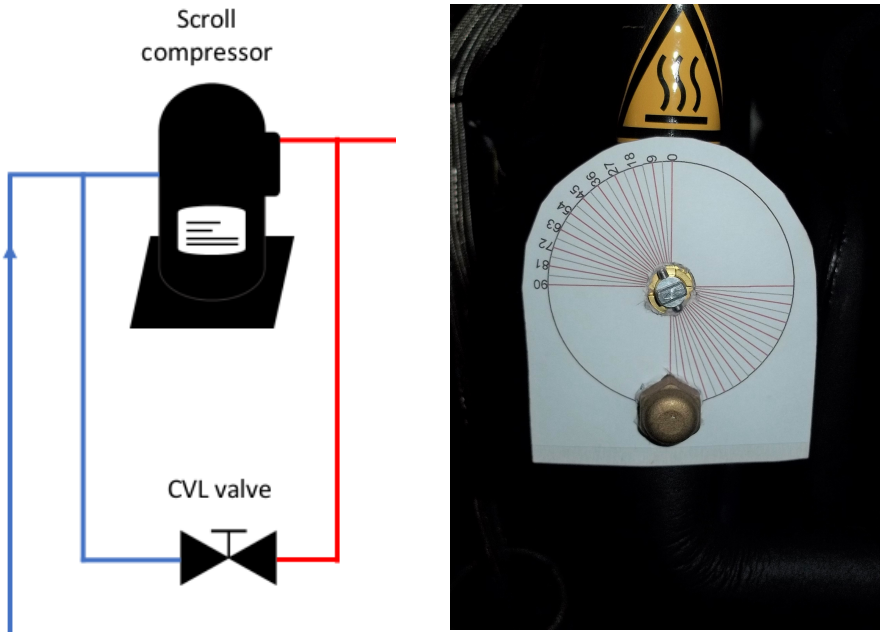

(a) (b)

Figure 4.5: Bypass valve to emulate the CVL fault a) schematic, b) actual bypass valve with a cardboard goniometer to know the angular position of the valve.

The FI for this fault is shown in Equation 4.2.

$$\mathrm{FI_{CVL}} = \frac{\dot{\mathrm{m}}_{\mathrm{r\_fault}} - \dot{\mathrm{m}}_{\mathrm{r\_ff}}}{\dot{\mathrm{m}}_{\mathrm{r\_ff}}} \tag{4.2}$$

where $\dot{m}_{r\_fault}$ is the refrigerant mass flow for the fault condition, and $\dot{m}_{r\_ff}$ is the refrigerant mass flow for fault-free condition. In devices with variable speed compressors, the refrigerant mass flow depends on the compressor speed, the action of the expansion valve and the thermodynamic properties of the refrigerant. During the test, the compressor speed changed when a fault occurs. Therefore, the $\dot{m}_{r\_ff}$ changed with the compressor speed. If this is not take into account, the FI_{CVL} could show a zero value because the mass flow is maintained due to the increase of compressor speed to overcome the fault. Therefore, it was need to know the correlation between compressor speed and refrigerant mass.

To do so, the compressor was tested at different speeds without any fault and measured the refrigerant mass flow at steady-state. Nevertheless, due to a tight timetable, the compressor speed test could not be performed before the CVL test. This means that, while doing the CVL test, the FI was not known. So, to define each level of CVL fault the valve position was used provisionally as an indicator.

The bypass valve was a ball valve with $90^{\underline{o}}$ operation with a poor linear response at the beginning and the end of the valve travel. A cardboard goniometer was used to know the position of the valve. However, with only a quarter-turn, the precision was very limited.

Table 4.3 shows the different fault levels tested. More levels were tested but, as they did not have any impact on the heat pump behaviour, they were not include in the table. The higher fault levels (CVL10.4 and CVL12.3) were near the limit of the heat pump operation, because they caused a high temperature at compressor outlet which had a protection to over-temperature. Therefore, the fault intensity was not increased further.

Table 4.3: CVL steady-state tests experimental plan.

Code	Load (kW)	Valve position ($^{\underline{o}}$)	FI_{CVL}
CVL10.1	10.2	22.5	-0.042
CVL10.2	10.2	27.0	-0.296
CVL10.3	10.2	31.5	-0.372
CVL10.4	10.2	36.0	-0.648
CVL12.1	12.3	27.0	-0.131
CVL12.2	12.3	31.5	-0.379
CVL12.3	12.3	34.0	-0.608

The FI_{CVL} on Table 4.3 was calculated after the tests. To do so, a correlation between compressor speed and refrigerant mass flow was obtained by running the compressor at different speeds without fault present. The test was made for both capacities at steady-state conditions, as shown in Figure 4.6. The regressions of both series had similar values, using the one from the 12 kW load to simplify. From the regression line, the Equation 4.3 was obtained. This equation relates the compressor frequency in rps and the refrigerant mass flow in g/s

for no-fault conditions. It may lose precision with faults present or different capacities, but it is enough to obtain the $\dot{m}_{r\_ff}$ for the FI_{CVL} calculation.

$$\mathrm{m_{r\_ff}} = 0.5206 * freq + 0.7082 \quad [\frac{g}{s}] \tag{4.3}$$

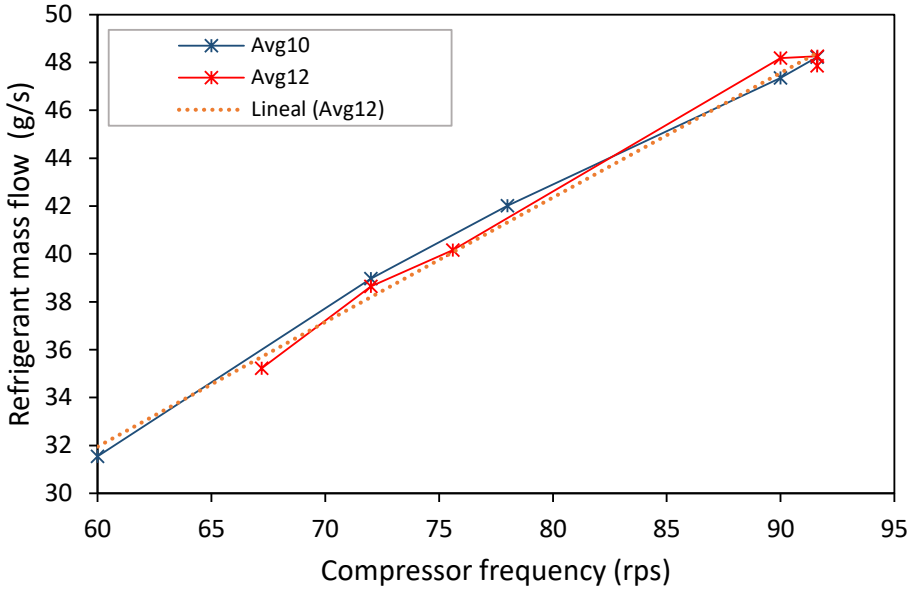

Figure 4.6: Relation between compressor frequency and refrigerant mass flow for the two load conditions. The average values are represented with a solid line and the regression is in doted line.

4.4.3 Liquid line restriction

The liquid line restriction (LL) appears when the filter/dryer located in the liquid line is clogged. To emulate this fault, the manufacturer placed a restriction valve in the liquid line to increase the pressure drop, as shown in Figure 4.7.

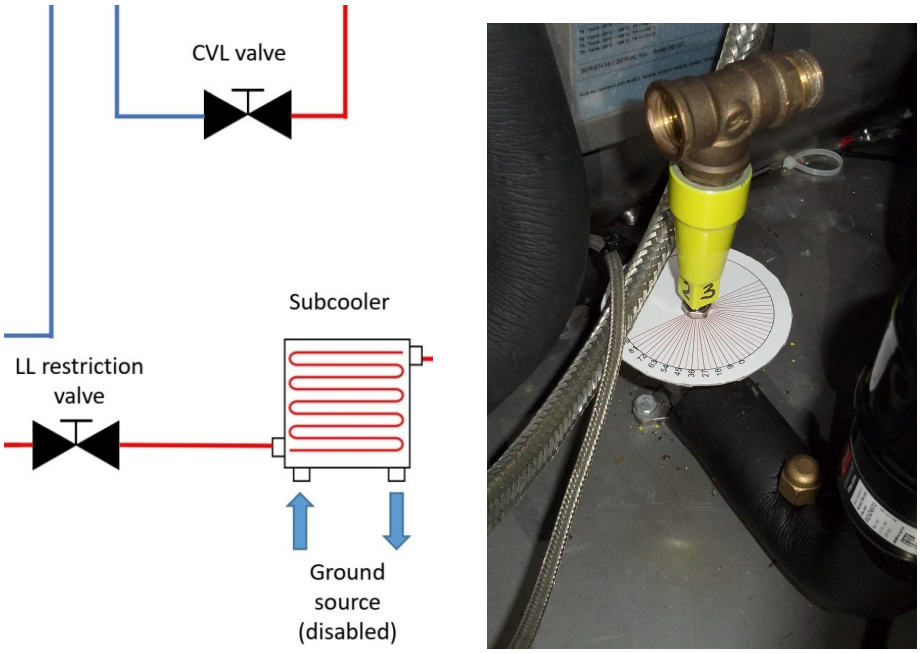

Figure 4.7: Restriction valve to emulate the LL fault a) schematic, b) actual restriction valve with a cardboard goniometer to know the angular position of the valve.

The FI of this fault is related to the pressure drop variation in the liquid line as Equation 4.4 shows.

$$\mathrm{FI_{LL}} = \frac{\Delta \mathrm{P_{LL}} - \Delta \mathrm{P_{ff}}}{\Delta \mathrm{P_{ff}}} \tag{4.4}$$

where ΔP_{LL} represents the liquid line pressure drop with the fault and ΔP_{ff} the liquid line pressure drop without the fault. The pressure drop in the liquid line was calculated as the pressure difference between the discharge and suction lines. However, during the test procedure, the angular position of the valve was used to define each fault level. It was a regulation valve with an operation of 3 turns and three-quarters of a turn. However, there was no effect for the first three and a half turns. Therefore, only the last quarter was used to emulate the fault. The experimental plan is shown in Table 4.4. The valve position indicates the angle starting from half of the last turn, so a valve angle of

10^{o} will correspond to the 190^{o} of the third turn.

Table 4.4: LL steady-state tests experimental plan.

Code	Load (kW)	Valve position (^{o})	FI_{LL}
LL10.1	10.2	54.0	0.103
LL10.2	10.2	58.5	0.181
LL10.3	10.2	63.0	0.267
LL10.4	10.2	67.5	0.418
LL10.5	10.2	72.0	0.743
LL12.1	12.3	54.0	0.055
LL12.2	12.3	58.5	0.168
LL12.3	12.3	63.0	0.281
LL12.4	12.3	67.5	0.404
LL12.5	12.3	72.0	0.648

4.4.4 Refrigerant overcharge

The refrigerant overcharge (OC) fault may appear during maintenance if the heat pump is filled with more refrigerant than recommended by the manufacturer. To emulate this fault, the heat pump was overcharged by 10% above the nominal amount. The FI_{OC} is the relative difference between the current and the nominal charge, as Equation 4.5 shows.

$$FI_{OC} = \frac{m_{r\_fault} - m_{r\_ff}}{m_{r\_ff}} \tag{4.5}$$

where m_{r_fault} is the propane charge for faulty conditions, and m_{r_ff} is the nominal propane charge. Table 4.5 shows the experimental plan. An overcharge of 20% was also tested, but the heat pump could not run properly. As the heat pump had a small nominal charge (720 gr), it may be more sensitive to charge variations.

Table 4.5: OC steady-state tests experimental plan.

Code	Load (kW)	FI_{OC}
OC10.1	10.2	0.1
OC12.1	12.3	0.1

4.4.5 Untested faults

In the first stages of the test planning, the non-condensable gas on the refrigerant, the internal heat exchanger fouling and the refrigerant undercharge were also considered as part of the test campaign. However, they were discarded or the test were not successful.

Non-condensables was discarded because of the difficulty of emulating the fault. This fault is emulated by adding dry-nitrogen into the refrigerant circuit. If it is wanted to test different faults intensities, between each fault level, all the refrigerant circuit must be purged. The dry-nitrogen mixes with the propane, therefore the only way of knowing the exact quantity of propane and dry-nitrogen of the circuit is at charging [99]. Because of the flammability of the propane, every operation of charge and discharge of refrigerant must be realized by an external service who can operate with flammable refrigerants. Therefore, this fault would be very time consuming and costly to reproduce.

The indoor heat exchanger fouling would be emulated by decreasing the water flow of the condenser. However, this would not cause any repercussions on the equipment. For the heat pump, this water flow descend would be the same as lowering the load. With variable speed heat pumps (VSHP), the compressor's frequency will decrease to adapt to the new load, therefore there is no much effect expected. This fault makes more sense when the compressor could not change its speed but was discarded for this heat pump.

Undercharged was included in the testing plan, because is a common fault that is relevant when the equipment has a flammable refrigerant. It was the last of the faults to be tested, just after overcharge. Undercharge levels of 10% and 20% were tested. However, the results showed that the pressure of the discharge and the suction lines were higher than for normal behaviour, which is contrary to the

expected. The system was purged and charged again to discard the non-condensables. However, the compressor could not run again. One of the explanations would be that the faults tests have damaged the compressor, for example by entering liquid refrigerant into it. The manufacturer also explained that, because of being a prototype with different and unorthodox parts due to using propane, it was less mature and robust than conventional heat pumps. Because of that, the undercharge test results are not included as they do not represent the undercharge behaviour.

4.5 Experimental results

Different heat pump features can be affected by each fault. The features taken into account for this study were the COP, compressor power consumption (W_{comp}), heat duty (Q_{heat}), subcooling (T_{sc}), superheating (T_{sh}), evaporation temperature (T_{evap}), condensing temperature (T_{cond}), compressor outlet temperature (T_{co}), liquid line temperature (T_{ll}), refrigerant mass flow ($\dot{m}_r$) and compressor frequency (f).

In VSHP, the refrigerant mass flow depends on the compressor speed, the expansion valve action and the inlet density, which in turn depends on the evaporation temperature. When a fault occurs, the heat pump may change the compressor speed to meet the new demand, changing considerably the mass flow rate. Therefore, the refrigerant mass flow should be interpreted in terms of compressor speed. Because of this, the ratio between the refrigerant mass flow rate and the compressor speed (MSR) is used to express that relation as Equation 4.6 shows.

$$MSR = \frac{\dot{m}_r}{f} \quad [\frac{g}{rev}] \tag{4.6}$$

Equation 4.7 shows the normalized value of MSR ($NMSR$), which is more intuitive.

$$NMSR = \frac{MSR_{fault}}{MSR_{nominal}} \tag{4.7}$$

Figures 4.8 to 4.10 show the effects of the different faults and Table 4.6 shows the effect for OC, which are expressed on a table because of being only one fault level. Only the features affected by each fault are shown. For T_{sc}, T_{sh}, T_{evap}, T_{cond}, T_{co} and T_{ll}, the difference between the no-fault value (T_{ff}) and the current level fault (T_{fault}) was used (see Equation 4.8). The ΔT for FI of 0, is 0.

$$\Delta T = T_{fault} - T_{ff} \quad [C] \tag{4.8}$$

4.5.1 Outdoor heat exchanger fouling

Figure 4.8 shows the effects of outdoor heat exchanger fouling fault (OHXF) in different features. For OHXF, reducing the water flow lowered the evaporator pressure, which decreased the evaporation temperature. The compressor speed increased so that demand could still be covered, which decreased NMSR and increased power consumption.

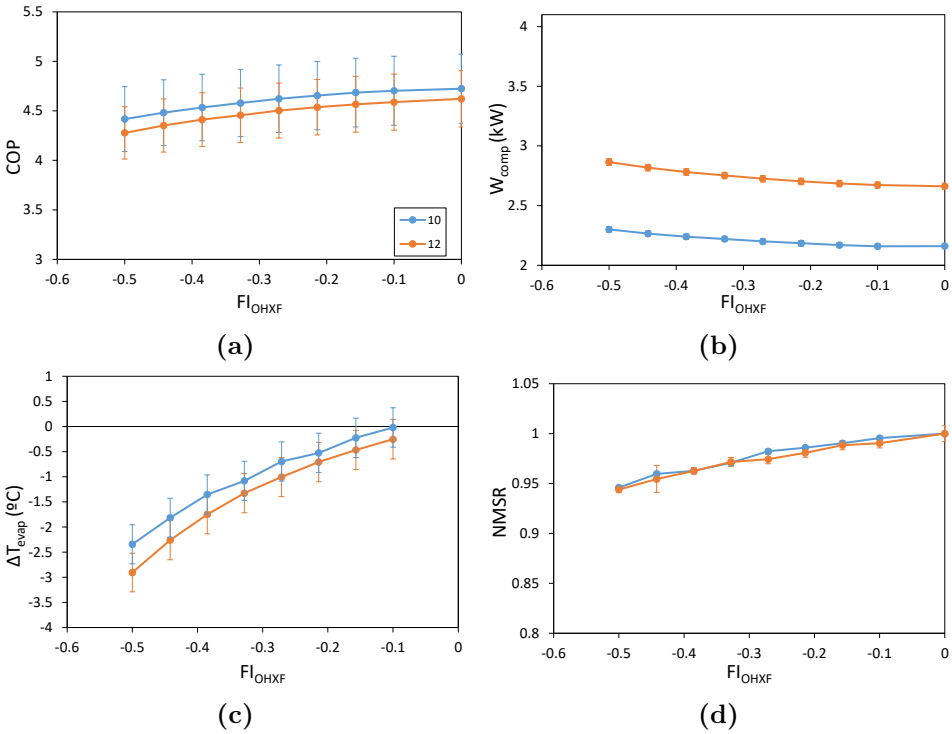

Figure 4.8: Relevant features affected by the outdoor heat exchanger fouling fault (OHXF) for the 10 kW and 12 kW steady-state tests. Effect on: a) COP, b) compressor power consumption, c) evaporator saturation temperature and d) NMSR.

4.5.2 Compressor valve leakage

Figures 4.9 display the affected features of the compressor or 4-way valve leakage (CVL). The CVL fault increased the pressure at the suction line while the discharge pressure remained the same. To compensate for all the refrigerant that went through the bypass, the compressor increased the speed, which increased the power consumption and the compressor outlet temperature.

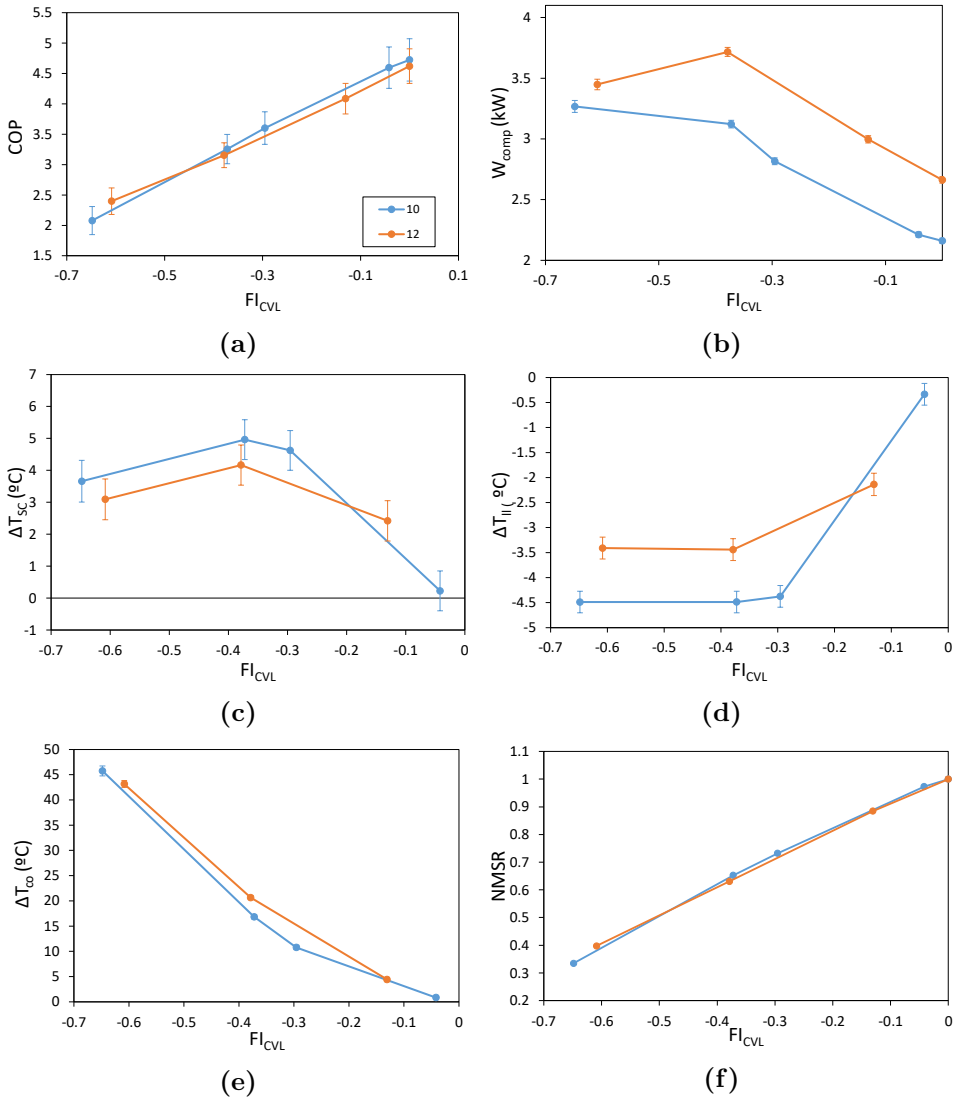

Figure 4.9: Relevant features affected by the compressor valve leakage (CVL) fault for the 10 kW and 12 kW steady-state tests. Effect on: a) COP, b) compressor power consumption, c) subcooling, d) liquid line refrigerant temperature, e) compressor outlet refrigerant temperature and f) NMSR.

This increase in the outlet temperature triggered a safety limitation of the compressor speed. This limitation caused a decrease in power consumption at the highest fault level, as Figure 4.9b shows. At that fault level, the refrigerant mass flow in the circuit was so small that

the demand could not be covered. The outlet temperature increased, forcing the compressor to stop for its safety.

4.5.3 Liquid line restriction

Figure 4.10 presents the repercussion of liquid line restriction (LL) fault. The LL caused an additional pressure loss between condensation pressure and suction pressure. With low restriction values, the two expansion valves opened simultaneously and there was no effect on the COP or other variables. When the restriction increased, the main valve (EEV1) was fully open, superheat at the evaporator outlet increased while the other valve (EEV2) closed. This reduced the refrigerant liquid line temperature by 4.5 ºC and 3.5 ºC for the lower and the higher load, respectively.

Since the first FI value, the EEV1 reached its capacity limit, and the refrigerant started to be retained in the condenser leading to more subcooling. Because there was liquid trapped in the condenser, the temperature of the refrigerant at the outlet of the condenser approached the temperature at the inlet of the water side, therefore the T_{ll} values were constant for all the fault levels. The condensation temperature increased while the evaporation temperature decreased. The compressor speed increased to cover the demand, which decreased the NMSR and increased the power consumption.

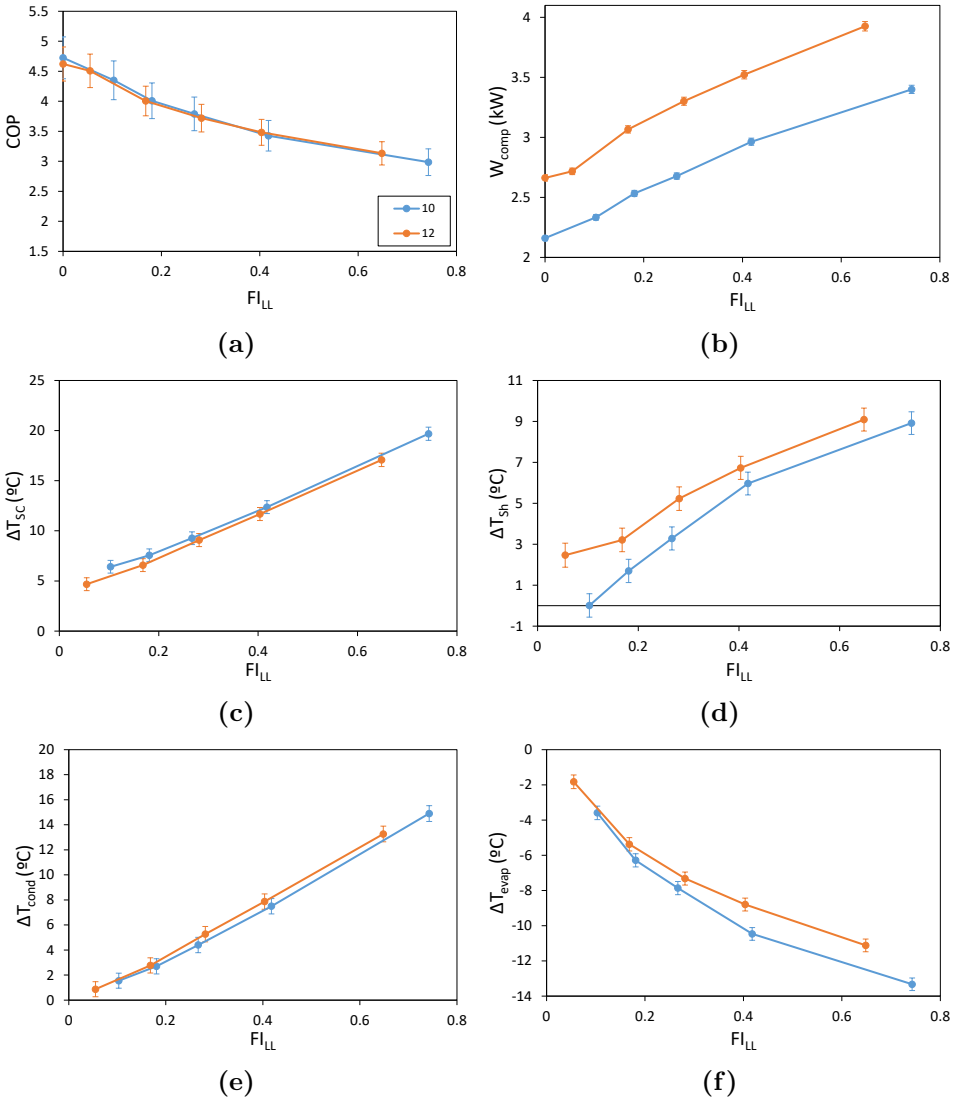

Figure 4.10: Continues

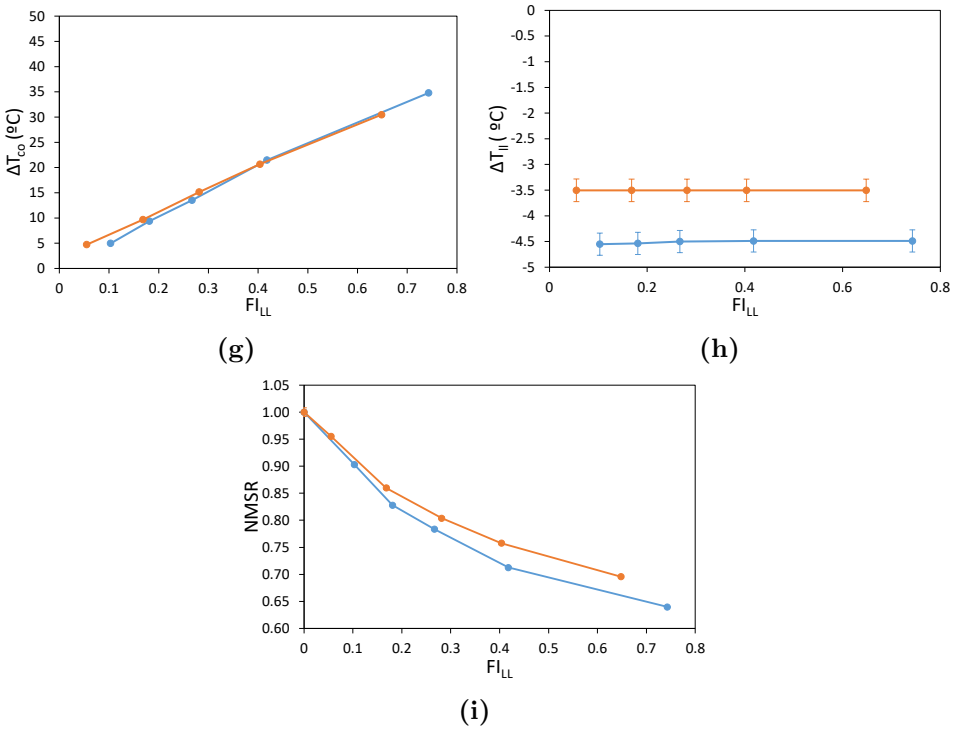

Figure 4.10: Relevant features affected by the liquid line restriction (LL) fault for the 10 kW and 12 kW steady-state tests. Effect on: a) COP, b) compressor power consumption, c) subcooling, d) superheating, e) condenser saturation temperature, f) evaporator saturation temperature, g) compressor outlet refrigerant temperature, h) liquid line refrigerant temperature and i) NMSR.

4.5.4 Refrigerant overcharge

As refrigerant overcharge (OC) was tested with only one fault level, the results are displayed in Table 4.6. The OC fault increased the liquid trapped in the condenser, which increased the condensation temperature. The evaporation temperature increased due to an increase in suction pressure. The subcooling and the compressor outlet temperatures rose. The refrigerant mass flow rate slightly increased while the speed of the compressor dropped, which increased the NMSR. This fault has little or no effect on systems with a liquid receiver [20].

Table 4.6: Results for the overcharge test for 10 kW and 12 kW . FI: fault intensity, COP, W_{comp}: compressor electrical power consumption, Q_{heat}: condenser heating power, T_{sc}: subcooling, T_{sh}: superheating, T_{evap}: evaporator saturation temperature, T_{cond}: condenser saturation temperature, T_{co}: compressor outlet refrigerant temperature, T_{ll}: liquid line refrigerant temperature, $\dot{m}_r$: refrigerant mass flow, f: compressor speed.

Code	FI	COP	W_{comp} kW	Q_{heat} kW	T_{sc} K	T_{sh} K	T_{evap} °C	T_{cond} °C	T_{co} °C	T_{ll} °C	$\dot{m}_r$ $g\ s^{-1}$	f Hz
NoFault10	0	4.7	2.2	10.2	2.0	11.0	4.5	46.8	63.4	44.6	29	57
Uncertainty		±0.35	±0.02	±0.75	±0.44	±0.40	±0.28	±0.42	±0.30	±0.15	±0.04	±0.03
OC10.1	0.1	3.6	2.8	10.1	24.9	10.7	7.0	64.8	84.8	40.0	29	52
Uncertainty		±0.27	±0.03	±0.75	±0.49	±0.41	±0.29	±0.48	±0.30	±0.15	±0.04	±0.03
NoFault12	0	4.6	2.7	12.3	4.1	8.7	4.0	47.0	61.9	42.6	36	69
Uncertainty		±0.28	±0.03	±0.75	±0.45	±0.41	±0.28	±0.42	±0.30	±0.16	±0.10	±0.04
OC12.1	0.1	3.7	3.3	12.2	25.7	9.9	6.8	64.6	83.5	39.1	35	62
Uncertainty		±0.23	±0.03	±0.75	±0.50	±0.41	±0.29	±0.41	±0.30	±0.15	±0.04	±0.03

4.6 Discussion and conclusions

This section has shown the experimental procedure to test different faults on a variable speed heat pump and their results. The faults were tested in the SEILAB, a laboratory for testing HVAC solutions using the HiL methodology.

The tested faults were the outdoor heat exchanger fouling, which was emulated reducing the evaporator water flow; the compressor valve leakage, which was emulated increasing the bypass of refrigerant between suction and discharge lines of the compressor; the liquid line restriction, which consisted in increasing the pressure drop of the liquid line; and the refrigerant overcharge. Each fault was tested for 10 kW and 12 kW load and, except for OC, with different fault intensities. To compare the COP degradation of each fault, the fault impact ratio (FIR) on COP is used. Equation 4.9 shows how it is calculated.

$$FIR_{COP} = \frac{COP_{fault}}{COP_{nominal}} \tag{4.9}$$

A FIR_{COP} with a value of one indicates no degradation. Figure 4.11 shows the FIR_{COP} for each fault.

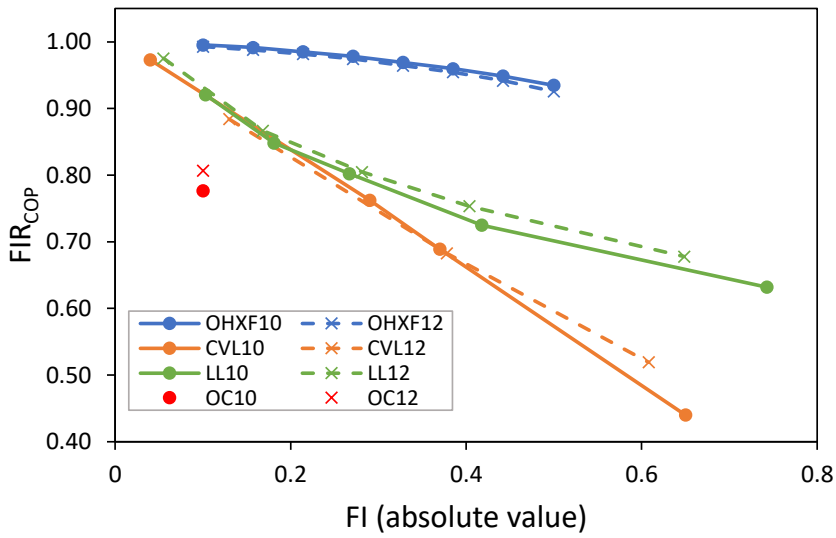

Figure 4.11: Fault impact ratio on COP for each fault intensity. The fault intensity is shown in absolute value. The solid lines with dot marks represents the test with 10 kW load, and the dotted lines with cross marks are for the 12 kW load.

The results of the fault tests have shown that every fault has lowered the COP, being OHXF and CVL the ones with minimum and maximum impact, respectively. In general, the compressor speed has increased to overcome the fault effects, which has increased the electric power consumption. The demand was covered for each fault except for the highest value of CVL.

Table 4.7 summarizes the results of the faults tested, indicating if the feature had an increasing or decreasing trend or if it was not affected. When the deviation of the feature is above the value of the grey-shadowed rows, ↑ or ↑↑ rows, or below the ↓ or ↓↓ rows, the corresponding arrows are applied.

Table 4.7: Trend for each of the features. ↑↑: high increasing trend, ↑: increasing trend, ↓: decreasing trend, ↓↓: high decreasing trend. The last two rows describe the criteria applied for constructing the table.

Fault	COP	W_{comp}	Q_{heat}	T_{sc}	T_{sh}	T_{evap}	T_{cond}	T_{co}	T_{ll}	$\dot{m}_r$	f	MSR
OHXF	↓	↑				↓					↑	
CVL	↓↓	↑↑	↓↓	↑				↑↑	↓	↓↓	↑↑	↓↓
LL	↓↓	↑↑		↑↑	↑↑	↓↓	↑↑	↑↑	↓	↓↓	↑↑	↓↓
OC	↓	↑↑		↑↑		↑	↑↑	↑↑	↓		↓	↑
↑↑,↓↓	±1	±0.5 kW	±1 kW	±5 °C	±5 °C	±5 °C	±5 °C	±5 °C	±5 °C	±5 $g\ s^{-1}$	±15 Hz	±15 $g\ r^{-1}$
↑ , ↓	±0.1	±0.1 kW	±0.2 kW	±2 °C	±2 °C	±2 °C	±2 °C	±2 °C	±2 °C	±2 $g\ s^{-1}$	±3 Hz	±3 $g\ r^{-1}$

The impact of OHXF has been small despite cut in half the evaporator water mass flow, being the decrease of T_{evap} the most relevant effect. CVL has impacted severely the COP due to a high increase of W_{comp}. This increase in consumption was caused by the rise of the compressor's speed which compensate for all the refrigerant that went to the bypass. This also caused the increment of the compressor outlet temperature. At the highest fault levels, the heat pump could not cover the demand and it was near its safety limit for the compressor's outlet temperature.

The LL had a high impact on the COP and affected nearly every feature of the heat pump. The refrigerant gets trapped in the condenser, increasing the subcooling. The expansion valves get saturated, so they cannot prevent the superheating increase.

The OC fault has decreased the COP and increased W_{comp}. However, for this fault, the compressor speed slightly decreased. The refrigerant mass flow and the compressor frequency have not changed, but the compressor outlet temperature has increased.

As stated previously in Chapter 2, the data about faults on VSHP is scarce. The most similar study to compare the test results was the one by Kim and Kim [20], which used a brine-to-water heat pump in cooling mode. They tested the faults CVL, OC, OHXF, IHXF and UC. The features that match ours are T_{cond}, T_{sc}, T_{co} and f. Table 4.8 compares the obtained results with their ones.

Table 4.8: Trend for each of the features for the present study and the study by Kim and Kim[20] .↑: increasing trend, ↓: decreasing trend.

Fault	COP	T_{sc}	T_{co}	f
OHXF	↓		↑	↑
OHXF_Kim	↓		↑	↑
CVL	↓	↑	↑	↑
CVL_Kim	↓		↑	↑

Kim and Kim did not find any effect on T_{sc} for CVL, but this could be because their maximum fault intensity was 0.2 while in our test an FI of 0.6 was reached. However, in our tests, for a FI near 0.2, it was not observed an effect on subcooling.

OHXF was difficult to compare because the heat pump tested was on heating mode and with brazed plate heat exchanger, whereas in theirs, it was in cooling, and with concentric heat exchanger. Therefore, the heat exchanger was acting as an evaporator in the tests and as a condenser in their study. Additionally, they tested OHXF reducing the secondary fluid passage by bypassing it at the ports installed at the end of each heat exchanger subsection. Nevertheless, they found a severe effect on the COP (COP reduction between 10% and 30%) for OHXF while in the present experimental test was smaller (less than 5%).

The OC had a negligible effect on their system, mainly because their system had a liquid receiver, which, as has been observed in another study [100], causes a high tolerance to the overcharge.

The experimental tests required tight surveillance as, despite all the security measures of the heat pump, there were transitory conditions that caused superheating values near 0 $^{\text{o}}$C. This means that liquid refrigerant could enter the compressor, which could damage it permanently. However, different faults have been tested and their effects quantified. This entails that more data is available to the development of FDD monitors for VSHP.

UNIVERSITAT ROVIRA I VIRGILI
AUTOMATIC FAULT DETECTION IN DOMESTIC HEAT PUMPS
Ivan Bellanco Bellanco

CHAPTER 5

Performance of the fault detection and diagnosis monitor with experimental data

UNIVERSITAT ROVIRA I VIRGILI
AUTOMATIC FAULT DETECTION IN DOMESTIC HEAT PUMPS
Ivan Bellanco Bellanco

5.1 Introduction

This chapter describes the validation of the Fault Detection and Diagnosis (FDD) monitor developed in Chapter 3 with the experimental data from Chapter 4. The FDD monitor was running in parallel on an industrial computer and in a pocket sized computer with a Quad Core 64 bit CPU and 1 GB RAM. The results are the same for both implementations, demonstrating the computational efficiency of the solution.

The correct operation of the steady-state detector (SSD) and the Input Space is tested with real time data. The Fault detection and the diagnosis are also validated with the set of experimental data. The changes needed to adapt from simulation data to real data are explained and the performance of the monitor quantified.

Finally, the results in terms of accuracy and other indicators of the FDD performance are compared with similar FDD solutions found in the literature.

5.2 Steady-state detector

In this section, the results of the SSD module with the real time data of the faults tests are explained. The SSD was used to eliminate the non-stationary points from the incoming data. The SSD was tested with simulation data in Section 3.4.2, but the lack of disturbances and noise of the simulation data, makes it necessary to check the performance with real data.

The easiest way to see the SSD performance was by visually check the detections of steady-state in the signal. Figure 5.1 shows three different moments of the steady-state detector with fault-free data. As stated in Section 3.5.3, Q_{heat} was the feature used for searching steady-state. The *Steady state* variable has a value of 1 when steady-state is detected.

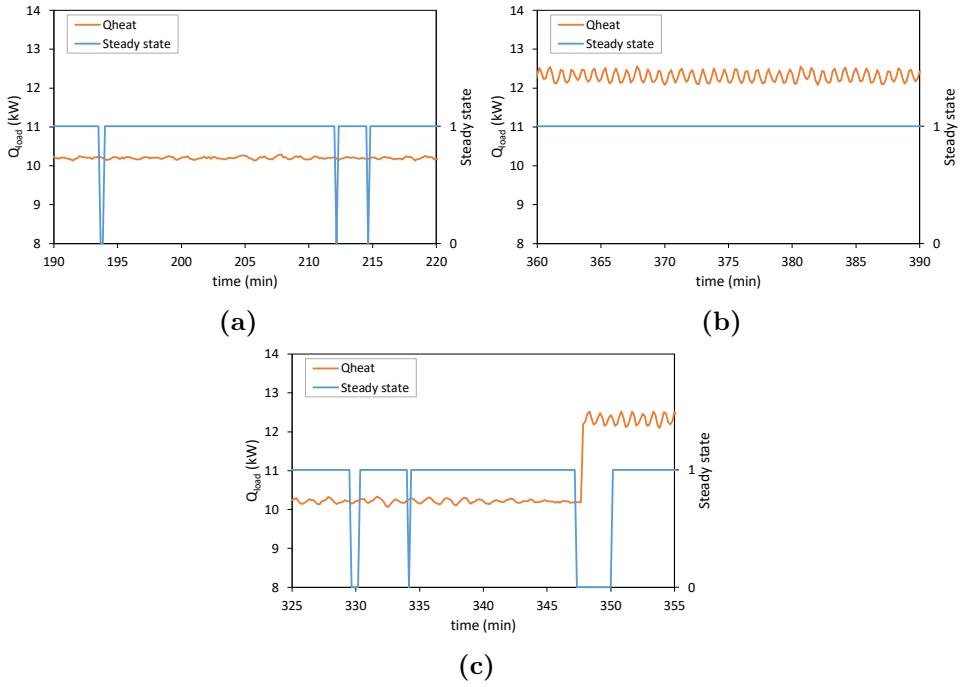

Figure 5.1: Results for the steady-state detector applied to the Q_{heat} signal. Steady state is 0 when the signal is not in steady-state. a) SSD for the 10.2 kW condition, b) for the 12.3 kW condition and c) for the change between both conditions.

Figure 5.1a shows the value of Q_{heat} for the 10.2 kW condition. As can be seen, the data could be defined as steady, and the SSD detected nearly all the period as steady-state with the exception of some points. Figure 5.1b shows the period of 12.3 kW. In this case, the data was also steady but it had more oscillations. However, the SSD adapted to this oscillations and detected the steady-state. Figure 5.1c shows the transition between the 10 kW and 12 kW series. For this case, the SSD filtered the discontinuity between both loads and adapted to the new series.

The strength of the SSD method developed is the self-adaptability to the different characteristics of the signal without external tuning. However, this data pertains to static experiments and more tests need to be done with more dynamic conditions to know the response of the SSD.

5.3 Input space

The Input Space was used to have different no-fault models depending on the value of the driving variables, to increase the accuracy of the models.

In Section 3.4.3, the specified driving variables were the T_{amb}, $T_{cond,out}$ and f_{comp}. This configuration was used for the TRNSYS model with an air-to-water heat pump. As the tested heat pump was water-to-water, T_{amb} was changed for $T_{evap,in}$, and $T_{cond,out}$ for $T_{cond,in}$, which are more representative of the external conditions.

Initially, for the experimental faults tests with the real heat pump, the frequency of the compressor was also considered, however, it was observed that the compressor speed changed to adapt to the faults. When this happened, the new data had a different speed than during training, and therefore, pertaining to a different group of the input space. As this new group was not trained, the algorithm could not do predictions. For the validation with experimental data, the fault parametrization equations did not include any effect on the compressor speed. Therefore, for that case, using the compressor speed as driving variable worked well, but was because of a lack of data.

The conclusion was that the driving variables should pertain to the external conditions of the heat pump, which are less affected by the faults. Therefore the f_{comp} was eliminated of the input space and the no-fault models after realising that the results were satisfactory with only two variables ($T_{cond,in}$ and $T_{evap,in}$).

Figure 5.2 shows how the training data of the fault-free tests had been distributed in the Input Space. All the training data is located in the red square in Figure 5.2a. Figure 5.2b shows that area zoomed, where there are clearly two main groups. The group circled in green (1936 data points) was assigned to the upper right centre, while the group circled in yellow (349 data points) was assigned to the lower right centre. Therefore, for these two groups, a no-fault model was trained.

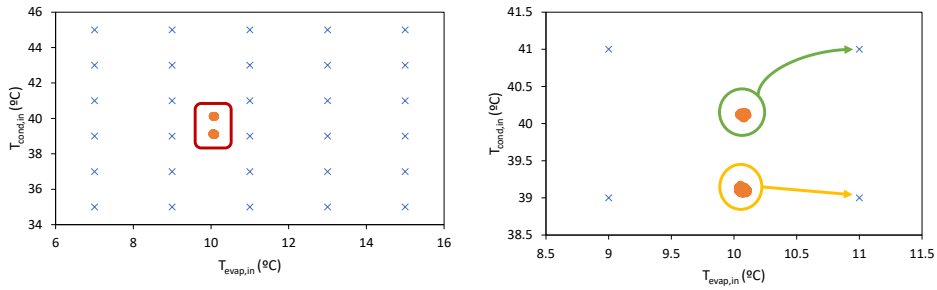

(a) **(b)**

Figure 5.2: Visual representation of the Input space. a) The blue crosses represent the centres of the groups and the orange dots are the data points used for the training. b) Zoom of the red square of figure a). Each group of data points are classified with the nearest centre.

Figure 5.3 shows some of the variables for the 10.2 kW condition in steady state.

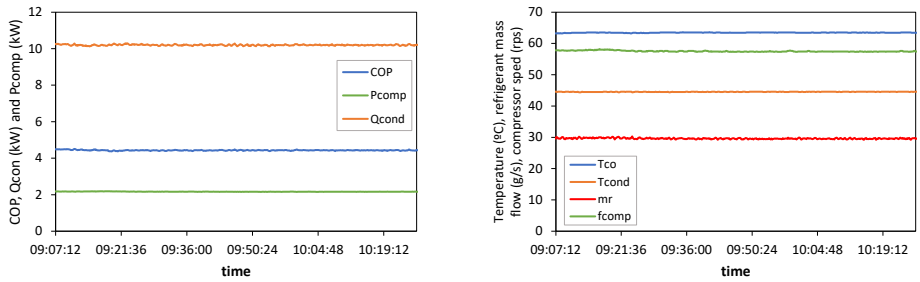

(a) **(b)**

Figure 5.3: Representation of different feature values in steady state for the 10.2 kW condition.

5.4 Fault free-models and fault detection

To generate the fault-free models, a total of five and a half hours of 10.2 kW load and nearly one hour of 12.3 kW data was used, taking into account that a minimum of 50 data points were needed for training a no-fault model. Those two load conditions correspond to two different clusters of the Input Space. For each of these clusters, fault-free models

were created for different features. The regression equation is showed in Equation 5.1.

$$\begin{aligned}\hat{y} =&\theta_0 + \theta_1 \mathrm{T}_{\mathrm{evap,in}} + \theta_2 \mathrm{T}_{\mathrm{cond,in}} + \theta_3 \mathrm{T}^2_{\mathrm{evap,in}} + \theta_4 \mathrm{T}^2_{\mathrm{cond,in}} + \\ &\theta_5 \mathrm{T}_{\mathrm{evap,in}} \mathrm{T}_{\mathrm{cond,in}} + \theta_6 \mathrm{T}^3_{\mathrm{evap,in}} + \theta_7 \mathrm{T}^3_{\mathrm{cond,in}} + \\ &\theta_8 \mathrm{T}^2_{\mathrm{evap,in}} \mathrm{T}_{\mathrm{cond,in}} + \theta_9 \mathrm{T}^2_{\mathrm{cond,in}} \mathrm{T}_{\mathrm{evap,in}}\end{aligned} \tag{5.1}$$

Table 5.1 shows the regression parameter values obtained for the COP and for T_{co} for the 10 kW and 12 kW conditions.

Table 5.1: Regression parameters for the COP and T_{co} for the 10 kW and 12 kW conditions.

Feature ($\hat{y}$)	θ_0	θ_1	θ_2	θ_3	θ_4	θ_5	θ_6	θ_7	θ_8	θ_9
COP10	0.00E+00	2.03E-04	-2.83E-03	3.28E-04	-5.06E-04	-2.82E-03	4.54E-04	-4.24E-05	-1.08E-03	-2.81E-03
COP12	0.00E+00	4.46E-03	-9.66E-03	4.95E-03	1.13E-03	-9.79E-03	5.44E-03	3.37E-03	-2.47E-03	-9.91E-03
$T_{co}10$	0.00E+00	3.48E-03	1.48E-03	3.15E-03	3.58E-03	1.52E-03	2.81E-03	3.19E-03	3.51E-03	1.55E-03
$T_{co}12$	0.00E+00	-3.61E-02	2.83E-02	-3.60E-02	-2.83E-02	2.78E-02	-3.58E-02	-3.28E-02	-1.72E-02	2.74E-02

Figure 5.4 shows the results of the training of the 10.2 kW cluster. As can be seen in the figure, the data had more noise than the validation with simulated data. This increased the root-mean-square error (RMSE) obtained during training, which in turn, increased the error margin of the prediction (green area) that was two times the training RMSE. Therefore, the faults will be detected at higher COP degradations.

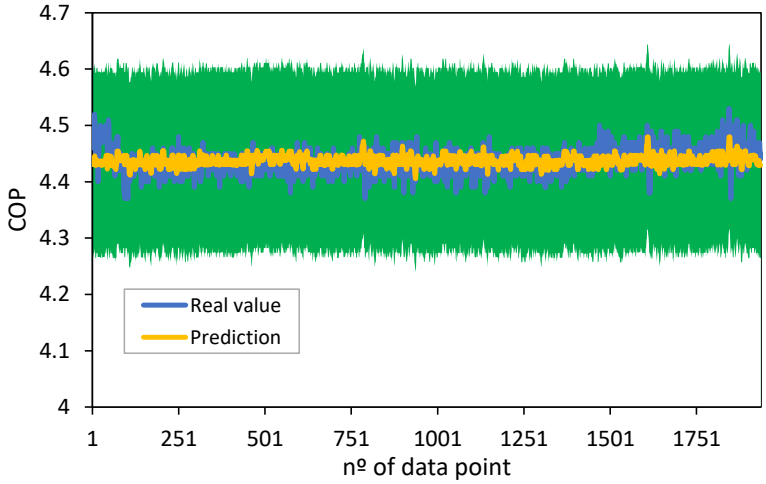

Figure 5.4: Training results of one the 10.2 kW cluster with experimental data. The green area is the error margin applied to the prediction of the no-fault model.

With the data from the TRNSYS model, the fault detection module ensured that a during a period of 50 minutes, the fault was present 80% of the time. As the experimental data had a data frequency of 10 seconds, the period needed to detect a fault was adapted to 10 minutes. Figure 5.5 shows the result of the fault detection module for the 12 kW series with the CVL fault.

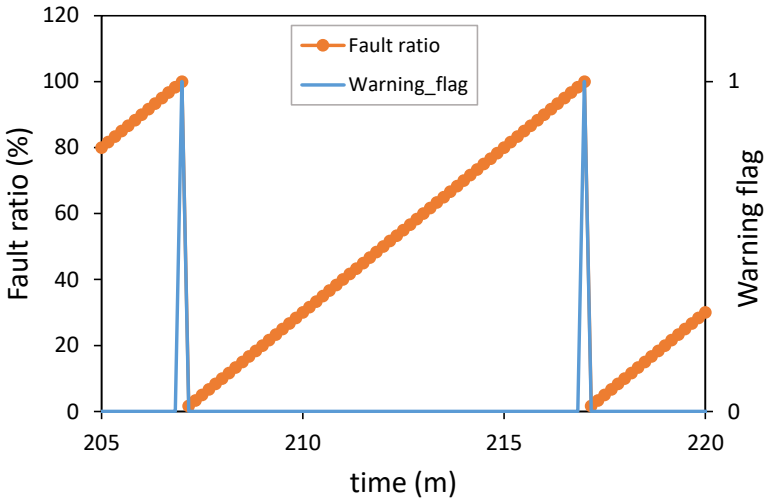

Figure 5.5: Fault detection module with the 12 kW with CVL fault. After a period of 10 minutes, when the fault ratio is higher than 80% the Warning flag has a value of 1.

The same indicators defined in Section 3.5.3 were used to quantify the performance of the FDD monitor with the experimental data. Those indicators are the false alarm rate (FAR), missed detection rate (MDR), accuracy, detection time (Dt) and fault impact ratio (FIR). There is a new indicator, the COP drift, showed in Equation 5.2, which is complementary to the FIR_{COP} but more intuitive, as it is the decrease in COP from the no-fault state.

$$COPdrift = \frac{COP_{ff} - COPfault}{COP_{ff}} * 100 \tag{5.2}$$

where COP_{ff} is the COP at fault-free condition and COP_{fault} is the COP when there is a fault. Table 5.2 shows for all the static tests, the value of the performance indicators.

Table 5.2: Performance values for the FDD. "-": FDD did not reach a prediction.

Code	FAR (%)	MDR (%)	Accuracy (%)	Dt (min)	FIR_{COP}	COP drift (%)
OHXF10.1	0	-	100	-	1.00	0
OHXF10.2	0	-	100	-	1.00	0
OHXF10.3	0	-	100	-	0.99	1
OHXF10.4	0	-	100	-	0.99	1
OHXF10.5	0	-	100	-	0.98	2
OHXF10.6	0	33	100	22	0.97	3
OHXF10.7	0	16	100	9	0.96	4
OHXF10.8	0	19	100	5	0.95	5
OHXF12.1	0	-	100	-	0.99	1
OHXF12.2	0	-	100	-	0.99	1
OHXF12.3	0	-	100	-	0.98	2
OHXF12.4	0	-	100	-	0.97	3
OHXF12.5	0	-	100	-	0.97	3
OHXF12.6	0	-	100	-	0.96	4
OHXF12.7	0	-	100	-	0.94	6
OHXF12.8	0	16	100	11	0.93	7
CVL10.1	0	-	100	-	1.00	0
CVL10.2	0	-	100	-	1.00	0
CVL10.3	0	-	100	-	1.00	0
CVL10.4	0	-	100	-	0.98	2
CVL10.5	0	31	100	14	0.78	22
CVL10.6	0	15	100	6	0.71	29
CVL10.7	0	-	100	-	0.79	21
CVL12.1	0	-	100	-	1.00	0
CVL12.2	0	-	100	-	1.00	0
CVL12.3	0	-	100	-	1.00	0
CVL12.4	0	19	100	13	0.89	11
CVL12.5	0	0	100	6	0.69	31
CVL12.6	0	30	100	10	0.53	47
LL10.1	0	-	100	-	1.00	0
LL10.2	0	23	100	22	0.93	7
LL10.3	0	31	100	17	0.86	14
LL10.4	0	-	100	12	0.82	18
LL10.5	0	33	100	19	0.74	26
LL10.6	0	26	100	17	0.65	35
LL12.1	0	-	100	-	0.98	2
LL12.2	0	33	100	17	0.87	13
LL12.3	0	25	100	7	0.81	19
LL12.4	0	7	100	15	0.76	24
LL12.5	0	-	100	-	0.69	31
RO10	0	33	100	17	0.79	21
RO12	0	33	100	13	0.81	19

The FAR and the Accuracy had ideal values which indicate that there were no false alarms. The FDD monitor detects that a fault was occurring when the COP drift was between 3% and 7% to above. The 3% value was for the data corresponding to the 10 kW series, while the 7% was for the 12 kW. This is because they correspond to different clusters, and therefore, have different error margins. For the experimental test with higher levels of CVL (CVL10.7), the heat pump could not cover the demand, increasing the condenser temperatures. This caused that the algorithm could not predict the heat pump behaviour because the conditions were far from those of the training.

The MDR values are very dependent on the test itself. A false negative is considered when the algorithm detects 10 minutes of steady-state data, the COP has decreased 0.05 and the FDD algorithm does not trigger a warning. As the tests have a duration of 60 minutes and, discarding all the noisy data, there are small quantity of those periods. Therefore, there was a lot of oscillation in the values of this indicator. The extension in time of the tests would improve this indicator. Nevertheless, the higher MDR was 33%, which is a good result.

The Dt was below 22 minutes. Without considering the unsteady area at the beginning of each test due to the FI increase, the Dt was usually 10 minutes, which is remarkable.

The $FIR_{COPdiagno}$ used in section 3.5.3 was not used with the experimental data, as it could be misleading. Note that $FIR_{COPdiagno}$ is used when the diagnosis of the fault is reached, whereas FIR_{COP} is used for any moment of the series. When the diagnosis is reached, FIR_{COP} is equals to $FIR_{COPdiagno}$. For the validation with simulation data, the fault effects were increasing continuously while with experimental data, the effects increased in an stepped way corresponding to each fault level. This could be observed in the faults RO, CVL and LL, where the FIR_{COP} increases fast with lower fault levels. If the $FIR_{COPdiagno}$ was used, it would have high values due to experimental limitation. For example, CVL at 10 kW started with a COP drift of 2% and the next fault level had a 22% drift. Therefore, despite the FDD monitor could diagnose for COP drifts as low as 3%, the $FIR_{COPdiagno}$ for CLV would be 0.78 (22% drift), that could be interpreted as a poor performance of the FDD monitor when it is due to experimental limitation.

The FDD monitor detected the faults for COP drifts of 3% for the 10.2 kW and 7% for the 12.3 kW. These drifts correspond to the uncertainty of each group of the input space. Those values comply with the objective of detecting a fault before a 10% of COP drift.

5.5 Fault diagnosis

The diagnosis methodology was based on expert knowledge. The trends expected from the literature research, that were used for the first validation with the TRNSYS model, differ from those obtained in the fault tests with a real heat pump. Table 5.3 shows the comparison between the results expected from literature and the ones obtained experimentally.

Table 5.3: Comparison between the feature trends from the literature and from the experimental tests. _lit: literature trends, _exp: fault test trends, ↑: increasing trend, ↓: decreasing trend.

Fault	COP	W_{comp}	Q_{heat}	T_{sc}	T_{sh}	T_{evap}	T_{cond}	T_{co}	T_{ll}	$\dot{m}_r$
OHXF_lit	↓	↑				↓		↑		
OHXF_exp	↓	↑				↓				
CVL_lit	↓	↑			↑			↑		↓
CVL_exp	↓	↑	↓	↑				↑	↓	↓
LL_lit	↓	↑		↓	↑				↑	
LL_exp	↓	↑		↑	↑	↓	↑	↑	↓	↓
OC_lit	↓	↑		↑			↑			↓
OC_exp	↓	↑		↑		↑	↑	↑	↓	

The following discrepancies were found:

- For OHXF: the compressor outlet temperature did not change on the tests, but an increase was expected from the literature and Dymola simulation.
- For CVL: the tests shows and increase in subcooling, decrease in liquid line temperature and no effect on superheating, while in

the literature they displayed no effect on subcooling and liquid line temperature, and increase in superheating.

- For LL: in the literature, subcooling decreased, superheating and liquid line temperature increased, but in the tests, subcooling, condenser temperature, and compressor outlet temperature increased, liquid line temperature and refrigerant mass flow decreased.
- For OC: the literature showed a decrease in refrigerant mass flow, but the tests displayed no change of it, and also an increase in compressor outlet temperature and evaporating temperature, and decrease of liquid line temperature.

The differences observed corresponded to a lack of literature data to generalize the fault effects for different heat pump architectures. Appling the first diagnosis logic (Figure 3.11) showed that none of the test faults with the real heat pump could be diagnosed correctly, being confound with another fault. Therefore, the diagnosis module was updated with the trends of the tested heat pump, ending with the diagnosis table showed in Figure 5.6.

Feature Fault	COP	W_{comp}	Q_{heat}	T_{sc}	T_{sh}	T_{evap}	T_{cond}	T_{co}	T_{ll}	m_r	Fault code
UC	↓	↑	=	↓		=	↓	↑		↑	-155-1151
OC	↓	↑	=			↑	↑	↑	↓		55111-15
CVL	↓	↑	=			↑	=	↑	↓	↓	55101-1-1
IHXF	↓	↑	=				↑	↑			5551155
OHXF	↓	↑	=		=	↓	=	=			50-10055
LL	↓	↑	=		↑	↓	↑	↑			51-11155

Figure 5.6: Fault diagnosis chart adapted to the real heat pump. The arrows facing up or down means increasing or decreasing trend, respectively, and the equals means that the feature does not change. Each of the faults has a code based on the tendency of the features (-1: decreasing, 1: increasing, 0: equals and 5:not relevant).

With the updated table of diagnosis, the indicator missdiagnosis rate (MR) was used to quantify the performance of the diagnosis. Table 5.4 shows the MR values for each fault tested.

Table 5.4: Misdiagnosis rate (MR) values for the updated diagnosis module

Code	MR (%)
OHXF10	-
OHXF12	-
CVL10	0
CVL12	0
LL10	0
LL12	0
RO10	0
RO12	0

With the update, there were no misdiagnosis for any fault. However, for OHXF the algorithm could not diagnose the fault because the effects were not high enough.

5.6 Discussion and conclusions

To put into context the results of the developed FDD monitor, it is required to compared it with similar solutions. From Section 3.2, the collected values Accuracy and the False Alarm Rate (FAR) of literature solutions could be compared with the ones obtained in the present chapter. However, it is hard to do a direct comparison between methodologies because the systems tested or the input data are different. Table 3.1 is reproduced below to see the accuracy and FAR values from the literature.

Table 3.1: Performance comparison between different FDD methods. CH: chiller, HP: heat pump, RTU: rooftop unit, MS: multi-split, Simu.:data from simulation, No.Sens.: number of sensors, P: pressure sensor, T: temperature sensor, m: air flow rate sensor, Accu.: Accuracy, FAR:false alarm rate and "-":Unspecified. (repeated from page 46)

Category	Method	Device	Data	No.Sens.	Accu.	FAR	Ref.
Knowledge-based	Machine Learning	HP	Real	4T,3P and 2m		1.6%	[53]
Analytical-based	Grey-box	HP	Real	4-5T		5.3%	[54]
Analytical-based	Black-box	CH	Real	7T,3P	93.0%		[81]
Knowledge-based	Machine Learning	RTU	Simu.	-		35.0%	[82]
Knowledge-based	Machine Learning	RTU	Simu.	-		55.0%	[82]
Knowledge-based	Machine Learning	RTU	Simu.	-		15.0%	[82]
Knowledge-based	Machine Learning	MS	Real	28T	94.0%		[83]
Knowledge-based	Machine Learning	MS	Simu.	28T	80.6%		[83]

Considering fault detection, the FAR obtained was 0%, being lower than which was found in literature. Taking a more concise look to each of those articles, the first study [53] obtained a FAR value of 1.6%. That study was about an FDD for multiple simultaneous faults in a roof top unit (RTU). They commented that the higher FAR values were caused by the LL fault which interferes with their refrigerant mass flow virtual sensor. They run their FDD with 6 faults happening simultaneously. Taking that into account, the FAR they obtained was small. In comparison, the current FDD solution was limited to one-by-one faults, with unknown results for simultaneous faults.

For another study [82], the authors evaluated the performance of three different commercial and open FDD protocols. They used four different types of input sets to do the evaluation. The FAR values were considerably high for two of the FDD (FAR between 20% and 90%) and lower for the other one (between 5% and 20%). The high FAR values could be the result of using different inputs sets than the used for the development of each FDD. The FDD monitor developed in this thesis, showed that the COP drift threshold for detection changed between different clusters of the input space, therefore, it could perform differently with another set of inputs.

In this thesis, only a small part of the operation region was tested and the results were good. It remains uncertain if the performance could change for other conditions, but the results encourage to commit with more development and validation of the developed monitor.

With respect to diagnosis performance, Table 3.1 also gives Accuracy values, which could be compared with the obtained results. However, they refer to diagnosis accuracy while, in this thesis, the accuracy has been used for the fault detection while for the diagnosis the indicator the misdiagnosis rate (MR) was used, which is the inverse of the diagnosis accuracy. Accordingly, the diagnosis accuracy values obtained with the FDD monitor were of a 100% for each fault except for OHXF which was not diagnosed.

Taking this into account, the first study [81] developed a fault diagnosis technique for chillers based on Bayesian network. They used as input data the results from a previous study from Comstock and Braun [22] about faults on a chiller. They obtained diagnosis accuracies higher than 70%. However, they did not define the accuracy calculation, being possible that they also took into account when a fault was not diagnosed. In this thesis, for the diagnosis part, it has been only take into account when a fault was wrong diagnosed. Therefore, using the same basis, they could had higher accuracy values, but that remains uncertain. They also note that when the fault intensity was higher, the accuracy increased because the fault effects were higher.

In other article [83], the use of an improved decision tree for fault diagnosis in variable speed heat pumps showed good results. They obtained a diagnosis accuracy of 94.44% for experimental data. When

the test conditions were different, the accuracy decreased until 69.18%.

There is the same uncertainty about the calculation of the accuracy, but in general terms, the diagnosis of the FDD monitor developed are even better that other FDD methodologies found in the literature.

The FDD monitor developed has performed well while working in real-time. During the faults test, the FDD used the heat pump measurements, detecting steady-state and monitoring the COP in real-time. Despite conditions were not changing, it only required almost seven hours of training to obtain the results showed.

This section has shown the result of the FDD developed with data from a real heat pump with emulated faults. The steady-state detector worked correctly and filtered the non-stationary data. Despite the data being very steady and without dynamic changes, the algorithm was able to adapt to the different noise levels and the discontinuities between both conditions.

The input data was classified correctly into two different clusters, corresponding to two different conditions. No-fault models were trained for both clusters with error margins of 3% and 7% for the 10 kW and 12 kW conditions, respectively. The last one had less quantity of data points and more noise which could explain the increase in error margin.

The FDD monitor had high accuracy without any false alarms. The use of the SSD and ensuring the constance of the fault, guaranteed the veracity of the detections. The detection time was below 20 minutes including the transition phase from one fault level to another.

All the faults were correctly diagnosed except for OHXF which a diagnosis could not be reached. However, the diagnosis table had to be changed between the first validation with simulated data and the second with experimental data. This means that more work is needed to be able to be generalized to different heat pump typologies. As already explained in Section 4.6, the different heat pump architectures affect the fault repercussions. If more data of fault effects were accessible, the diagnosis module could take into account different fault effects and be more adaptable to other conditions.

The FDD monitor worked as intended with low computational re-

quirements. The FDD was running on a computer with average hardware, but in parallel, the same FDD was running on a pocket-size computer with low resources. The results were the same between both implementations. This opens the possibility to install the monitor insite.

CHAPTER 6

Summary and outlook for future research

UNIVERSITAT ROVIRA I VIRGILI
AUTOMATIC FAULT DETECTION IN DOMESTIC HEAT PUMPS
Ivan Bellanco Bellanco

6.1 Final summary

The objective of this doctoral thesis was to develop and validate a Fault Detection and Diagnosis (FDD) monitor for domestic heat pumps. The monitor has been developed to work with variable heat pumps.

The first part of this thesis was dedicated to do a literature review of the faults that commonly affect to vapour compression systems, which are: outdoor heat exchanger fouling and outdoor unit mechanical component failure, indoor heat exchanger fouling and indoor unit mechanical component failure, compressor and 4-way valve leakage, non-condensable gas in the refrigerant circuit, refrigerant over and under charge, restriction in the liquid line, errors in sensor measurements and other less common errors. From the literature, the effects of those faults were summarized and quantified. The different emulation techniques that have been used to induce faults in real equipment were described, as well as the modelling of faults for virtual simulation.

The different methodologies to create an FDD monitor were explored to choose the one that best covers the aims of the research. Despite the lack of homogenization to describe the performance of the FDDs, a table was created to compare the performance of the different methodologies. The method selected to develop the FDD consist of the creation of no-fault models of different features with polynomial regressions and diagnosis of faults using expert knowledge. The FDD consisted of additional modules as the steady-state detector, the input space and the fault detection module, to increase the accuracy of the results. The steady-state detector eliminates the non-stationary data, for this, a new methodology that adapts to different input conditions was developed. The input space is used to group the data by the working conditions, giving the capability of self train the algorithm when data from new condition is detected. The no-fault models created with polynomial regression models represent the behaviour of the heat pump when there is no fault present in the equipment. The comparison of the COP value between the results of the models and the heat pump measurement serves as indicator of a fault. To avoid the possibility of false alarms due to measurement noise or outliers in the measurement, the fault detection module ensures that the fault is present during a certain period before giving notice of the fault. From the expert knowledge

obtained by reviewing the literature of faults effects, a diagnosis table was created to knowing the trend of different features and determine the occurring fault.

The FDD monitor was first validated with data from a simulation model. Using the TRNSYS software, the model of an air-to-water heat pump with a variable speed compressor was created. However, the model was not complex enough to induce the faults in the different components. To tackle the situation, different fault parametrization equations were generated. The equations were applied to the data of the non-faulted heat pump TRNSYS model, obtaining the data with the fault effects to validate the FDD monitor. The faults simulated were under and over charge, valve leakage, indoor heat exchanger fouling, outdoor heat exchanger fouling and liquid line restriction. Using this data, the monitor could detect that a fault was happening before a 5% reduction in COP occurred without any false alarm. All the faults simulated were correctly diagnosed by the FDD. The self training capability was used along the simulation when new conditions appeared. If these new conditions appeared when the equipment had a fault, the algorithm could learn this faulty behaviour as normal and delaying the detection of the fault.

The monitor was also validated with a real heat pump, a prototype of a 10 kW, water-to-water, variable-speed compressor heat pump charged with propane, developed within the framework of the European project TRI-HP. The heat pump was tested in normal conditions and with faults induced. The tests were carried out under laboratory conditions in the SEILAB, which is a testing laboratory based on the Hardware-in-the-Loop methodology. The faults emulated were outdoor heat exchanger fouling, compressor valve leakage, liquid line restriction and refrigerant overcharge. The tests were performed with different fault intensities and with heat duties of 10 kW and 12 kW. The effects of the faults were analysed, focusing on the COP, the electrical power consumption and internal parameters of the refrigerant circuit as refrigerant mass flow, superheat, subcooling and compressor outlet, liquid line, evaporation and condensing temperatures. All the faults decreased the COP, being compressor valve leakage the fault that had a higher impact and outdoor heat exchanger fouling the one with the least effect. The results of the faults differ from the ones obtained from the literature review, mainly because of the different architectures

between the tested heat pump and the ones from literature. Because of that, the diagnosis table developed had to be adapted to the new data.

While the faults were being tested, the FDD monitor was running in real time, supervising the heat pump status. The monitor was trained with the data of the heat pump without faults. Then, it monitored the rest of the tests. The FDD monitor detected that a fault was happening before the COP decreased 8%, achieving a detection before a 4% drift for the 10 kW load. The detection time was less than 25 minutes without any false alarm. All the faults were correctly identified, except for outdoor heat exchanger fouling which was detected as a fault but could not be discerned from the others. Despite that was difficult to do a direct comparison with other FDD methodologies found in the literature review, the FDD monitor developed showed better results than other methodologies. Furthermore, this new monitor also works with variable speed compressors, which were not commonly used for FDD development and requires of low computational resources.

The main objective of the thesis has been achieved. Almost all the specific objectives were fulfilled. Despite the monitor has been validated with simulation data and experimental data with two different types of heat pumps, the diagnosis methodology needs more work to achieve the specific objective of developing a monitor that could work with different types of heat pumps.

6.2 Future work

The objective of this thesis has been accomplished, however there are more actions that can be done to improve the overall performance of the FDD monitor.

Different faults has been tested in a real heat pump, yet faults as undercharge, non-condensables gases and sensor errors could not be tested within the time frame of the experimental campaign. If in a future research, these faults want to be tested, the first two fault will needed to have a real heat pump to induce the faults, with the possibility of damaging the equipment if liquid refrigerant enters the

compressor. The sensor error could be emulated by manipulating the data from the tests done. However, sensors provide the input data to the FDD, being difficult to know if a measurement corresponds to a real situation or to a drift in the measurement. The methodologies required to detect sensor errors are inside the group of pattern recognition techniques. Therefore, the FDD monitor will require to count with this type of methodologies to identify a sensor error, needing a total rebuild.

As has been shown, the diagnosis logic obtained with the literature review does not work correctly for the tested heat pump. More efforts need to be done to obtain a diagnosis that could work with a high variety of heat pump systems. To do so, more tests are required with different heat pumps or the obtention of information from maintenance services about faults. The self-train capability gives flexibility to the solution; however, for the case of the OC fault with the validation with simulated data, the FDD monitor self-trained when the equipment had a fault. Therefore, the self-training capability needs to be redefined to avoid the training when the heat pump has a fault, for example, by stopping the self-learning after a fault has been detected.

With the test of the FDD monitor in the laboratory with static conditions, the Technology Readiness Level (TRL) achieved was 4. The TRL is used to measure the maturity level of a technology. Doing the same tests but under dynamic conditions, the TRL achieved would be 5. But one of the most interesting steps to do to improve the solution, is to implement it in a heat pump in field. This will provide valuable information about the performance of the solution along the year and the needs and expectations of the final users. With this demonstration, another TRL level will be acquired (6), and the technology will be accessible to the domestic heat pump market.

BIBLIOGRAPHY

UNIVERSITAT ROVIRA I VIRGILI
AUTOMATIC FAULT DETECTION IN DOMESTIC HEAT PUMPS
Ivan Bellanco Bellanco

[1] IPCC. *Climate Change 2014, Synthesis Report*. 2014, p. 151. ISBN: 9789291691432. DOI: 10.1016/S0022-0248(00)00575-3.

[2] Intergovernmental Panel on Climate Change. *Climate Change 2022 - Mitigation of Climate Change - Summary for Policymakers (SPM)*. 1. 2022, pp. 1–30. ISBN: 9781107415416.

[3] UNFCCC. *UNFCCC Kyoto Protocol to the United Nations Framework Convention on Climate Change*. Kyoto, Japan, 1997.

[4] UNFCCC. *UNFCCC The Paris Agreement to the United Nations Framework Convention on Climate change*. Paris, France, 2015.

[5] European Parliament. *The European Parliament declares climate emergency*. 2019. URL: https://www.europarl.europa.eu/news/en/press-room/20191121IPR67110/the-european-parliament-declares-climate-emergency (visited on 02/06/2022).

[6] O. Lucon et al. *2014: Buildings in Climate Change 2014: Mitigation of Climate Change. Contribution of Working Group III to the Fifth Assessment Report of the Intergovernmental Panel of Climate Change*. Cambridge Univeristy Press, 2014.

[7] *Energy consumption in households - Statistics Explained*. 2020. URL: https://ec.europa.eu/eurostat/statistics-explained/index.php?title=Energy_consumption_in_households#Energy_consumption_in_households_by_type_of_end-use (visited on 26/06/2019).

[8] IEA. *Heat Pumps*. 2021. URL: https://www.iea.org/reports/heat-pumps (visited on 21/06/2022).

[9] European Commission. *Energy performance of buildings directive*. URL: https://www.energy.ec.europa.eu/topics/energy-efficiency/energy-efficient-buildings/energy-performance-buildings-direcive_en#:~:text=The%20Directive%20amending%20the%20Energy,and%20to%20increase%20building%20renovations. (visited on 23/06/2022).

[10] IEA. *Net Zero by 2050: A Roadmap for the Global Energy Sector*. Tech. rep. 2021, p. 224.

[11] European Heat Pump Association (EHPA). *European Heat Pump Market and Statistics, Report 2021*. Tech. rep. 2021.

[12] Mark S. Breuker and James E. Braun. "Common faults and their impacts for rooftop air conditioners". In: *HVAC and R Research* 4.3 (1998), pp. 303–318. ISSN: 10789669. DOI: 10.1080/10789669.1998.10391406.

[13] Todd M Rossi. "Unitary air conditioner field performance". In: *International Refrigeration and Air Condtioning Conference* (2004).

[14] Tom Downey and John Proctor. "What Can 13 , 000 Air Conditioners Tell Us ?" In: *ACEEE Summer Study Proceedings*. 2002, pp. 53–68.

[15] Bob Davis and David Robison. "Field Monitoring of High-Efficiency Heat Pumps". In: *ACEEE Summer Study on Energy Efficiency in Buildings* (2008), pp. 63–74.

[16] Robert J Mowris et al. "Field Measurements of Air Conditioners with and without TXVs". In: *ACEEE Summer study on Energy Efficiency in Buildings* (2004), pp. 212–227.

[17] Srinivas Katipamula and Michael R. Brambley. "Review article: Methods for fault detection, diagnostics, and prognostics for building systems—a review, part I". In: *HVAC and R Research* 11.1 (2005). DOI: 10.1080/10789669.2005.10391133.

[18] A. P. Rogers, F. Guo and B. P. Rasmussen. "A review of fault detection and diagnosis methods for residential air conditioning systems". In: *Building and Environment* 161.July (2019), p. 106236. ISSN: 03601323. DOI: 10.1016/j.buildenv.2019.106236.

[19] R.S. Adhikari et al. "Energy Savings through Variable Speed Compressor Heat Pump Systems". In: *Energy Procedia* 14 (2012), pp. 1337–1342.

[20] Minsung Kim and Min Soo Kim. "Performance investigation of a variable speed vapor compression system for fault detection and diagnosis". In: *International Journal of Refrigeration* 28.4 (2005), pp. 481–488. ISSN: 01407007. DOI: 10.1016/j.ijrefrig.2004.11.008.

[21] *TRI-HP Project*. URL: https://www.tri-hp.eu/ (visited on 05/05/2022).

[22] M. C. Comstock, J. E. Braun and E. A. Groll. "The sensitivity of chiller performance to common faults". In: *ASHRAE Transactions* 108 PART 1 (2002), p. 467. ISSN: 00012505.

[23] Kyle A. Brownell, Sanford A. Klein and Douglas T. Reindl. "Refrigeration System Malfunctions". In: *ASHRAE Journal* 41.2 (1999), pp. 40–47. ISSN: 00012491.

[24] Young Chull Ahn et al. "An experimental study of the air-side particulate fouling in fin-and-tube heat exchangers of air conditioners". In: *Korean Journal of Chemical Engineering* 20.5 (2006), pp. 873–877. ISSN: 02561115. DOI: 10.1007/BF02697291.

[25] Hatef Madani and Erica Roccatello. "A comprehensive study on the important faults in heat pump system during the warranty period". In: *International Journal of Refrigeration* (2014). ISSN: 01407007. DOI: 10.1016/j.ijrefrig.2014.08.007.

[26] Martin Zogg. "History of Heat Pumps. Swiss Contributions and International Milestones". In: *9th International IEA Heat Pump Conference, 20 – 22 May 2008, Zürich, Switzerland* May (2008), pp. 20–22.

[27] Yuebin Yu, Denchai Woradechjumroen and Daihong Yu. "A review of fault detection and diagnosis methodologies on air-handling units". In: *Energy and Buildings* 82 (2014), pp. 550–562. ISSN: 03787788. DOI: 10.1016/j.enbuild.2014.06.042.

[28] James Braun. "Automated Fault Detection and Diagnostics for Vapor Compression Cooling Equipment". In: *Journal of Solar Energy Engineering* (2003).

[29] Necati Kocyigit, Huseyin Bulgurcu and Cheng Xian Lin. "Fault diagnosis of a vapor compression refrigeration system with hermetic reciprocating compressor based on p-h diagram". In: *Energy Economics* 45 (2014), pp. 44–54. ISSN: 01409883. DOI: 10.1016/j.ijrefrig.2014.05.027.

[30] D Noël et al. "Experimental Characterization of Fault Impacts on the Functioning Variables of an Inverter Driven Heat Pump". In: *10th International Conference on System Simulation in Buildings* (2018).

[31] Seok Ho Yoon, William Vance Payne and Piotr A Domanski. *Residential Heat Pump Heating Performance with Single Faults Imposed*. Tech. rep. 2010.

[32] Samuel Boahen, Kwang Ho Lee and Jong Min Choi. "Refrigerant charge fault detection and diagnosis algorithm for water-to-water heat pump unit". In: *Energies* 12.3 (2019). ISSN: 19961073. DOI: 10.3390/en12030545.

[33] Mehdi Mehrabi and David Yuill. "Fouling and Its Effects on Air-cooled Condensers in Split System Air Conditioners (RP-1705)". In: *Science and Technology for the Built Environment* 25.6 (2019), pp. 784–793. ISSN: 2374474X. DOI: 10.1080/23744731.2019.1605197.

[34] Yabin Guo et al. "An expert rule-based fault diagnosis strategy for variable refrigerant flow air conditioning systems". In: *Applied Thermal Engineering* 149.November 2018 (2019), pp. 1223–1235. DOI: 10.1016/j.applthermaleng.2018.12.132.

[35] Ian H. Bell, Eckhard A. Groll and Holger König. "Experimental analysis of the effects of particulate fouling on heat exchanger heat transfer and air-side pressure drop for a hybrid dry cooler". In: *Heat Transfer Engineering* 32.3-4 (2009), pp. 264–271. ISSN: 01457632. DOI: 10.1080/01457632.2010.495618.

[36] Mehdi Mehrabi and David Yuill. "Generalized effects of refrigerant charge on normalized performance variables of air conditioners and heat pumps". In: *International Journal of Refrigeration* 76 (2017), pp. 367–384. ISSN: 01407007. DOI: 10.1016/j.ijrefrig.2017.02.014.

[37] Minsung Kim et al. "Performance of a residential heat pump operating in the cooling mode with single faults imposed". In: *Applied Thermal Engineering* 29.4 (2009), pp. 778–786. ISSN: 1359-4311. DOI: 10.1016/j.applthermaleng.2008.04.009.

[38] Zhimin Du, Piotr A. Domanski and W. Vance Payne. "Effect of common faults on the performance of different types of vapor compression systems". In: *Applied Thermal Engineering* 98 (2016), pp. 61–72. ISSN: 13594311. DOI: 10.1016/j.applthermaleng.2015.11.108.

[39] Li Yang, James E. Braun and Eckhard A. Groll. "The impact of fouling on the performance of filter-evaporator combinations". In: *International Journal of Refrigeration* 30.3 (2007), pp. 489–498. ISSN: 01407007. DOI: 10.1016/j.ijrefrig.2006.08.006.

[40] Minsung Kim et al. "Performance of a residential heat pump operating in the cooling mode with single faults imposed". In: *Applied Thermal Engineering* 29.4 (2006), pp. 770–778. ISSN: 13594311. DOI: 10.1016/j.applthermaleng.2008.04.009.

[41] Mehdi Mehrabi and David Yuill. "Normalized effect of condenser fouling and refrigerant charge on performance of vapor compression air conditioning systems". In: *International Compressor Engineering, Refrigeration and Air Conditioning, and High Performance Buildings Conferences*. 2016, pp. 1–10.

[42] H. M. Hashemian. *Effects of normal aging on calibration and response time of nuclear plant resistance temperature detectors and pressure sensors*. 1994.

[43] X. J. Luo et al. "Development of clustering-based sensor fault detection and diagnosis strategy for chilled water system". In: *Energy and Buildings* 186 (2019), pp. 17–36. ISSN: 03787788. DOI: 10.1016/j.enbuild.2019.01.006.

[44] Guannan Li and Yunpeng Hu. "An enhanced PCA-based chiller sensor fault detection method using ensemble empirical mode decomposition based denoising". In: *Energy and Buildings* 183 (2019), pp. 311–324. ISSN: 03787788. DOI: 10.1016/j.enbuild.2018.10.013.

[45] Peter R. Armstrong et al. "Detection of rooftop cooling unit faults based on electrical measurements". In: *HVAC and R Research* 12.1 (2006), pp. 151–175. ISSN: 10789669. DOI: 10.1080/10789669.2006.10391172.

[46] Mohammad Abuasbeh. "Fault Detection and Diagnosis for Brine to Water Heat Pump Systems". PhD thesis. Royal Institute of Technology, KTH, 2016.

[47] H. Han et al. "Important sensors for chiller fault detection and diagnosis (FDD) from the perspective of feature selection and machine learning". In: *International Journal of Refrigeration* 34.2 (2011), pp. 586–599. ISSN: 01407007. DOI: 10.1016/j.ijrefrig.2010.08.011.

[48] B Chen, Bin Chen and James E Braun. "Simple Fault Detection and Diagnosis Methods for Packaged Air Conditioners Packaged Air Conditioners". In: *International Refrigeration and Air Conditioning* (2000).

[49] Todd M. Rossi and James E. Braun. "A statistical, Rule-Based fault detection and diagnostic method for vapor compression air conditioners". In: *HVAC and R Research* 3.1 (1997), pp. 19–37. ISSN: 10789669. DOI: 10.1080/10789669.1997.10391359.

[50] Derek Noël, Philippe Riviere and Dominique Marchio. "Non-Intrusive Performance Assessment Method For Heat Pumps : Experimental Validation And Robustness Evaluation Facing Faults". In: *17 th, International Refrigeration and Air Conditioning Conference*. 2018.

[51] Alex Janecke, Trevor J. Terrill and Bryan P. Rasmussen. "A comparison of static and dynamic fault detection techniques for transcritical refrigeration". In: *International Journal of Refrigeration* 80 (2017), pp. 212–224. ISSN: 01407007. DOI: 10.1016/j.ijrefrig.2017.04.020.

[52] Necati Kocyigit. "Fault and sensor error diagnostic strategies for a vapor compression refrigeration system by using fuzzy inference systems and artificial neural network". In: *International Journal of Refrigeration* 50 (2015), pp. 69–79. ISSN: 01407007. DOI: 10.1016/j.ijrefrig.2014.10.017.

[53] Haorong Li and James E. Braun. "A Methodology for Diagnosing Multiple-Simultaneous Faults in Rooftop Air Conditioners". In: *HVAC and R Research* 13.2 (2004), pp. 369–95.

[54] D. Zogg, E. Shafai and H. P. Geering. "Fault diagnosis for heat pumps with parameter identification and clustering". In: *Control Engineering Practice* 14.12 (2006), pp. 1435–1444. ISSN: 09670661. DOI: 10.1016/j.conengprac.2005.11.002.

[55] Rajeev Namdeo, Smita Manepatil and Suvandan Saraswat. "Detection of Valve Leakage in Reciprocating Compressor Using Artificial Neural Network (Ann)". In: *International Compressor Engineering Conference at Purdue* (2008), pp. 1–8.

[56] Guannan Li and Yunpeng Hu. "Improved sensor fault detection, diagnosis and estimation for screw chillers using density-based clustering and principal component analysis". In: *Energy and Buildings* 173 (2018), pp. 502–515. ISSN: 03787788. DOI: 10.1016/j.enbuild.2018.05.025.

[57] Fu Xiao, Shengwei Wang and Jianping Zhang. "A diagnostic tool for online sensor health monitoring in air-conditioning systems". In: *Automation in Construction* 15.4 (2006), pp. 489–503. ISSN: 09265805. DOI: 10.1016/j.autcon.2005.06.001.

[58] Zhijian Hou et al. "Data mining based sensor fault diagnosis and validation for building air conditioning system". In: *Energy Conversion and Management* 47.15-16 (2006), pp. 2479–2490. ISSN: 01968904. DOI: 10.1016/j.enconman.2005.11.010.

[59] Marco Bonvini et al. "Robust on-line fault detection diagnosis for HVAC components based on nonlinear state estimation techniques". In: *Applied Energy* 124 (2014), pp. 156–166. DOI: 10.1016/j.apenergy.2014.03.009.

[60] Yanfei Li and Zheng O'Neill. "A critical review of fault modeling of HVAC systems in buildings". In: *Building Simulation* 11.5 (2018), pp. 953–975. ISSN: 19968744. DOI: 10.1007/s12273-018-0458-4.

[61] B. H. Cheung and J. E. Braun. "Simulation of fault impacts for vapor compression systems by inverse modeling. Part II: System modeling and validation". In: *HVAC and R Research* (2013).

[62] David P Yuill, Howard Cheung and Pur James E. Braun. "Evaluating Fault Detection and Diagnostics Tools with Simulations of Multiple Vapor Compression Systems". In: *International Refrigeration and Air Conditioning Conference* July (2014).

[63] Rongpeng Zhang and Tianzhen Hong. "Modeling and Simulation of Operational Faults of HVAC Systems Using Energyplus". In: *ASHRAE and IBPSA-USA SimBuild 2016 Building Performance Modeling Conference* (2016).

[64] Howard Cheung and James E. Braun. "Inverse Modeling to Simulate Fault Impacts for Vapour Compression Equipment Part I: Component Modeling and Validation". In: *International Refrigeration and Air Conditioning Conference at Purdue* (2012).

[65] R. Zhang and T. Hong. "Modeling of HVAC operational faults in building performance simulation". In: *Applied Energy* (2017).

[66] Yanfei Li and Zheng O'Neill. "An EnergyPlus/OpenStudio-biased Fault Simulator for Buildings". In: *2016 ASHRAE Winter Meeting*. June. 2016.

[67] Mangesh Basarkar et al. "Modeling and simulation of HVAC faults in EnergyPlus". In: *Proceedings of Building Simulation 2011: 12th Conference of International Building Performance Simulation Association* January (2011), pp. 2897–2903.

[68] S Bendapudi. "Development and evaluation of modeling approaches for transients in centrifugal chillers". PhD thesis. Purdue University, 2004.

[69] Kevin Otto et al. "Prioritizing Building System Energy Failure Modes Using Whole Building Energy Simulation". In: *Proceedings of SimBuild* 5.1 (2012), pp. 545–553.

[70] Piotr A. Domanski, Hugh Henderson and W. Vance Payne. "Effect of heat pump commissioning faults on energy use in a slab-on-grade residential house". In: *Applied Thermal Engineering* (2015). ISSN: 13594311. DOI: 10.1016/j.applthermaleng.2015.05.090.

[71] M. Yoshimura and N. Ito. "Effective diagnosis methods for air-conditioning equipment in telecommunications buildings". In: *Conference Proceedings., Eleventh International Telecommunications Energy Conference*. 1989, 21.1/1–21.1/7 vol.2. DOI: 10.1109/INTLEC.1989.88347.

[72] T Kumamaru et al. "A fault diagnosis system for district heating and cooling facilities". In: *Proceedings IECON'91: 1991 International Conference on Industrial Electronics, Control and Instrumentation* (1991).

[73] Venkat Venkatasubramanian et al. "A review of process fault detection and diagnosis part I: Quantitative model-based methods". In: *Computers and Chemical Engineering* 27.3 (2003), pp. 293–311. ISSN: 00981354. DOI: 10.1016/S0098-1354(02)00160-6.

[74] V. Venkatasubramanian, R. Rengaswamy and S. N. Kavuri. "A review of process fault detection and diagnosis part II: Qualitative models and search strategies". In: *Computers and Chemical Engineering* 27.3 (2003), pp. 313–326. ISSN: 00981354. DOI: 10.1016/S0098-1354(02)00161-8.

[75] V Venkatasubramanian et al. "A review of fault detection and diagnosis. Part III: Process history based methods". In: *Computers and Chemical Engineering* 27 (2003), pp. 327–346.

[76] Srinivas Katipamula and Michael R. Brambley. "Review article: Methods for fault detection, diagnostics, and prognostics for building systems—a review, part II". In: *HVAC and R Research* 11.2 (2005), pp. 169–187. ISSN: 10789669. DOI: 10.1080/10789669.2005.10391133.

[77] Woohyun Kim and Srinivas Katipamula. "A review of fault detection and diagnostics methods for building systems". In: *Science and Technology for the Built Environment* 24.1 (2018), pp. 3–21. ISSN: 2374474X. DOI: 10.1080/23744731.2017.1318008.

[78] Yang Zhao et al. "Artificial intelligence-based fault detection and diagnosis methods for building energy systems: Advantages, challenges and the future". In: *Renewable and Sustainable Energy Reviews* 109.November 2018 (2019), pp. 85–101. ISSN: 18790690. DOI: 10.1016/j.rser.2019.04.021.

[79] David P. Yuill and James E. Braun. "Evaluating the performance of fault detection and diagnostics protocols applied to air-cooled unitary air-conditioning equipment". In: *HVAC and R Research* 19.7 (2013), pp. 882–891. ISSN: 10789669. DOI: 10.1080/10789669.2013.808135.

[80] Zixiao Shi and William O'Brien. "Development and implementation of automated fault detection and diagnostics for building systems: A review". In: *Automation in Construction* 104 (2019), pp. 215–229. ISSN: 09265805. DOI: 10.1016/j.autcon.2019.04.002.

[81] Yalan Wang et al. "A practical chiller fault diagnosis method based on discrete Bayesian network". In: *International Journal of Refrigeration* 102 (2019), pp. 159–167. ISSN: 01407007. DOI: 10.1016/j.ijrefrig.2019.03.008.

[82] David P. Yuill and James E. Braun. "Effect of the distribution of faults and operating conditions on AFDD performance evaluations". In: *Applied Thermal Engineering* 106 (2016), pp. 1329–1336. ISSN: 13594311. DOI: 10.1016/j.applthermaleng.2016.06.149.

[83] Guannan Li et al. "An improved decision tree-based fault diagnosis method for practical variable refrigerant flow system using virtual sensor-based fault indicators". In: *Applied Thermal Engineering* 129 (2018), pp. 1292–1303. ISSN: 13594311. DOI: 10.1016/j.applthermaleng.2017.10.013.

[84] Jaehyeok Heo et al. *Self Training of a Fault-Free Model for Residential Air Conditioner Fault Detection and Diagnostics*. Tech. rep. National Institute of Standards and Technology, 2015.

[85] Minsung Kim et al. "Design of a steady-state detector for fault detection and diagnosis of a residential air conditioner". In: *International Journal of Refrigeration* (2008). ISSN: 01407007. DOI: 10.1016/j.ijrefrig.2007.11.008.

[86] Elena Fuentes and Jaume Salom. "Validation of black-box performance models for a water-to-water heat pump operating under steady state and dynamic loads". In: *E3S Web of Conferences* 111 (Jan. 2019), p. 01068. DOI: 10.1051/e3sconf/201911101068.

[87] Thibault Péan, Ramon Costa-Castelló and Jaume Salom. "Price and carbon-based energy flexibility of residential heating and cooling loads using model predictive control". In: *Sustainable Cities and Society* 50 (2019), p. 101579. DOI: 10.1016/j.scs.2019.101579.

[88] Shengwei Wang, Qiang Zhou and Fu Xiao. "A system-level fault detection and diagnosis strategy for HVAC systems involving sensor faults". In: *Energy and Buildings* 42.4 (2010), pp. 477–490. ISSN: 03787788. DOI: 10.1016/j.enbuild.2009.10.017.

[89] Haorong Li and James E. Braun. "Decoupling features and virtual sensors for diagnosis of faults in vapor compression air conditioners". In: *International Journal of Refrigeration* 30.3 (2007), pp. 546–564. ISSN: 01407007. DOI: 10.1016/j.ijrefrig.2006.07.024.

[90] G Bigot, L. Palandre and D Clodic. "Optimized Design of Heat Exchangers for "Reversible" Heat Pump Using R-407C ". In: *Eighth International Refrigeration Conference at 39 Purdue University, West Lafayette* (2000).

[91] Mehdi Mehrabi and David Yuill. "Generalized effects of faults on normalized performance variables of air conditioners and heat pumps". In: *International Journal of Refrigeration* 85 (2018), pp. 409–430. ISSN: 01407007. DOI: 10.1016/j.ijrefrig.2017.10.017.

[92] H Cheung and J. E. Braun. "Modeling of fault impacts for a multi-split ductless heat pump system ". In: *IEA Heat Pump Conference 2014* (2014).

[93] Minsung Kim, W Vance Payne and Piotr A Domanski. "Cooling mode fault detection and diagnosis method for a residential heat pump". In: *National Institute of Standards and Technology Special Publication 1087* (2008), p. 98.

[94] GmbH TKL Thermo. *TILMedia Suite*. Braunschweig, Germany.

[95] Aurelien Geron. *Hands-on machine learning with Scikit-Learn and TensorFlow : concepts, tools, and techniques to build intelligent systems*. OReilly Media, 2017. ISBN: 9781491962299.

[96] Ivan Bellanco et al. *Common faults tested on a variable-speed propane-charged heat pump on heating mode*. 2021. DOI: 10.5281/zenodo.5155136.

[97] Thibault Péan and Jaume Salom. *Laboratory facilities used to test energy flexibility in buildings*. Tech. rep. IEA EBC Annex 67 Energy Flexible Buildings, 2017. URL: http://www.annex67.org/media/1373/lab-description-report-first-edition.pdf.

[98] Joint Committee for Guides on Metrology. *Evaluation of measurement data — Guide to the expression of uncertainty in measurement*. Tech. rep. September. 2008, p. 134.

[99] ASHRAE. *Laboratory Method of Test of Fault Detection and Diagnostics Applied to Commercial Air-Cooled Packaged Systems*. Tech. rep. 2015.

[100] Yifeng Hu et al. “An experimental study of the behavior of a high efficiency residential heat pump in cooling mode with common installation faults imposed”. In: *Applied Thermal Engineering* 184 (2021). ISSN: 13594311. DOI: 10.1016/j.applthermaleng.2020.116116.

UNIVERSITAT ROVIRA I VIRGILI
AUTOMATIC FAULT DETECTION IN DOMESTIC HEAT PUMPS
Ivan Bellanco Bellanco